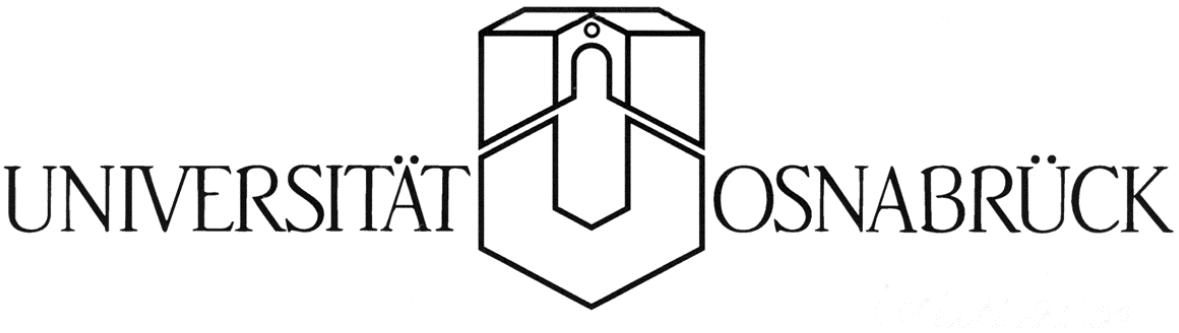

Site-specific modification strategies for unravelling energetics and dynamics of type I interferon receptor complex

Dissertation

Presented to the department of Biology/Chemistry, University of Osnabrück in partial fulfilment of the requirements for the degree of

"Doctor Rerum Naturalium"

Yulia Podoplelova

Osnabrück

February 2013

TABLE OF CONTENTS

1 Introduction

Living beings coordinate their activities at every level of their organization through complex biochemical signalling systems. A multitude of these communications is mediated through high affinity cell surface receptors such as G protein-coupled receptors, receptor tyrosine kinases (RTKs) and cytokine receptors, all membrane-spanning type of proteins. Among these, RTKs and cytokine receptors share certain principles of function and responsible for relaying signals for cell growth, differentiation and immunoregulation. Chemical external signals like hormones, polypeptide growth factors and cytokines are specifically or promiscuously recognized by these receptors on the cell surface. Commonly signalling pathway comprises a specific interaction of a messenger molecule with an extracellular receptor subunit, a mechanism for transmitting the ligand-binding event to the cell interior and a series of intracellular responses that may involve a cascade of chemical changes catalysed by kinases and phosphatases.

Whereas ligand recognition by ectodomains among these receptor groups has a lot in common or ultimately can be explored by conventional approaches, little is understood in each case for a mechanism how signal translocates across the membrane and sensed by the cytosolic catalytic pathway components. Based on the presence or absence of catalytic domains, some of these receptors can be classified as receptors with intrinsic enzymatic activity, containing cytoplasmic tyrosine kinase domain (receptor tyrosine kinases - RTKs), and those without it but associated with protein kinases at their cytosolic part (cytokine receptors). Indeed, the most common model for activating kinases appears to be ligand-induced crosslinking of two receptor proteins, bringing the kinases in proximity for trans-phosphorylation of the dimerized monomers. Apparently this is unlikely for receptors existing in unliganded state as preformed dimers where the cytosolic interaction of catalytic motifs is suppressed. Activation of such receptor complexes appears to be induced through a conformational change or relative displacement of individual receptor subunits upon ligand binding that the resulting rearrangements in the architecture of transmembrane segments unlock the intracellular kinase activity. Though in the most cases the detailed nature of these signal propagation mechanism remains concealed. This makes it difficult to explain how some receptors fine-tune the same mechanisms for relaying signals from promiscuous binding of various ligands to initiate distinct intracellular response pathways – a phenomenon termed as differential signalling. The elucidation of the reasons for differential signal propagation may be fulfilled by expanding knowledge on the interaction of these ligands with their receptors with respect to the structure

and dynamics as well as by comparing with readily studied examples of receptor activation modes.

The classic model of receptor tyrosine kinases assume that in the absence of ligand they exist on a plasma membrane as monomeric protein subunits with a single transmembrane helix. Binding of a soluble ligand, such as different growth factors, to an RTK receptor induces receptor dimerization, activation of intrinsic tyrosine kinase activity, and trans-phosphorylation of the dimerized monomers. Phosphorylation allows access of substrates and ATP to the activated catalytic domain and additional phosphorylated residues on the non-catalytic domain create docking sites for adapter proteins. The insulin receptor [1] and several epidermal growth factor receptor (EGFR) homologues [2-4] are exceptions from this model in that they are dimers in unliganded state. These receptors are now thought to be activated by a ligand-induced conformational change.

A hallmark for understanding RTK signalling is the most studied activation mechanism of epidermal growth factor receptor complex. It belongs to epidermal growth factor receptor-family (EGFR-family), an important class of RTKs involved in transmission of biochemical signals governing cell fate. Four human EGFR-family receptor members (ErbB-1 - ErbB-4) are proteins with a single-pass transmembrane helix. They form numerous homo- and heterodimer combinations and bind different epidermal growth factor-related ligands, thus performing diverse functions in a complex signalling network.

A complicated interrelation of ligand-induced conformational change in extracellular domains, allostery, interaction with surrounding lipid environment and transmembrane communication with cytoplasmic kinase domains has been shown to modulate an activation of epidermal growth factor receptor (EGFR or ErbB-1) (Figure 1.1). In the case of the EGFR, structural studies show that ligand binding promotes conformational rearrangement of its four extracellular domains from a tethered to an extended conformation in which a loop, termed the dimerization arm, becomes exposed and mediates formation of symmetric receptor dimers [5]. More recent findings suggest that a portion of cell-surface receptor pool exist as preformed dimers [2, 4] where the cytosolic kinase domains are perhaps autoinhibited in some way prior to ligand binding. In the ligand-activated state of EGFR dimer the kinase domains form an asymmetric, head to tail dimer, in which the binding of one kinase domain (denoted as the activator kinase) (Figure 1.1 A) stabilizes the active conformation of the second kinase domain (denoted as the receiver kinase), essential for the transphosphorylation [6]. This interaction of the kinases is additionally regulated by the juxtamembrane helical segments forming a short antiparallel coiled-coil dimer, which is coupled to the dimerization of the

transmembrane domains (TMDs) of the receptor [7, 8]. The ligand-induced dimerization of the TMDs of the EGFR family was documented by mutational [9] and NMR analysis of transmembrane helices [10, 11]. They provided a clue as to how certain consensus sequences composed by residues with small side chains enable the dimerized TMDs to adopt more than one conformation upon so-called rotation-coupled activation [4] of the receptor thus suggesting a mechanism of signal propagation across membrane for these representatives of RTKs.

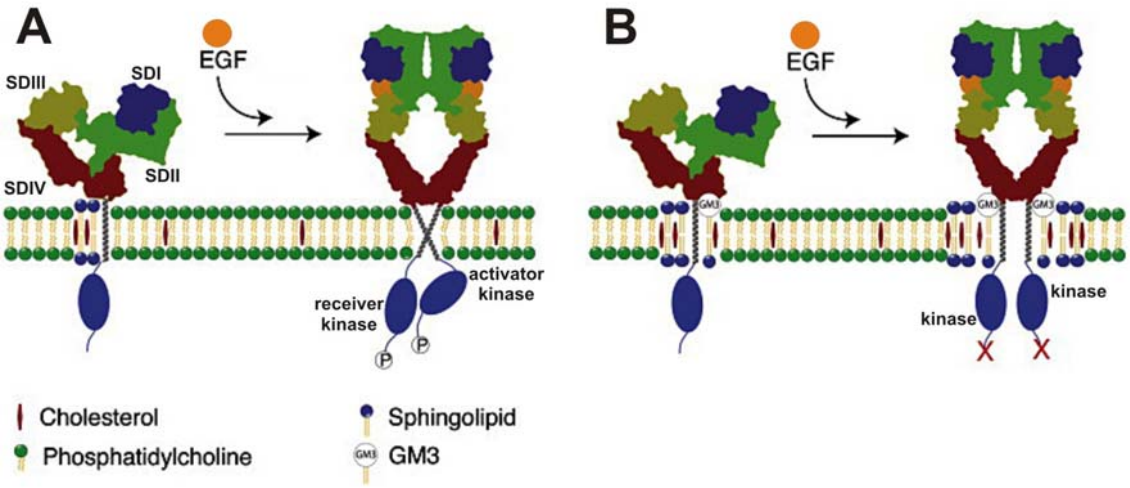

Figure 1.1 A model for the formation of signalling complex between EGF and EGFR, conformational change and receptor activation.

A EGFR extracellular domain without bound ligand adopts a tethered low-affinity conformation with an intramolecular tether (shown between subdomains SDII and SDIV) or the extended high-affinity conformational state and can switch between the states by dynamic fluctuations mainly at the hinge between SDII and SDIII [2]. In the absence of ligand monomers of EGFR exist primarily in the tethered state, and the formation of homodimers biases the structure of EGFR toward extended state-like conformations with high association rates to EGF. When EGF binds at SDI and SDIII at one side of an EGFR dimer, EGFR undergoes an allosteric conformational change, making it easier for the second EGF to bind to the dimer than to the monomer. Next, the so-called rotational activation mechanism [4] was proposed to relay the ectodomain conformational change into the transmembrane helix-helix packing rearrangement. The resulting change in angle between two transmembrane domains can be ascribed to the activation of the EGFR intracellular kinase domains [10, 11]. **B** Additionally, EGFR activation is proposed to be regulated by the ganglioside GM3 of the outer lipid bilayer leaflet [12, 13]. When GM3 is present in the bilayer, the direct association of GM3 with the EGFR ectodomain leads to the inactivation of the EGFR kinase activity. Modified from [13].

Cytokines are required for the growth and differentiation of nearly all cell types, but are particularly important for regulation of the immune and hematopoietic systems. Type I and type II cytokine receptors function as oligomeric complexes consisting of typically two to four receptor chains that may be the same or different. In single subunit receptors the subunits

fulfil the dual role of binding to cytokines and signalling. In multi-subunit receptors the different subunits may perform specialized functions such as ligand-binding or signal transduction. The erythropoietin receptor, the growth hormone receptor and the interleukin 6 receptor belong to the type I cytokine receptor family. The IFNα/β receptor and IFNγ receptor represent the family of type II cytokine receptors (Interferon receptor family). Typically cytokine receptor assembly involves homo- or heterodimerization of two receptors by a single, less frequently, by a dimeric cytokine molecule. All receptor subunits are proteins with one single transmembrane domain, an extracellular located N-terminal citokine-binding domain and an intracellular non-catalytic C-terminal domain that is associated with Janus kinases (Jaks). The active kinases phosphorylate the C-terminal intracellular tails of the receptors on specific tyrosine residues, creating binding sites for pathway-associated effector molecules such as STAT (signal transducer and activator of transcription) which, upon phosphorylation by the active Jaks, translocate to the nucleus where they activate transcription of cytokine-responsive genes.

Currently it is still under debate, how kinase activation is mediated by cytokine binding. The classical model is the ligand-induced cross-linking of extracellular subunits which is responsible for bringing the cytoplasmic domains into proximity leading to signal propagation. For some cytokine receptors, however, pre-assembly of receptors in an inactive state is proposed. This hypothesis suggests that ligand binding leads to a conformational change of the pre-assembled subunits and not to a ligand-induced assembly.

As one of examples, binding of human growth hormone (GH), to the cell surface receptor (GHR), a member of the type I cytokine receptor family, is accompanied by a conformational rearrangement in the extracellular part (Figure 1.2) which is propagated via the transmembrane domains then leading to activation of Jak2, the Janus kinases associated with the cytoplasmic domains [14, 15]. The dimerization of two identical receptor subunits alone by one hormone molecule is insufficient to activate the full-length GHR. Increasing evidences strongly suggest that in the absence of ligand the human GHR receptor exists as a preformed inactive dimer through the contact of TMDs. If the unliganded human GHR exists as a preformed dimer on the surface of a cell, activation must be mediated by conformational changes induced by the binding of GH, as opposed to receptor association model. Interestingly, a detailed comparison of unliganded and liganded receptor ectodomain structures revealed that only minor conformational changes result from ligand binding [14, 16].

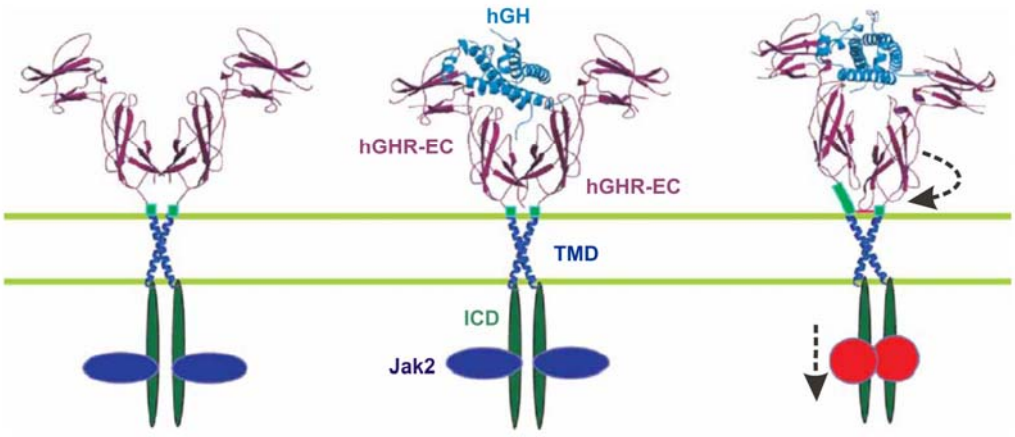

Figure 1.2 A schematic model of human GHR activation.

The first diagram shows the unliganded preformed human growth hormone receptor (hGHR) dimer (purple) on the cell membrane with the subunits sitting equivalently. In the centre diagram, a hormone molecule (blue ribbon) binds via high affinity site 1 to the left-hand receptor extracellular domain (hGHR-EC) as it has been observed in the 1:1 published complex structure. The dimerization domains of each receptor (cyan) located in the C-terminal domains are far from complementary because of charge repulsions and steric clashes. The right-hand diagram shows the structure as observed in the crystal structure of the published 2:1 complex. On binding to site 2 of the hormone, the second receptor molecule must move with respect to the first molecule so that the dimerization contacts are optimized, involving a rotation and a vertical movement. This then causes a rotation of the TMD and juxtamembrane regions, resulting in rotation and activation by transphosphorylation of the Jak2 molecules bound to intracellular domain (ICD), and the initiation of the GHR signalling cascade. The red line indicates disulfide bond formation by Cys241, which occurs as a result of receptor activation. Modified from [14].

Hormone binding occurs in two-steps involving high-affinity interaction with the first receptor subunit of the dimer with subsequent recruitment of a second receptor molecule to form the asymmetric 1:2 signalling complex (Figure 1.2). The second receptor interaction interface is characterized by the low binding energy conferred through a single hydrophobic hotspot and the additive contribution of many residues [16]. Upon hormone binding several residues of this diffuse interface serve to orient and lock the productive receptor conformation involving a relative subunit rotation and a vertical movement (Figure 1.2). The conformational rearrangement in the extracellular part is followed by the clockwise rotation within the TMDs of about 40° leading to the interaction of the Box1 and Box2 motifs of intracellular domains (ICDs) and subsequent activation of Jak2 kinases and intracellular signalling. This conclusion was supported by insertion of four alanines in the TMD resulting in its relative vertical transition and in the constitutively active GHR [14].

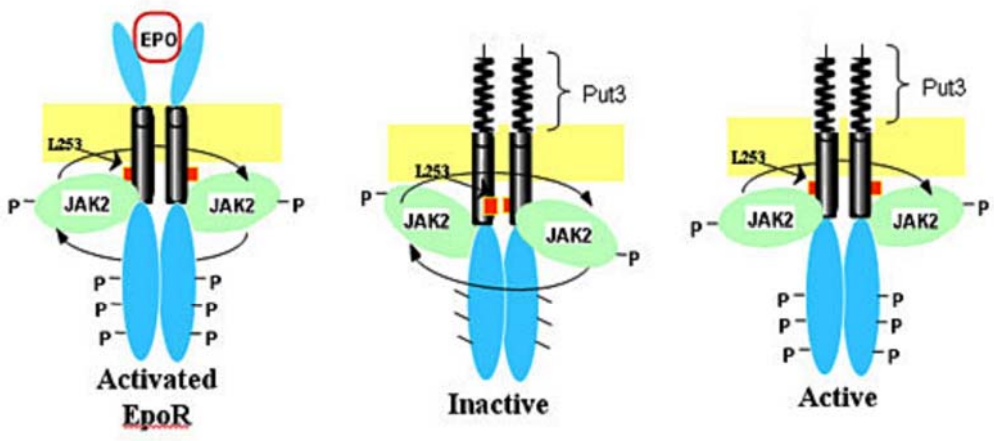

Figure 1.3 Mechanism of erythropoietin receptor activation.

The first diagram: Epo (red) binding to the extracellular domains (cyan) EpoR subunits stabilizes the conformation induced by TMD self-assembly and promotes a conformational switch that is compatible with activation of cytosolic Jak2, phosphorylation (-P) of the receptor tyrosine residues and downstream signalling. The centre diagram shows one of inactive conformations of fusion EpoR obtained by the replacement of extracellular domains by a dimeric coiled coil of the yeast transcription factor Put3 (Put3) in order to functionally probe the orientation requirements of TMDs (black) [17]. The right-hand diagram shows an active fusion protein identified from the total seven possible orientations. This orientation enables the proper rotational movement of transmembrane helices and results in the initiation of signal transduction through EpoR as indicated by Jak2 activation and tyrosine phosphorylation of EpoR ICDs. L259 (orange) indicates the hydrophobic residue involved in the interhelical interaction in the TMD region and in the stabilization of the inactive EpoR conformation. In the active orientation L259 is predicted to be outside of the TMD dimer interface [17, 18]. The diagram is based on information from Ref. [17, 18].

Another cytokine receptor system where the mechanism of signal propagation is studied in detail is the erythropoietin receptor (EpoR). Like growth hormone, erythropoietin (Epo) is proposed to induce a conformational change in EpoR by binding sequentially on the membrane to one high affinity and one low affinity receptor subunits which in the absence of ligand also form a preassembled dimer. In contrast to GHR, showing now evident contact of ectodomains (ECs) in the absence of hormone, the X-ray structures of the unliganded erythropoietin receptors differ in that the EpoR ECs interact between each other to form the basis for the constitutive dimer [19]. Structural evidences suggest that in the unliganded homodimer form EpoR exists in the conformation which is unproductive for signalling [19, 20]. This dimeric conformation is stabilized by self-assembly of TMDs in the orientation precluding the convergence and activations of ICD-associated Jaks [21]. If Epo binds, the receptor is hypothesized to be activated by a rotation of extracellular subunits [17, 22] which promotes a rotation of the TMDs and closer and correct proximity of the intracellular domains and permits phosphorylation of Jak2 and EpoR ICDs (Figure 1.3). The role of TMD rotational

movement in the signal propagation was corroborated by engineering the TMD EpoR fusion proteins with ectodomains replaced by a dimeric coiled coil where the helical TMDs were constrained in seven possible relative orientations, one of which resulted in full and one in partial Jak2 activation (Figure 1.3) [17]. Unlike for GHR, serial alanine insertions below the EpoR TMD did not produce constitutive activation of EpoR but fully impaired the ability of Jak2 to phosphorylate the receptor [18], pointing toward that the ligand-induced conformational change of EpoR does not involve a downwards receptor displacement. This not only strongly supports the hypothesis that ligand-induced rotation of the receptor subdomains might represent a general mechanism of activation within the cytokine receptor superfamily, but also suggests that the domains facilitating receptor dimerization and conformational change may differ between cytokine receptors.

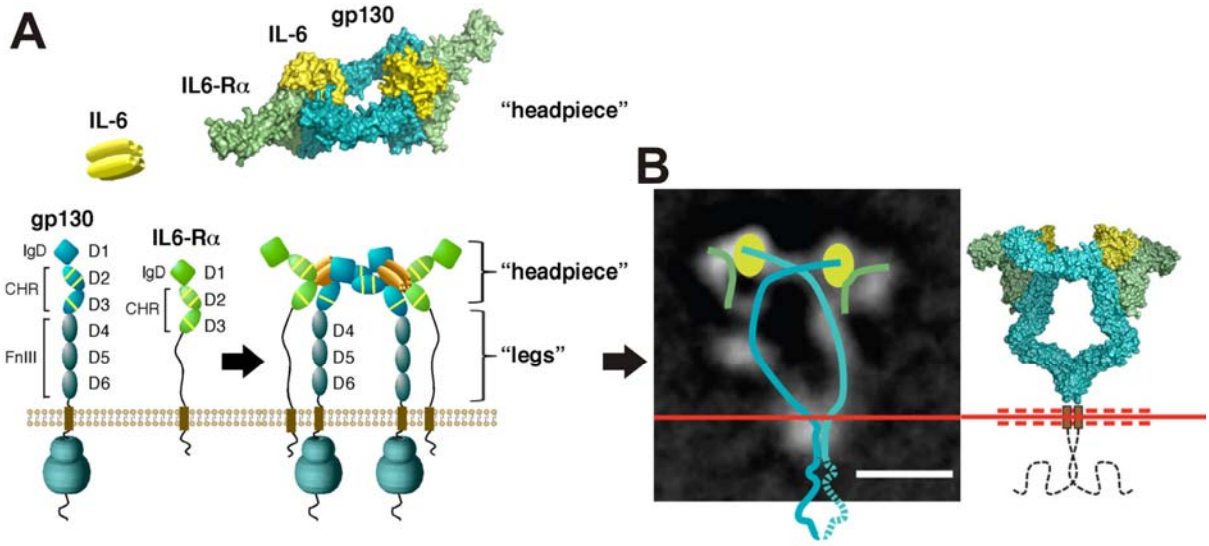

Figure 1.4 Assembly of the full-length IL-6/IL-6Rα/gp130 signalling complex.

A Components of the IL-6/IL-6Rα/gp130 2:2:2 complex in pre- and post-assembly state. A surface rendering of the structure of the signalling hexamer is shown on the top. IgD denotes Ig-like domain, CHR denotes cytokine-binding homology region, and FnIII denotes Fibronectin-III-like domain. ICD-associated Janus kinases are shown as blue bubbles. **B** The holocomplex class average electron microscopy image (left) modelled to the IL-6/IL-6Rα/gp130 complex (right) suggests that homodimerization of gp130 by IL-6 locks the extracellular/transmembrane domains of gp130 together into a rod-like unit that can sensitively transduce a conformational signal through the plasma membrane (red line) to Jaks (not shown) that are bound at the extreme juxtamembrane regions of the ICDs (dotted line) and imitate the signal activation. Modified from [23].

In addition to the ligand binding-induced conformational change it appears to be common that extracellular membrane-proximal domains of cytokine receptors are close in the activated complex, as it is seen for interleukin-6 (IL-6) receptor (Figure 1.4). The X-ray structures of unliganded full-length "tall" gp130 receptor (domains D1-D6) [24] and the hexameric

IL-6/IL-6Rα/gp130 complex [25] including only the membrane-distal domains D1-D3 of gp130 were determined at ~3.6 Å resolution. Superimposition of these structures shows that ligand binding induces a conformational kink in gp130 which brings the membrane-proximal extracellular domains of two gp130 molecules into very close proximity but there is no clear evidence whether these receptors interact directly in their C-terminal regions. Recently the full transmembrane IL-6/IL-6Rα/gp130 hexametric complex have been reconstituted and the Jaks associated with intracellular domains of gp130 have been purified for electron microscopy (EM) imaging [23]. These images of the complex indicate very close proximity of two gp130 membrane-proximal domains as well as intimate interaction between TMDs and juxtamembrane cytosolic domains (Figure 1.4 B).

Whereas type I cytokine receptors are often dimers comprised of subunits which share similar overall architecture but differ in binding affinities, type II cytokine receptor family represented by IFNα/β and IFNγ receptors are heteromeric receptors composed of functionally dissimilar protein chains. Interferon γ, the sole member of type II IFNs, signals as a dimer. Accumulating evidences have suggested that the IFNγ receptor actually has a tetrameric structure consisting of two IFNγ Receptor Chain 1 (IFNγR1) molecules and two IFNγ Receptor Chain 2 (IFNγR2) molecules [26], forming with the IFNγ dimer a hexameric signalling complex. Each individual IFNγ binds to a heterodimer consisting of the IFNγR1, which provides binding affinity, and IFNγR2, which is involved in signal transduction. Binding of IFNγ leads to a conformational change and subsequent signal transduction [27]. For type I IFNs exerting their functions through heterodimeric IFNα/β receptor, however, the mechanism of receptor activation still remains nebulous.

1.1 Type I interferon receptor

Type I interferons form a family of pleiotropic, multifunctional cytokines initially described more than half a century ago as agents that interfere with viral infection [28] but now also recognized as major elements of the early immune response [29, 30]. In addition to their antiviral and strong immunomodulatory activities, IFNs exhibit antiproliferative effects on cells. Consequently, they have substantial medical potential and are already used in the treatment of viral hepatitis (IFN2α) and multiple sclerosis (IFNβ) as well as several kinds of cancer [31]. Based on the receptor system that mediates their effects, IFNs are grouped into type I, type II, and type III interferons [32]. The type I IFNs act on, and are produced by, almost every nucleated cell and comprise 16 members with approximately 20%–60% sequence identity. Amongst them the human genome encodes 12 α subtype proteins, and a single subtype of β, ω, κ and ε [33, 34]. IFNγ is the only known type II interferon.

Additionally four IFN-like cytokines, defined as type III interferons [34], have been reported recently: IFNλ1 (IL-29), IFNλ2 (IL-28A) and IFNλ3 (IL-28B) are found in humans and other mammals. Here, only type I IFNs and their signalling will be discussed in more detail.

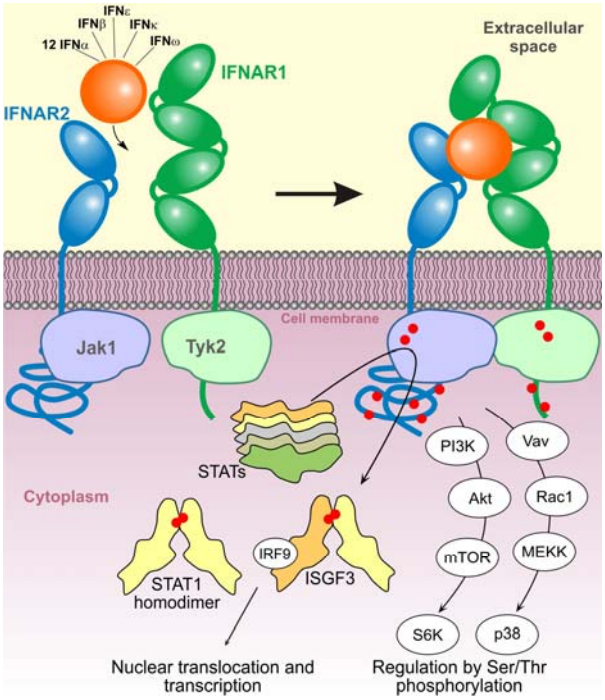

Figure 1.5 The type I interferon signalling network.

By simultaneous interaction of IFNs with the two receptor subunits IFNAR1 and IFNAR2 the active signalling complex is formed. Subsequently, the kinases Tyk2 and Jak1 associated with IFNAR1 and IFNAR2, respectively, transphosphorylate each other and phosphorylate specific tyrosine residues of IFNAR1 and IFNAR2 (indicated as red dots). These serve as docking sites for effector proteins of the STAT family. Upon phosphorylation, STAT1 and STAT2 form homo- and heterodimers, which translocate into the nucleus to activate transcription. Additionally type I IFNs are shown to activate the phosphatidylinositol 3-kinase pathway and MAP kinase pathway.

Exposure of cells to viruses or double stranded RNA (dsRNA) induces the production of IFNαs, IFNβ and IFNω. The level of each expressed IFN depends on the tissue of origin and the nature of viral challenge. All of them apparently signal through the same receptor complex comprised of the transmembrane receptor subunits IFNAR1 and IFNAR2. The intracellular domain of each receptor chain binds constitutively to a single specific member of the Janus kinase family: IFNAR1 to tyrosine kinase 2 (Tyk2) and IFNAR2 to Jak1 (Figure 1.5 and Figure 1.6) [35, 36].

Ligand binding induces the transphosphorylation of Jak1 and Tyk2, they phosphorylate several intracellular tyrosine residues on the membrane-distal intracellular part of both receptor subunits which then serve as docking sites and activation of STAT proteins (STAT1, STAT2, STAT3, STAT4, and STAT5) (Figure 1.5). STAT2 has also been speculated to

preassociate constitutively with IFNAR2 [37, 38]. Phosphorylated STATs, in turn, form homo- and heterodimers, dissociate from the receptor, and translocate into the nucleus, providing the primary mechanism through which gene expression of interferon-stimulated genes (ISGs) is induced [35]. Other important signalling pathways activated by type I IFNs include the phosphatidylinositol 3-kinase pathway [39, 40] and the MAP kinase pathway (Figure 1.5) [41, 42]. Despite their common biological activities and sequence homologies, type I IFNs are not redundant but rather induce their activities differentially [43, 44] by acting in different types of cells and initiating different specific signals and patterns of gene expression. However, it should be noted that for some cellular activities IFNs have equal potencies whereas for other responses they have very different potencies. Thus, for instance, higher IFNα2 concentrations mimic most IFNβ activities.

Altering the binding affinities of IFN towards both receptors in parallel has shown that the overall affinity towards the ternary complex dictates the activity pattern [45, 46]. In addition, differential IFN activities were proposed to be determined by different lifetimes and ligand affinities towards the receptor subunits, which dictate assembly and dynamics of the signalling complex in the plasma membrane [46, 47]. The transient formation of a small number of ternary interferon receptor complexes is sufficient to promote antiviral activity [46, 47]. Conversely, a high number of complexes, formed over a prolonged period of time, is required for antiproliferative activity.

The shared cell surface receptor mediating signalling activities of all 16 human type I IFNs consists of the two transmembrane subunits IFNAR1 and IFNAR2 [48] which bind a single ligand, forming a heteromeric ternary complex in a 1:1:1 ratio. The current view is that IFNAR2 is responsible for high affinity binding and that the IFN/IFNAR2 binary complex subsequently recruits the lower affinity subunit IFNAR1 on the membrane (Figure 1.6). This is due to that all IFNs bind IFNAR2 with nanomolar (typically 0.4-5 nM) affinity and the IFNAR1 receptor with micromolar (ranging from 0.5-5 μM) affinity [49, 50]. The tightest binding interferon is IFNβ which binds IFNAR2 with 0.1 nM affinity and IFNAR1 with 100 nM affinity [51]. The binding affinity of IFNω (2 nM towards IFNAR2 and 0.4 μM towards IFNAR1) is closer to that of IFNα2 (5 nM and 5 μM, respectively) [50]. All IFNs rapidly bind to IFNAR2 with association rate constants of 10^6-10^7 $M^{-1}s^{-1}$, whereas the association to IFNAR1 is relatively slow with association rate constant of ~$5 \cdot 10^5$ $M^{-1}s^{-1}$ [49-51]. Differences in binding affinities between different IFNs are mainly manifested as differences in the dissociation rate constants. Based on the proposed two-step assembly mechanism the dynamic equilibrium between binary and ternary complexes on the plasma

membrane appears to be determined by the affinity of IFN towards IFNAR1 ($K^{T}_{D,1}$) (Figure 1.6) and the concentration of receptor subunits. The life time of individual signalling complexes with IFNα2 is ~1 s [52], while it is ~100 s in case of IFNβ. For IFNAR1 and IFNAR2, preassociation of the receptors has not been detected in living cells neither for extracellular subunits nor through their cytosolic domains [53].

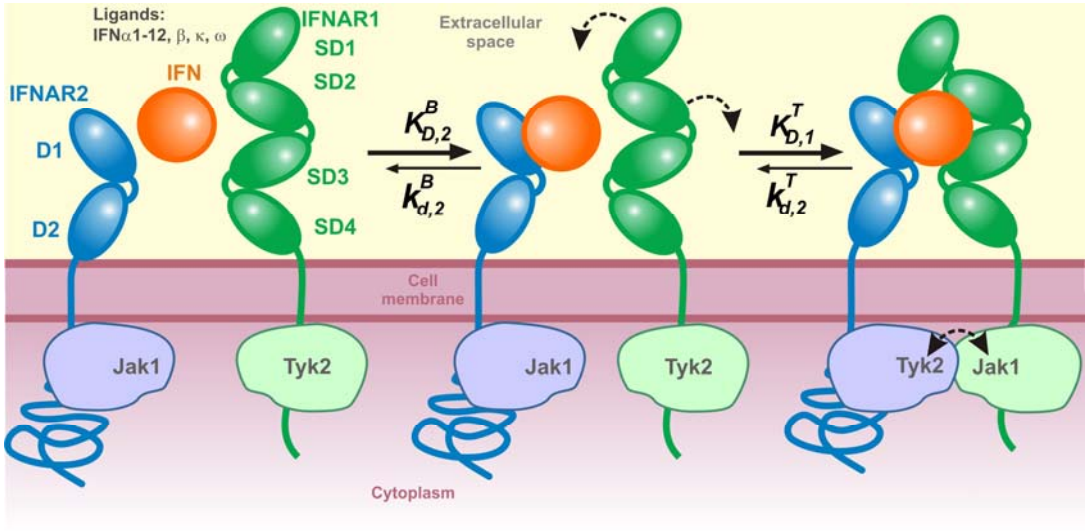

Figure 1.6 Model of type I Interferons receptor assembly and dynamics in the plasma membrane.

Sixteen human type I interferon (IFN) ligands (orange) signal through the same cell-surface transmembrane receptor subunits, IFNAR1 (green), comprised of four subdomains (SD1-SD4) and IFNAR2 (blue), comprised of two domains (D1-D2). Assembly of the ternary IFN receptor complex is proposed to occur in two steps. Rapid and high-affinity binding of IFN to IFNAR2 and formation of binary complex is followed by recruitment of IFNAR1 into the ternary complex. The dynamic equilibrium between binary and ternary complexes depends on the 2D dissociation constant $K^{T}_{D,1}$ and concentrations of the receptor subunits. After the ligand-induced assembly of a heterotrimeric complex, the IFN signal is then propagated through cell membrane to cytoplasm. The cytosolic receptor domains are associated with Janus kinases Tyk2 and Jak1 which are transphosphorylated upon assembly.

To demonstrate the affinity-potency correlation of specific IFNs, the antiproliferative activity of IFNα2 has been previously enhanced by increasing its binding affinity to either IFNAR1 [45, 54] or IFNAR2 [55]. The H57A-E58A-Q61A (HEQ mutant) [54] and H57Y-E58N-Q61S (YNS mutant) [45] triple mutants exhibited not only ~50-fold (~50-60-fold for YNS) tighter IFNAR1 binding than the wild type (WT), but ~100-fold-higher antiproliferative potency, while a mutation on IFNα2, where the C-terminal tail was replaced with that of IFNα8 (IFNα2-α8tail mutant) [55], resulted in 20-fold increased binding affinity to IFNAR2 and 10-fold-increased antiproliferative potency. Moreover, the repertoire of IFNα2 variants has

been further extended by generating a mutant possessing both the α8tail and YNS (IFNα2-YNS-α8tail) and thus the maximum integral affinity [47].

How can such differences in activity of various IFNs with a broad range of affinities be communicated through the same cell surface receptor? Initially, specific, additional components have been suspected to be responsible, but these have never been found. The elucidation of the reasons for type I IFNs differential activities may in part have been by limited for a long time by incomplete information on the interaction of these molecules with their receptor due to the absence of the sufficient structural data. Therefore a detailed analysis of the differences in the interaction mode of IFN subtypes with their cognate cell surface receptor might provide an understanding of the structure-function relationships.

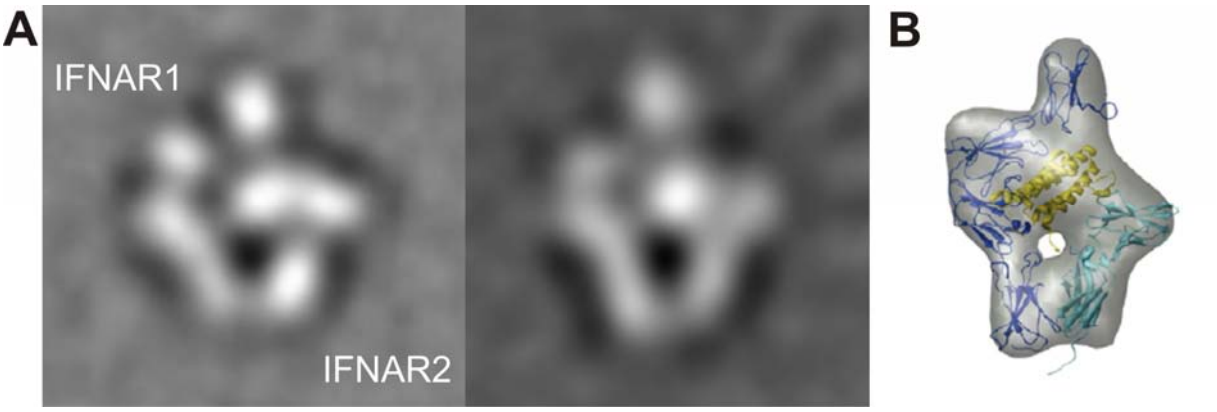

Figure 1.7 Low resolution EM structures of ternary complex formed with different type I IFNs.
A Average single particle EM images of the ternary complex with IFNα2-HEQ (left) and IFNβ (right). Complexes are formed with the full length (FNIII-like domains 1-4) of IFNAR1. **B** 3D reconstruction of the ternary IFNα2/IFNAR1-EC/IFNAR2-EC complex in negative stain. Density map with the fit atomic models of the components (yellow: IFNα2, blue: IFNAR1-EC, cyan: IFNAR2-EC). From [56].

The two chains of the shared human type I interferon receptor, IFNAR1 and IFNAR2 are both transmembrane type II cytokine receptors with an extracellular (EC) domain responsible for cytokine binding, a single-pass α-helical transmembrane domain and an unstructured intracellular domain associated with Jak1 (IFNAR2) and Tyk2 (IFNAR1) (Figure 1.6) [32, 57]. Like other receptors in this class, the ectodomain of the high-affinity subunit IFNAR2 (K_D in the nM range) comprises two fibronectin type III (FNIII)-like subdomains [58] (with canonical three-stranded and four-stranded antiparallel β-sheets and one disulfide bond), consisting of ~100 residues referred to as D1 and D2, respectively. The low-affinity receptor chain IFNAR1 (K_D in the μM range), however, consists of ~400 residues, twice of the size of IFNAR2-EC, and four FNIII-like subdomains 1 to 4 (SD1 to SD4), which most likely emerged from gene duplication [59]. IFNAR2-EC forms one cytokine binding module and the structure was solved by NMR [60] followed by the X-ray and NMR structures of the binary

IFN–IFNAR2 complex with human IFNα2b [61]. The IFNAR1-EC four-subdomain organization suggests two cytokine binding modules and a more complex stoichiometry than the 1:1:1 signalling complex. In addition, low-resolution structures of the ternary complexes harbouring IFNβ and IFNα2 mutant HEQ with enhanced affinity to IFNAR1, respectively, were obtained by single particle EM (Figure 1.7) [56]. These correctly deduced the general 1:1:1 stoichiometry and architecture of the ternary complex and showed no difference in binding mode of these two IFNs (Figure 1.7).

More recently, the structures of two heterotrimeric type I IFN receptor-ligand complexes have been determined by X-ray crystallography (Figure 1.8), in addition to the high-resolution structures of unliganded IFNAR1 and the binary IFNα2/IFNAR2 complex [62]. These two solved ternary complex structures contain two different ligands with distinct physiological activities, IFNω and IFNα2–YNS. Similarly to EM results, despite the different physiological activities of the two ligands, the heterotrimeric receptor-ligand complexes share the same architecture and the superimposed structures of the two complexes overlap with a root-mean-square deviation (RMS) of 0.9 Å.

IFNAR1 and IFNAR2 bind on opposing sides of the IFN ligand in an almost orthogonal arrangement that is unique among cytokine-receptor complexes. IFNAR2–EC shares with a ligand ~1800 $Å^2$ of binding surface area which is formed between parts of helices A, E, and the A–B loop of IFN and the D1 subdomain of IFNAR2 (Figure 1.8). Unlike most type I and II cytokine-receptor complexes, the IFN ligand does not bind at the apex of the elbow region between the D1 and D2 subdomains of IFNAR2, but its long axis shows almost parallel alignment with the beta strands of D1 [62, 63]. The IFNAR2 interface is characterized by the presence of several hotspot residues. The IFNAR1–IFN interface buries ~2200 $Å^2$ of surface area and is formed by contacts between helices B, C, and D of the IFN molecule and SD1–3 of IFNAR1. The large binding surface on IFNAR1 confers relatively low binding energy, thus implying that this receptor subunit might be designed for the conformational change. The IFN ligand primarily binds to IFNAR1 at the level of the hinge between the SD2 and SD3 domains, with the SD1 domain “capping” the top of the IFN molecule and the membrane-proximal SD4 is not involved in ligand binding [64]. There was no electron density for the SD4 of IFNAR1 in the maps of both ternary complexes, suggesting that it is flexible.

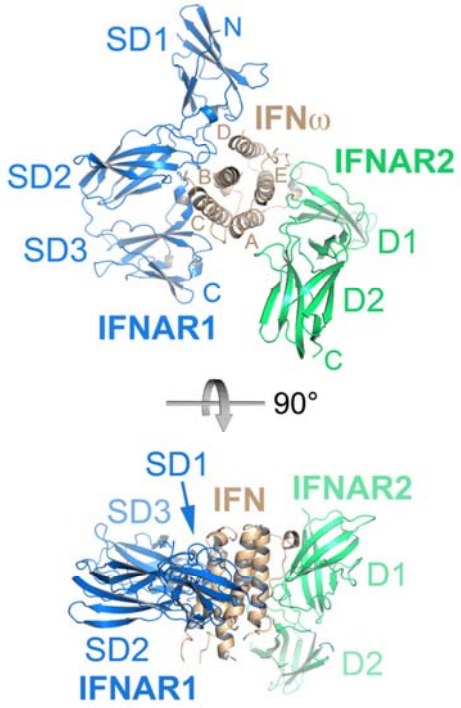

Figure 1.8 X-ray structure of type I IFN receptor ternary complex.

X-ray structure of IFNω (brown) in complex with IFNAR1–ECD (blue) and IFNAR2–ECD (green). The helices of IFNω are labelled with the letters A–E. The FNIII-like domains of IFNAR1 (SD) and IFNAR2 (D) are numbered starting from the N-terminus.

Consequently, though the two membrane-proximal domains of IFNAR1 and IFNAR2 are shown to be very close in EM images (Figure 1.7), there is still no high resolution structural evidence of contact between them as this interaction would be expected for other cytokine receptors. Based on the assumption of IFNAR1 SD1–SD2 homology to SD3–SD4 due to gene duplication, it was possible to model the orientation of SD4 with respect to the remaining complex (Figure 1.9 B). Overall, again, the binding mode of IFNAR1 is unique among cytokine-receptor interactions. The IFN ligand forms a broad interaction interface by binding to IFNAR1 at the hinge between SD2–SD3 such that the helical bundle is perpendicular to the receptor long axis, in contrast to other type I and II cytokine receptor systems, where the ligands interact with the loops in the "elbow" region of the receptor.

Comparison of the unbound receptor subunits with the bound forms in X-ray structures revealed a large movement in the receptor orientation and an outwards movement of IFN (Figure 1.9). When the unliganded IFNAR1ΔSD4 structure and IFNAR1ΔSD4 of the ternary complexes are superimposed, it becomes apparent that the N-terminal SD1 moves toward the ligand (Figure 1.9 A) and the SD2–SD3 portion of IFNAR1 shift relative to each other upon IFN binding, allowing all three subdomains of IFNAR1 to contact the ligand (Figure 1.9 B).

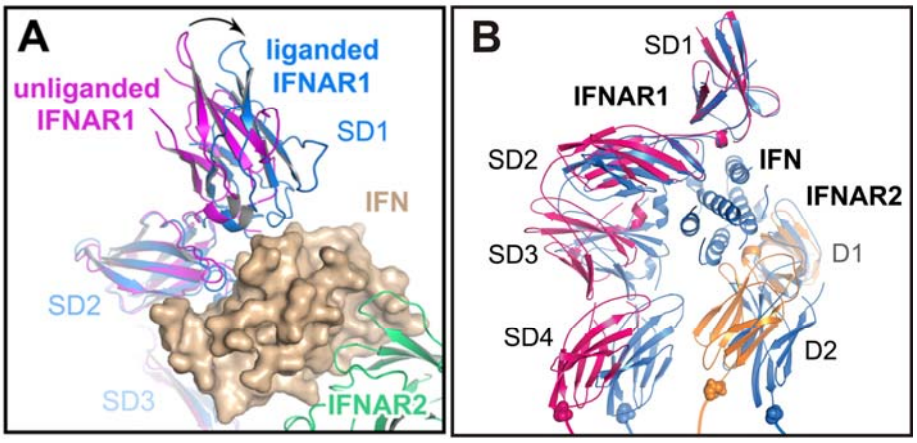

Figure 1.9 Ligand-induced conformational changes of IFNAR based on a comparison of unbound and bound structures.

A Domain movement in IFNAR1 upon IFN binding. Unliganded IFNAR1ΔSD4 (magenta) was superimposed onto subdomains 2 (SD2) and 3 (SD3) of IFNAR1 (blue) in the ternary complex. The difference in the position of the SD1 domain is depicted as an arrow. The ligand is shown in brown with its molecular surface. **B** Overlay of the unbound (magenta and yellow) and bound (blue) X-ray structures. SD4 of IFNAR1 was not visible in the X-ray structures and was modelled for clarity.

For cytokine receptors structural movements of receptor components upon ligand binding have previously been implicated to have an important role in signal propagation across the membrane. As described above, a mechanism that involves the transduction of a conformational change of a preformed extracellular receptor domain toward the intracellular domain and thus inducing signalling was suggested for IFNγ [27], growth hormone [14], erythropoietin [17, 65], thrombopoietin [66] as well as for some others [67]. In contrast, in the absence of ligand, the IFNα/β receptor does not form a preassembled dimer [53]. In addition, for some type I cytokine receptors (Figure 1.4) a ligand-induced conformational change in the membrane-proximal subdomains have previously been observed [24] suggesting their involvement in the activation of the receptor complex. So far there is no experimental evidence to correlate how the ligand-induced conformational change in the IFNα/β receptor ectodomain is fine-tuned to relay signals from different IFN subtypes through the membrane to evoke intracellular differential signalling responses. Since as it seen from the structural findings, all type I IFNs share the same receptor-binding mode and form ternary signalling complexes with highly similar architecture it is likely that differential recognition of IFNs by the receptor subunits IFNAR1 and IFNAR2 must be responsible for differential activity. Therefore a comprehensive picture of the energetics, dynamics and the conformational crosstalk of the IFN-receptor interactions is required.

1.2 Aim and objectives

This PhD project aims to establish techniques for exploring interactions and conformational changes involved in the formation of the type I IFN receptor complex *in vitro*. The assembly of IFN/IFNAR1/IFNAR2 complex represents a dynamic interaction of a three-body system. It may include not only the fine-tuned energetics of IFN recognition upon binding to two receptor ectodomains but receptor-receptor cross-talk or allosteric interaction as well as the conformational change accompanying the ternary complex assembly. Demonstrating these effects and uncovering molecular mechanisms behind them is challenging and requires site-specific modification of proteins for incorporation of fluorescent dyes in combination with approaches for tethering them to surfaces. Thus establishment of dedicated biochemical and biophysical techniques is the key prerequisites for elucidating a number of those biological questions.

For these purposes, the following objectives were followed:

1. Devising efficient strategies for site-specifically modifying IFNα2, IFNAR1 and IFNAR2 with fluorescent dyes, small probes and for stable tethering them to surfaces by means of enzymatic posttranslational modification of genetically encoded short peptide tags fused to the protein of interest. Exploring their activities, with respect to the interactions in binary and ternary complexes by *in vitro* solid phase binding studies using TIRFS/RIf detection. (Section 1).
2. Dissecting the energetics of the interferon/IFNAR1–EC binding interface by identifying the key receptor amino acid residues at the ligand binding interface, engaged in the interaction with various type I interferons, as well as the residues involved in stabilizing the conformation of the receptor and thus crucial for ligand binding. Exploring ligand binding site crosstalk, allosteric properties of the simultaneous IFNAR1-EC and IFNAR2-EC interaction with ligands and the role of membrane-proximal receptor subdomains in the stability of the ternary complex. (Section 3).
3. Stabilizing *in vitro* dual-colour labelled IFNα2/IFNAR1/IFNAR2 ternary complex for subsequent analysis by fluorescence cross-correlation spectroscopy (FCCS) and Förster resonance energy transfer (FRET). (Section 1).

1.3 Strategies

1.3.1 Genetically encoded peptide tags for posttranslational protein modifications

In the past decade, numerous chemical technologies have been developed to allow the site-specific post-translational modification of proteins. Traditionally covalent chemical protein modification has been accomplished by the attachment of synthetic groups to nucleophilic amino acids on protein surfaces. These chemistries, however, are rarely sufficiently selective to distinguish one residue due to the multiple copies of each amino acid residue within the protein that possess similar reactivity. Attempting to genetically replace redundant residues significantly affects protein stability or even obscures the production of the protein in a biologically active, homogenous form. One solution to this problem is to introduce a unique chemical handle into the target protein through a novel peptide sequence, which forms a biocompatible "tag" which is posttranslationally specifically modified to incorporate a probe of interest.

Among these tags, the interaction of oligohistidine peptide tag with multivalent chelator trisnitrilotriacetic acid (tris–NTA) has been recently shown as a powerful technique for site-specific posttranslational reversible labelling and surface anchoring of recombinant proteins [52, 68-71]. Fusion of proteins to a 6-10 histidine long peptide sequence was originally developed as a strategy for affinity chromatography. Transition metal ions such as Zn^{2+} or Ni^{2+} are reversibly immobilized by chelating agents such an iminodiacetic acid or nitrilotriacetic acid (NTA), thus maintaining 2 or 3 coordination sites free for histidines (Figure 1.10 A). This interaction can be very efficiently disrupted by competing coordinators such as imidazole, which selectively and rapidly remove the protein from the chelator under mild conditions. Synthesis of multivalent chelator head (MCH) groups, supramolecular entities with 2–4 NTA moieties incorporated onto branched and cyclic scaffolds significantly increased the stability of their multivalent interaction with oligohistidine tags [68]. Based on high association rate constants of tris–NTA (comprised of three NTA moieties) around 10^5 $M^{-1} \cdot s^{-1}$ and dissociation rate constants as low as $5 \times 10^{-5} \cdot s^{-1}$, subnanomolar affinities of such MCHs for hexa- or decahistidine-tagged proteins have been demonstrated. Since histidine is a relatively rare amino acid in native proteins, recombinantly expressed proteins fused to His-tags can be preferentially surface-immobilized on MCHs even in the presence of low concentration of a competitor or native proteins in the background (e.g. in expression supernatants). Thus the reversible tris-NTA/His-tag interaction is ideal for efficient

immobilization of oligohistidine-tagged proteins since surfaces can be completely regenerated for subsequent biding assays. By conjugation of tris–NTA with fluorescence dyes or biotin, the incorporation of these small molecule probes into His-tagged proteins is enabled in a remarkably selective site-specific manner (Figure 1.10 B) [68-70]. Employment of the vacant His-tags used for protein affinity purification and the simplicity of rapid *in situ* His/NTA coupling make this technique a suitable labelling tool for monitoring protein interactions *in vitro* and live cells. However the incorporation of transition metal ions into the labelled proteins upon labelling with tris-NTA leads to metal-ion mediated fluorescence quenching [69] which is inconvenient for some spectroscopic applications. Owing to the non-covalent nature of His/NTA interaction this labelling approach can suffer from gradual dissociation of spectroscopic probes at highly diluted working protein concentrations applied in some assays. In addition, this labelling technique is not fully orthogonal to the solid phase binding assays employing His tag-based protein tethering.

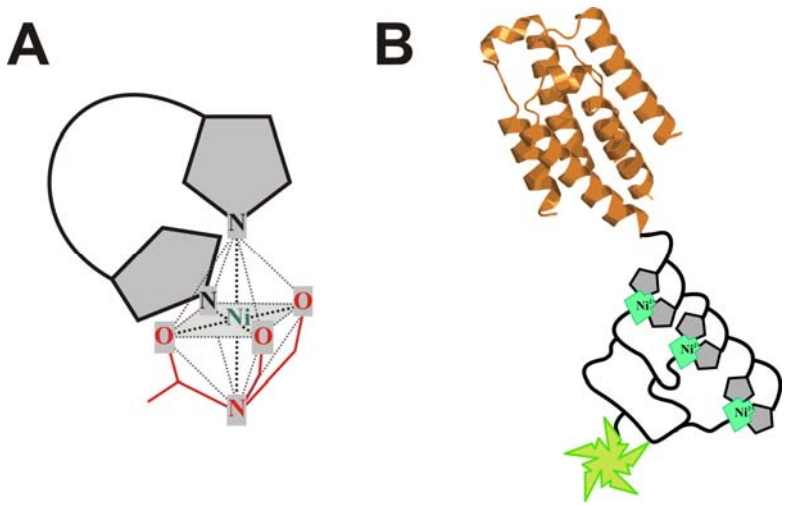

Figure 1.10 His-tag interaction with NTA moieties.

A One NTA molecule can occupy four coordination sites of Ni^{2+}, leaving two coordination sites vacant for histidines. **B** Schematic drawing of an *in situ* fluorescence probe incorporation into a protein via the multivalent interaction of tris–NTA/fluorophore conjugate with a histidine tag.

Incorporation of unnatural amino acids (UAAs) [72] has recently emerged as a generic technique to introduce translationally non-native functionality into proteins by engineering changes into the cellular protein translation pathways [73, 74]. For successful translation of a novel amino acid, the codon to which the unnatural amino acid is assigned cannot already code for one of the 20 natural amino acids. Usually a nonsense codon (stop codon, typically amber UAG) [75] or a four-base codon are used [76]. This approach requires devising a host organism with an orthogonal tRNA/aminoacyl-tRNA synthetase pair that specifically incorporates the UAA into the target protein in response to a nonsense codon. It allows UUAs

with diverse physicochemical and biological properties to be genetically encoded into different organisms such as bacteria [76], mammalian cells [77], *Saccharomyces cerevisiae* and *Pichia pastoris* [78], providing unprecedented opportunities for protein labelling. The label can be directly introduced or subsequently conjugated through the introduction of chemical functionalities not present on the canonical natural system. Extending this approach to a combination of site-specific labelling *via* an UAA and chemical labelling of a cysteine residue provides means for controlled site-specific orthogonal dual colour fluorescence labelling of a single protein for studying intramolecular FRET [79]. However currently this technique is limited to certain host organisms. Production of novel UAA-bearing target proteins such as interferon receptor subunit IFNAR1, which is an extracellular protein expressed in insect cells would require the time, effort and costs-consuming establishment of tRNA/aminoacyl-tRNA synthetase-orthogonal insect cell expression system.

A strategy, alternative to genetically encoded oligohistidine tags and unnatural amino acids, makes use of a recombinant peptide tag that is selectively and irreversibly modified by a reaction with the enzyme specific for the tag, transferring small molecules substrate analogues in a site-specific covalent fashion.

In this category of site-specific post-translational protein labelling, a number of peptide tags have been recently highlighted for modifying proteins with a variety of small synthetic molecules so that affinity, fluorescent, and photocrosslinking probes are posttranslationally attached as prosthetic groups to the proteins of interest to study their biological functions [80, 81]. However many current enzymatic methods often suffer drawbacks, such as high labelling background (tetracysteine tag) [82], deleterious *in vitro* labelling reaction conditions (AGT) [83], indirect protein labelling (biotin ligase BirA labelling with the use of streptavidin to attach the fluorophores in a second step [84], LplA acceptor peptide modifications require a secondary chemistry) [85], limited selection of the appropriately functionalized substrates (Q-tag) and the large size of the HaloTag protein (33 kDa) [86], AGT, SNAP and CLIP-tags (22 kDa) [87].

To overcome these limitations, phosphopantetheinyl transferases (PPTases) which catalyse the sequence-specific post-translational modification of different short PPT-tag peptide sequences derived from acyl (ACP) (Figure 1.11) or peptidyl carrier proteins (PCP) [88] have been implemented.

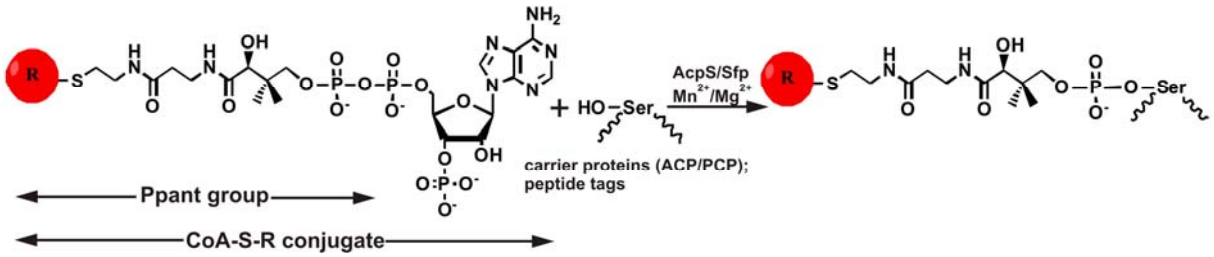

Figure 1.11 Phosphopantetheinylation reaction catalysed by PPTase.

Sfp- or AcpS-catalysed PCP, ACP, or peptide labelling reactions using small-molecule-CoA conjugates as the donor of the small-molecule-PPT group to a specific serine residue in PCP, ACP, or the peptide tags.

In nature, PPTase Sfp from *Bacillus subtilis* catalyses the posttranslational phosphopantetheinylation of the conserved serine residue of 8-10 kDa PCP domain from the biosynthetic machinery of the nonribosomal peptide synthetase [88]. Phage selection led to a significant reduction in size of peptide fragment recognized by Sfp from the native 80-100 residue PCP to an 11-residue fragment, a PPT-tag containing a conserved sequence around the serine side chain to be phosphopantetheinylated [89]. The identified 11-residue peptide termed ybbR-tag (DSLEFIASKLA) has the conserved DSL tripeptide sequence at the N terminus, matching the conserved sequence motif of a PCP, with the serine to which the 4'-phosphopantetheinyl (Ppant) moiety of coenzyme A (CoA) is transferred, resulting in a site-specific and covalent bond. The specific activity of the ybbR peptide tag ($k_{cat}/K_m \approx 1.4\times10^3$ $M^{-1}s^{-1}$) is similar to that of the full length PCP and has 30-fold higher Michaelis constant (K_m= 140 μM) compared to that of PCP [89]. However it was demonstrated that under mild physiological conditions in presence of Mn^{2+} or Mg^{2+} ions as co-factor, Sfp catalyses within half an hour the transfer of small molecule probes of divers structure attached to CoA (Figure 1.11) to the ybbR tag fused to a protein of interest, resulting in more than >80% of the protein being labelled, which makes it an attractive tool for site-specific fluorescence protein labelling using various CoA-fluorophore conjugates. Furthermore, ybbR- tag has been shown to be recognized by Sfp for labelling when fused to the N- and C- termini of target proteins or even inserted in a flexible loop in the middle of a target protein [89].

In fact, N-terminal extensions of the DSL motif on the ybbR tag did not affect the activity of ybbR peptides as a substrate of Sfp, suggesting the N terminus of ybbR-tag plays a minor role for interaction with Sfp.

Unlike non-essential N-terminal tag extensions, ybbR peptide C-terminal ASKLA residues are crucial for substrate modification by Sfp. The importance of C-terminal sequence of the tag can be dictated by its unique tendency to form an α-helical motif [89]with the serine residue from the site of Ppant modification, placed at the N-terminal tip of the helical region.

When the ybbR-tag is fused to the C terminus of a protein, the α-helical motif of ybbR may facilitate binding between the tag and Sfp enzyme [89]. In contrast, when the ybbR-tag is at the protein N terminus, the presence of all ASKLA residues in the ybbR-tag might not be necessary, because the tag is followed by the N-terminal residues of the target proteins, which might facilitate α-helical formation of the N-terminal ybbR-tag to be recognized by Sfp.

Interestingly, in spite of the seemingly minor role of N-terminal tag extension, the additional glycine residue upstream of the shared Asp-Ser-Leu motif is conserved in native PCPs, which are specifically modified by PPTases with the same K_{cat}/K_m catalytic efficiency as the ybbR-tag, but require 30 fold less substrate concentration (Michaelis constant K_m ~about 4 μM). Moreover, this glycine residue is flanking the conserved serine in the S6-peptide (with the sequence GDSLSWLLRLLN), an alternative PPT-tag, which was obtained in addition to ybbR from the further phage selection as a highly efficient substrate for recognition by Sfp. The S-peptide panel has been generated in order to develop a pair of short tags with useful level of orthogonality for selective recognition by two distinct PPTases, the Sfp from *Bacillus subtilis* to post-translationally modify the S-tags, and the AcpS transferase of *Escherichia coli* origin modifying A-tags [90]. The S6-tag seems to be a better peptide tag than the primarily identified ybbR-tag with a 2.4-fold lower K_m and >2-fold higher specificity (K_{cat}/K_m). Yet, due to the presence of tryptophan residues in the S peptide sequence it was not employed for fluorescence protein labelling in the current project to avoid effects by photo-induced electron transfer quenching, which was observed for some dyes such as Oregon Green 488. Since for two peptides the adjacent glycine residue upstream of the phosphopantetheinylattion motif led to the higher substrate specificity, its addition for enhancement of ybbR-tag has to be further systematically explored. Whereas S6-tag might be still employed to enzymatically immobilize a tagged protein of interest to surfaces. Taking into account the comparatively low values of catalytic efficiency for these enzymatic reactions ($k_{cat}/K_m \approx 3.2\times10^3$ $M^{-1}s^{-1}$ in saturating CoA concentrations) and Michaelis constant for S6 K_m~50 μM, it will require less concentration of S6-tagged protein for achieving desired surface densities than for ybbR-tagged proteins.

The full length 11-residue ybbR-tag is small enough as the affinity tags employed for protein purification and can be efficiently phosphopantetheinylated when fused to either the amino or carboxy protein terminus [89, 90], making this approach highly attractive for the use with recombinant proteins. Moreover, Sfp enzyme retains high substrate promiscuity with respect to transferring small-molecule probes of very different structure conjugated to CoA so that biotin [89], fluorophores [89, 91], quantum dots [92] or any other maleimide-linked small probe can be custom-conjugated to CoA in a one-step reaction [93], further improving the

versatility of Sfp-catalysed protein labelling. Yet, originally implemented for site-specific labelling, this strategy has been since extended for covalent biocompatible surface immobilization of ybbR-tagged proteins to a variety of CoA-functionalized substrates [94, 95]. Thus, the ybbR-tag/CoA approach combines the advantages of small size of the peptide tags (11 residues) for the construction of protein fusions with the minimum disturbance to the target protein structure and biological function; and one-step protein labelling for the direct conjugation of small molecule probes of diverse structures to the tagged target protein; high efficiency and specificity of the labelling reaction that can be carried out on cell surfaces, in expression supernatants without prior purification of the protein of interest or *in situ* in a flow cell.

1.3.2 Combined optical surface sensitive detection by TIRFS/RIf

Whereas a number of routine spectroscopic techniques for monitoring protein–protein interactions in solution are established, quantitative characterization of proteins in multi component and dynamic complexes remains challenging and frequently requires application of special techniques for studying molecular interactions at interfaces in real time. Surface-sensitive optical techniques such as attenuated total reflectance infrared spectroscopy (ATR-IR) [96, 97] using evanescent wave generated at ATR crystal by infrared radiation, surface plasmon resonance (SPR) [98-100] which probes change in refractive index by generating evanescent field evoked by horizontal electromagnetic wave and reflectometric interference spectroscopy (RIfS) [101] provide highly quantitative information about surface density and orientation of bound molecules, conformation, interaction stoichiometry, affinity, address thermodynamics, kinetics of association and dissociation reactions and provide high sensitivity of detection in real time.

TIRFS/RIf experimental setup used in these studies combines label-free detection based on reflectance interferometry (RIf) and fluorescence technique using evanescent field excitation (total internal reflection fluorescence spectroscopy; TIRFS) .Thus it provides not only quantification of molecular interactions on a surface by change of optical thickness but also overcomes limitations given by measuring very low affinity interactions and discrimination between different surface-bound species using highly sensitive quantitative fluorescence detection with much lower concentration of labelled analyte.

Rif detection is a technique for label free-detection and quantification of molecular interactions on a surface [101]. It is based on an interference layer obtained by coating a glass substrate (n ~ 1.52) with a silica layer (d=300-500 nm, n ~ 1.45). Owing to the differences in refractive index between the glass substrate and the silica layer, as well as the silica layer and

the environment (n ~ 1.33 for buffer), a light beam is partially reflected at these interfaces (Figure 1.12 A). The reflected beams have different optical path lengths and therefore a phase difference is formed.

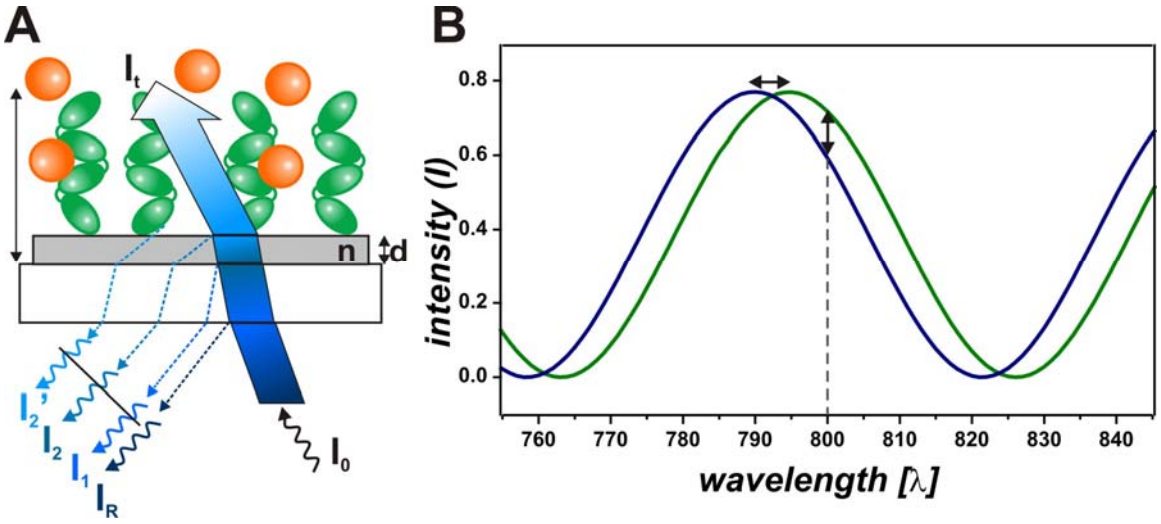

Figure 1.12 Principle of RIf detection.

A A glass chip with a thin silica layer (d) is illuminated with a white light beam that is partially reflected at each interface. n: refractive index, I: light intensity. **B** An interference pattern (intensity vs. wavelength) is obtained and detected at the fixed wavelength 800 nm, which changes (blue vs. green curve) upon binding of molecules to the silica layer.

Superposition of the two light beams leads to an interference pattern that depends on the phase shift between the two beams. At constant optical thickness ($n \cdot d$) of the interference layer, the reflected intensity as a function of the wavelength λ is modulated yielding an interference spectrum with maxima for constructive interference and minima for destructive interference. Changes in the optical thickness upon protein binding on the silica layer result in a shift of the interference spectrum, which can be probed by monitoring the position of an extremum or reflected intensity at a fixed wave length 800 nm in real time (Figure 1.12 B).

Therefore, by knowing the change in the interference pattern, the change in optical thickness ($n \cdot d$) as a result of surface binding can be calculated. Knowing the refractive index (n) of the molecule that is bound to the surface, the change in the thickness of the physical layer (d) upon binding can be ascertained. From this data, very quantitative information such as the molecular surface density of analytes can be inferred. RIf can measure surface binding in terms of mass/unit area (ng/mm^2) in real time with a sensitivity of ~ 0.02 ng/mm^2 (~ 6 x 10^{11} molecules/mm^2 for a 20 kDa protein) [102]. A change in surface loading by 1 pg/mm^2 leads to a shift of the interference minimum by 1.2 pm as determined by calibration experiments with radioactively labelled proteins [103].

RIf detection combined with fluorescence measurement [51] offers the ability to conduct highly sensitive quantitative analysis of surface binding. In order to make fluorescence analysis surface sensitive, a technique known as total internal reflection (TIRF) is used for illumination.

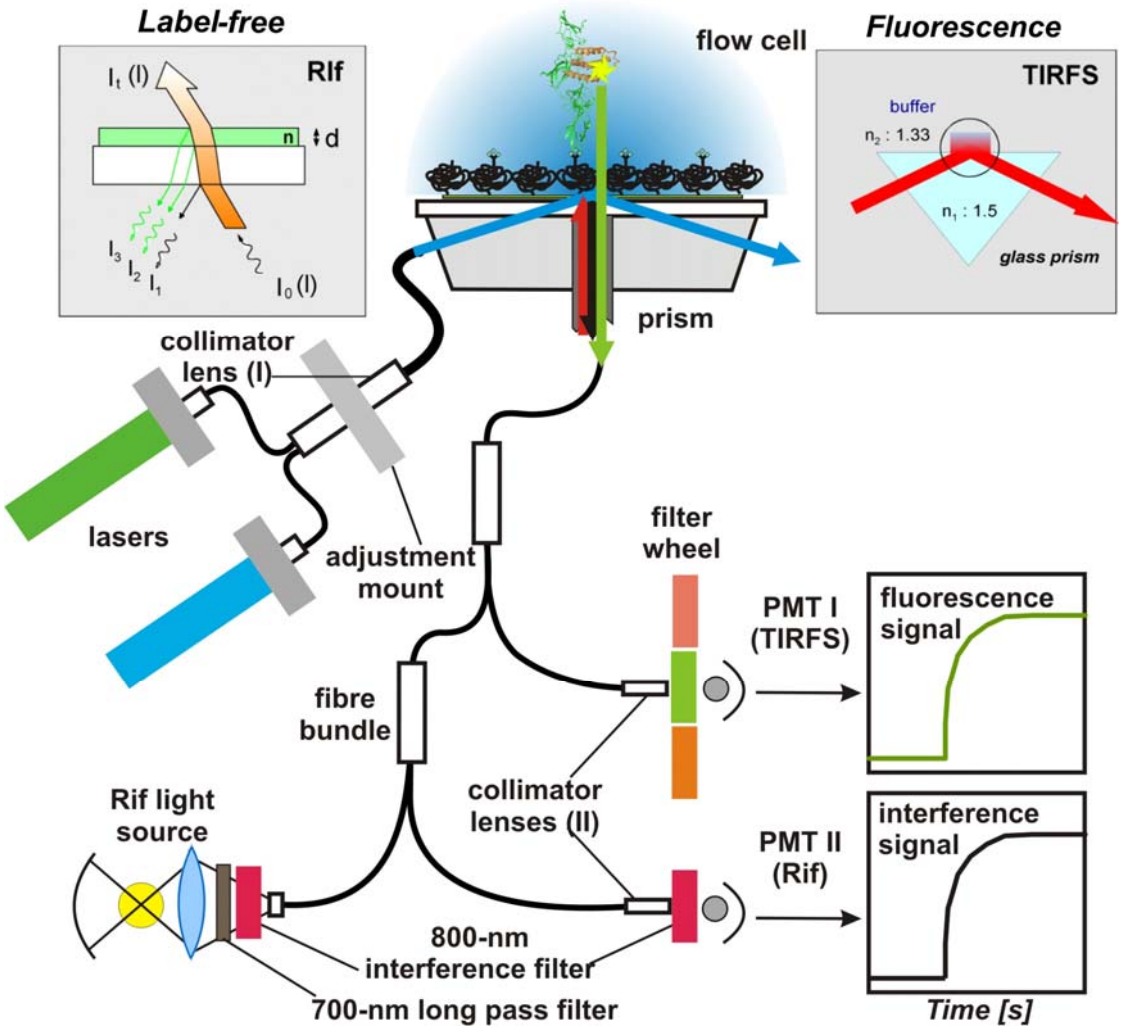

Figure 1.13 Schematic of the experimental setup for simultaneous TIRFS-Rif detection.

An excitation laser beam of a desired wavelength excites fluorescent species in a flow cell generating a TIRF signal which is detected by a photomultiplier (PMT I). Simultaneously a halogen lamp generates RIf signal, detected by the second photomultiplier (PMT II) at 800 nm; Modified from [52].

When light reaches the interface between two media, it is reflected and refracted. The incidence and refraction angles are related by Snell's law:

$$n_1 \cdot \sin\theta_1 = n_2 \cdot \sin\theta_2 \qquad \textbf{Equation 1.1}$$

Where n_1 and n_2 are refractive indices of the two media, θ_1 is the angle of incidence and θ_2 is the angle of refraction.

If the refractive index of the first medium is higher than that of the second ($n_1 > n_2$), then $\theta_1 < \theta_2$. The incidence angle when θ_2=90° is called the critical angle θ_c.

$$\theta_c = \sin^{-1} \cdot (n_2 / n_1)$$ **Equation 1.2**

If the angle of incidence is higher than θ_c, then the light is totally internally reflected and does not propagate into the second medium. However, some of the light still penetrates the medium of lower refractive index as an electromagnetic field called an 'evanescent wave'. A key characteristic of an evanescent wave is that it propagates parallel to the interface, vanishing exponentially with distance. The decay length (d_p) of the evanescent wave along the depth of field depends on the incident angle (θ), the wavelength of the excitation beam (λ) and the refractive indices of both media:

$$I_z = I_0 \exp(-z / d_p)$$ **Equation 1.3**

$$d_p = \frac{\lambda}{4\pi\sqrt{n_1^2 \cdot \sin^2 \theta - n_2^2}}$$ **Equation 1.4**

This means that using TIRF, only fluorophores that are very close (~100 nm) to the interface will be excited. Thus fluorescent species that are bound to the surface contribute to the major fluorescence, and unbound fluorophores in the background are not detected.
Detailed setup (Figure 1.13) description is provided in [52, 104].

1.3.3 Fluorescence cross-correlation spectroscopy

Fluorescence correlation spectroscopy (FCS) is as a single molecule technique, based on fluorescence intensity fluctuations, which arise from individual fluorophores diffusing in and out of a very small detection volume (Figure 1.14) [105]. It has a broad application in studying fluorescent biomolecules with intrinsic fluorescence properties like autofluorescent proteins or the ones with attached extrinsic fluorescent label. FCS allows quantitative determination of local concentrations, mobility constants and rate constants of intra- or intermolecular reactions and interactions *in vitro* and in live cells. In order to achieve optimum signal to noise levels, very low concentrations in the nanomolar regime are required in the observation volume. Less fluorophores result in more fluctuations, and more fluorophores result in smaller fluctuations and a more constant average signal. This makes method highly sensitive since only a few fluorophores are observed at one time in a minimized observation volume. Femtoliter volumes can be obtained with localized multiphoton excitation or by using confocal optics, where laser light is strongly focused by a high numerical aperture objective (N.A. > 0.9) into a diffraction limited spot with a beam waist of ~0.5 µm exciting only fluorophores in that region, and introduction of a pinhole blocks all light that does not originate from the focal plane.

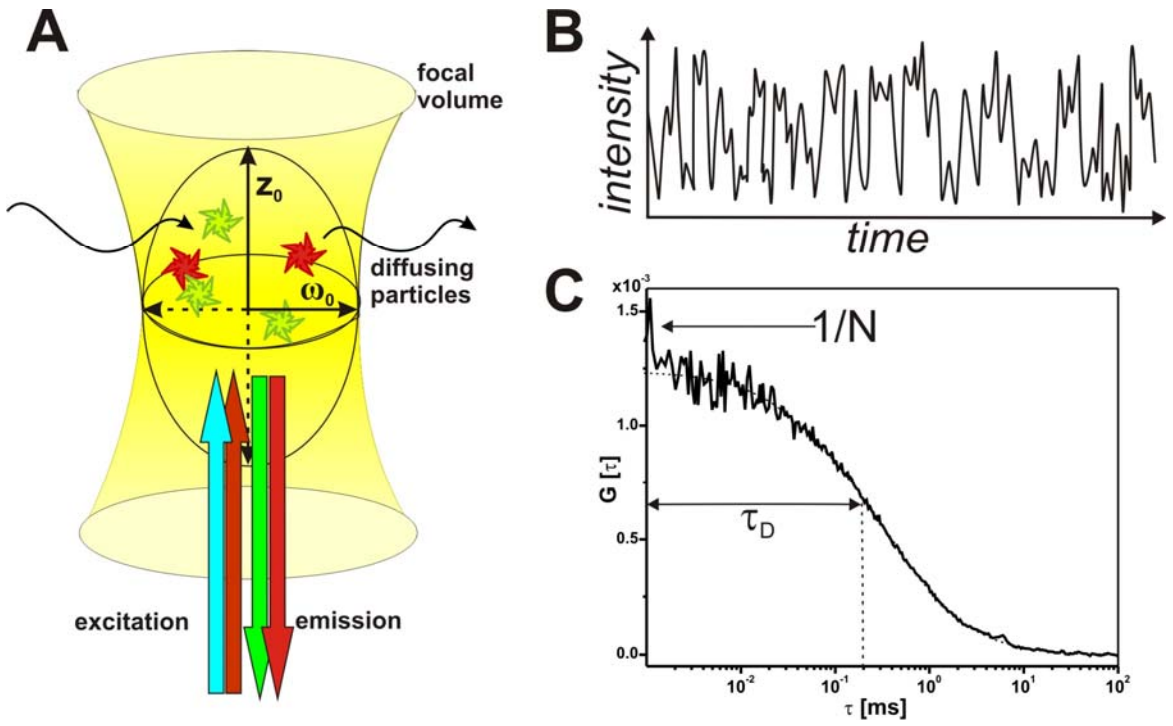

Figure 1.14 Schematic principle of FCS experiment.

A Fluorescent molecules passing a focused laser beam. **B** Fluorescence fluctuations are recorded over time as fluorescence intensity time trace, reflecting the statistical fluctuation of fluorophore distribution in the detection volume. **C** These fluctuations are collectively evaluated by an autocorrelation analysis and resulting autocorrelation curve produces the value of autocorrelation G(τ) at lag time τ. Lateral and vertical extensions of effective volume geometry are denoted as ω_0 and z_0 respectively, diffusion time as τ_D and inverse number of particles as 1/N.

The amplitude and speed of the fluctuations arising from molecules entering and leaving detection volume are used in autocorrelation analysis to calculate the correlation function (Figure 1.14). Autocorrelation analysis is a mathematical procedure to analyse the signal time series for self-similarity. If a molecule is detected at time *t*, it resembles the conditional probability of finding a molecule in the focal volume at a later time ($t + \tau$). This is expressed by the autocorrelation function $G(\tau)$ (Equation 1.5).

$$G(\tau) = \frac{\langle \delta F(t) \cdot \delta F(t+\tau) \rangle}{\langle F(t) \rangle^2} = \frac{\langle F(t) \cdot F(t+\tau) \rangle}{\langle F(t) \rangle^2} - 1 \qquad \textbf{Equation 1.5}$$

Where $\delta F(t)$ is the deviation of fluorescence signal fluctuations around the mean value from the temporal average of the signal $F(t)$, defined as $\delta F(t) = F(t) - \langle F(t) \rangle$ and $\langle ... \rangle$ is denomination of the mean value.

For a fluorescent molecule freely diffusing at thermal equilibrium in three-D a simple model of pure diffusion can be fitted (Equation 1.6).

$$G(\tau) = G(0) \cdot \left(1 + \frac{\tau}{\tau_D}\right)^{-1} \cdot \left(1 + \frac{1}{\kappa^2} \cdot \frac{\tau}{\tau_D}\right)^{-\frac{1}{2}}$$ **Equation 1.6**

Further analysis of autocorrelation function provides access to system parameters like diffusion time or molecule concentrations. Assuming that the signal intensity is proportional to the number of fluorophores in the volume, the correlation amplitude *G(0)* in the limit of time $\tau \rightarrow 0$ corresponds to the inverse average number of the particles *(N)* being observed in the focal volume $G(0) \sim 1/N$ (Equation 1.7).

$$G(0) = \frac{1}{N} = \frac{1}{C \cdot V_{eff}}$$ **Equation 1.7**

With correlation amplitude *G(0)*, *N* - average number and *c* – concentration of particles in observation volume V_{eff}.

If the size of the detection volume V_{eff} is known from a calibration measurement (Equation 1.8, Equation 1.9), information on the concentration *c* (Equation 1.10) and the diffusion coefficient, *D* (Equation 1.11), can be inferred from the autocorrelation curve.

$$\kappa = \frac{z_0}{\omega_0}$$ **Equation 1.8**

Where κ – eccentricity of the effective volume V_{eff}, described by the ratio of structural parameters z_0 to ω_0 - axial and - radial extensions of effective volume respectively (Equation 1.9).

$$V_{eff} = \pi^{\frac{3}{2}} \cdot \omega_0^2 \cdot z_0$$ **Equation 1.9**

$$c = \frac{N}{V_{eff} \cdot N_A}$$ **Equation 1.10**

Where *c* – concentration, N_A – Avogadro constant.

The diffusion time τ_D obtained from autocorrelation function fitting, represents the average time a molecule needs to pass the detection volume. It can be estimated for single component pure diffusion by the time τ at which the *G(0)* amplitude has decayed to half of its value (Figure 1.14 C) and it is related to the diffusion constant *D* by Equation 1.11.

$$D = \frac{\omega_0^2}{4 \cdot \tau_D}$$ **Equation 1.11**

Such parameters as hydrodynamic radius and approximate molecular weight of a diffusing particle can be calculated in further analysis as well.

Investigation of the interaction of molecules and their complexes with autocorrelation is ambiguous, because interactions can only be determined by a change in the diffusion time and diffusion coefficient. Two or more co-diffusing species can be efficiently separated if diffusion time differs at least by factor 1.6 and according to Stocks law for globular molecules, the mass of diffusing species must differ by a factor of 4. Dual-colour cross-correlation spectroscopy (FCCS) provides an elegant loophole, where two spectrally separated lasers are focused onto the same spot. Fluorescence from two spectrally different fluorophores diffusing through the effective volume is recorded in separate channels. The individual intensity traces are both auto- and cross-correlated. In the case that both fluorescent species co-diffuse within the focal volume, correlation between the spectral channels will be detected, which results in a positive cross-correlation.

The cross-correlation is calculated analogously (Equation 1.12) to the autocorrelation function [106].

$$G_X(\tau) = \frac{\left\langle \delta F_g(t) \cdot \delta F_r(t+\tau) \right\rangle}{\left\langle F_g(t) \right\rangle \cdot \left\langle F_r(t) \right\rangle} \qquad \textbf{Equation 1.12}$$

Where $F_g(t)$ and $F_r(t)$ denote fluorescence signal from two spectrally distinct (e.g. green and red) channels and G_X stands for the cross-correlation amplitude.

Free three-dimensional diffusion of cross-correlated species is fitted via Equation 1.13.

$$G_X(\tau) = G_X(0) \cdot \left(1 + \frac{\tau}{\tau_D}\right)^{-1} \cdot \left(1 + \frac{1}{\kappa_X^2} \cdot \frac{\tau}{\tau_D}\right)^{-\frac{1}{2}} \qquad \textbf{Equation 1.13}$$

An additional calibration and calculation (Equation 1.14) of the consensus effective volume $V_{eff,X}$ must be performed, since two different not perfectly overlapping volumes, caused by two different diffraction limited laser spots contribute to the geometry of cross-correlation effective volume.

$$V_{eff,X} = \pi^{\frac{3}{2}} \cdot \omega_g \cdot \omega_r \cdot \sqrt{z_g \cdot z_r} \qquad \textbf{Equation 1.14}$$

Where ω_g, ω_r, z_g, z_r, - radial and axial effective volume parameters of the green or red channel respectively.

Additional calculations must be performed for the structural parameters ω_X, z_X and κ_X of cross-correlation effective volume

$$\omega_{0,X} = \frac{\omega_{0,r} + \omega_{0,r}}{2} \qquad \textbf{Equation 1.15}$$

$$z_{0,X} = \frac{z_{0,g} + z_{0,r}}{2}$$ **Equation 1.16**

$$\kappa_X = \frac{z_{0,X}}{\omega_{0,X}}$$ **Equation 1.17**

Calculation of concentration for the cross-correlated species (Equation 1.18) takes into consideration the fitted and calculated autocorrelation parameters such as amplitude, effective volume and concentration .

$$c_x = \frac{G_{0,x} \cdot V_{eff,X} \cdot c_r}{G_{0,g} \cdot V_{eff,g}}$$ **Equation 1.18**

The percentage of double-labelled species in respect to the total amount of labelled species is given by the ratio of the cross-correlated amplitude $G_X(0)$ and the amplitude of the red species $G_r(0)$ (Equation 1.19).

$$\frac{G_X(0) \cdot V_{eff,X}}{G_g(0) \cdot V_{eff,g}} = \frac{c_X}{c_r}$$ **Equation 1.19**

In FCCS experiment possible spectral cross-talk can contribute to the increase of cross-correlation and thus concentration of doubly labelled species. It can be additionally filtered out by applying pulsed interleaved laser excitation and software-provided lifetime filters.

1.3.4 Förster resonance energy transfer

A common process which occurs in excited state of fluorescent species - is resonance energy transfer or in particular Förster resonance energy transfer (FRET). This process takes place whenever the emission spectrum of a fluorophore, called the donor (Figure 1.15), overlaps with the absorption spectrum of another molecule, called the acceptor. It is the radiationless transmission of an energy quantum from its site of absorption to the site of its utilization in the molecule, or system of molecules, via dipole-dipole interaction between chromophores, over distances considerably greater than interatomic, without conversion to thermal energy, and without the donor and acceptor coming into kinetic collision [107]. The extent of energy transfer is determined by the distance between the donor and acceptor, and the extent of spectral overlap which is characterized by an overlap integral J - the degree of overlap between the donor fluorescence emission spectrum and the acceptor absorption spectrum (Equation 1.20).

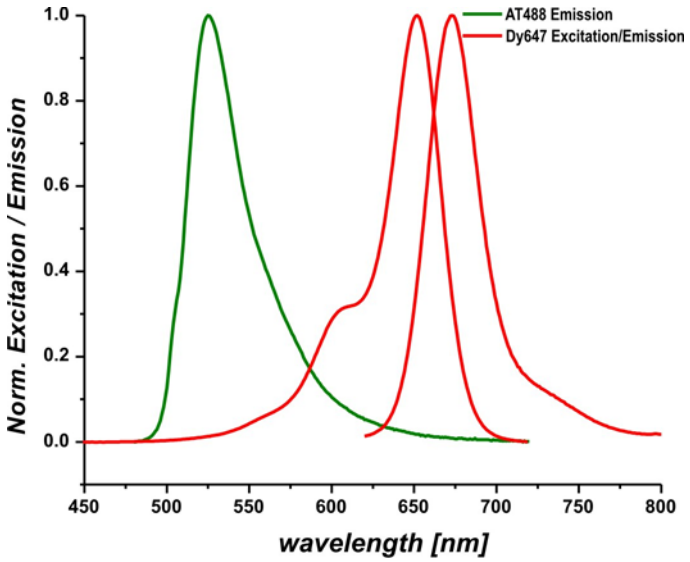

Figure 1.15 Emission and excitation spectra of the employed FRET pair.

Donor and acceptor spectral overlap. Normalized emission spectrum of ATTO-488 is shown in green, and excitation/emission spectra of DY-647 in red colour.

$$J = \int_0^\infty f_D(\lambda) \cdot \varepsilon_A(\lambda) \cdot \lambda^4 d\lambda$$ **Equation 1.20**

Where λ is the wavelength of the light, $\varepsilon_A(\lambda)$ is the molar extinction coefficient of the acceptor at that wavelength, and $f_D(\lambda)$ is the fluorescence spectrum of the donor normalised on the wavelength scale [107].

For convenience the spectral overlap is described in terms of the Förster distance (R_0). In our example Förster radius for ATTO-488 – Dy-647 FRET pair is about 5.1 nm. The rate of energy transfer $k_\tau(r)$ is given by Equation 1.21.

$$k_\tau(r) = \frac{1}{\tau_D} \cdot \left(\frac{R_0}{r}\right)^6$$ **Equation 1.21**

Where r is the distance between the donor (D) and the acceptor, and τ_D is the lifetime of the donor in the absence of energy transfer [108].The efficiency of energy transfer (E) for a single donor–acceptor pair at a fixed distance is proportional to the sixth power of the distance (Equation 1.22) and also can be calculated from donor fluorescence intensities in presence and absence of the acceptor (Equation 1.23).

$$E = \frac{R_0^6}{R_0^6 + r^6}$$ **Equation 1.22**

$$E = \frac{I_{DA}}{I_{DA} + I_D}$$ **Equation 1.23**

Where E is FRET efficiency, I_{DA} fluorescence intensity of donor molecule in presence of acceptor and I_D - intensity of the unaffected donor in absence of acceptor. FRET efficiency can also be determined using the lifetime of the donor in presence (τ_{DA}) and absence of the acceptor probe (τ_D) (Equation 1.24) or from the corresponding to these lifetimes total numbers of donor-emitted photons or the analogue intensity amplitudes A_i (Equation 1.25) [109].

$$E = 1 - \frac{\tau_{DA}}{\tau_D}$$ **Equation 1.24**

$$E = \frac{A_i}{\sum_i A_i}$$ **Equation 1.25**

There is a variety of approaches to design and observe FRET in experiment which depends on utilized chromospheres' properties, experimental objectives and used instrumentation for detection. One possibility includes measuring of sensitized fluorescence (emission) coming from fluorescence acceptor by excitation at a donor excitation wavelength. Another approach, the acceptor photobleaching method, is often used as a relatively straightforward approach for determining FRET. When FRET pairs are in close proximity, the donor energy is transferred to the acceptor molecule. Bleaching of the acceptor fluorophore eliminates the potential for the acceptor to participate in energy transfer and dequenches the donor resulting in an increase of donor emission. In similar approach the acceptor does not need to be fluorescent, but can be fluorescent as well. This type of FRET experiments deals with monitoring donor molecules only, quenched by resonance energy transfer to acceptor and resulting in lower donor emission intensity or presence of population with shorter lifetime. Depending on experimental setup one can either measure the fluorescence intensity or the lifetime of donor fluorophore in the absence or presence of quencher.

1.4 References

1. Ward, C., et al., *Structural insights into ligand-induced activation of the insulin receptor.* Acta physiologica, 2008. **192**(1): p. 3-9.

2. Teramura, Y., et al., *Single-molecule analysis of epidermal growth factor binding on the surface of living cells.* The EMBO journal, 2006. **25**(18): p. 4215-22.

3. Chung, I., et al., *Spatial control of EGF receptor activation by reversible dimerization on living cells.* Nature, 2010. **464**(7289): p. 783-7.

4. Moriki, T., H. Maruyama, and I.N. Maruyama, *Activation of preformed EGF receptor dimers by ligand-induced rotation of the transmembrane domain.* Journal of Molecular Biology, 2001. **311**(5): p. 1011-26.

5. Burgess, A.W., et al., *An open-and-shut case? Recent insights into the activation of EGF/ErbB receptors.* Molecular cell, 2003. **12**(3): p. 541-52.

6. Zhang, X., et al., *An allosteric mechanism for activation of the kinase domain of epidermal growth factor receptor.* Cell, 2006. **125**(6): p. 1137-49.

7. Jura, N., et al., *Mechanism for activation of the EGF receptor catalytic domain by the juxtamembrane segment.* Cell, 2009. **137**(7): p. 1293-307.

8. Jura, N., et al., *Catalytic control in the EGF receptor and its connection to general kinase regulatory mechanisms.* Molecular cell, 2011. **42**(1): p. 9-22.

9. Mendrola, J.M., et al., *The single transmembrane domains of ErbB receptors self-associate in cell membranes.* The Journal of biological chemistry, 2002. **277**(7): p. 4704-12.

10. Bocharov, E.V., et al., *Spatial structure of the dimeric transmembrane domain of the growth factor receptor ErbB2 presumably corresponding to the receptor active state.* The Journal of biological chemistry, 2008. **283**(11): p. 6950-6.

11. Mineev, K.S., et al., *Spatial structure of the transmembrane domain heterodimer of ErbB1 and ErbB2 receptor tyrosine kinases.* Journal of Molecular Biology, 2010. **400**(2): p. 231-43.

12. Coskun, U., et al., *Regulation of human EGF receptor by lipids.* Proceedings of the National Academy of Sciences of the United States of America, 2011. **108**(22): p. 9044-8.

13. Coskun, U. and K. Simons, *Cell membranes: the lipid perspective.* Structure, 2011. **19**(11): p. 1543-8.

14. Brown, R.J., et al., *Model for growth hormone receptor activation based on subunit rotation within a receptor dimer.* Nature structural & molecular biology, 2005. **12**(9): p. 814-21.

15. Thompson, K., et al., *Cerebral plasticity and recovery of function after childhood prefrontal cortex damage.* Developmental neurorehabilitation, 2009. **12**(5): p. 298-312.

16. Clackson, T., et al., *Structural and functional analysis of the 1:1 growth hormone:receptor complex reveals the molecular basis for receptor affinity.* Journal of Molecular Biology, 1998. **277**(5): p. 1111-28.

17. Seubert, N., et al., *Active and inactive orientations of the transmembrane and cytosolic domains of the erythropoietin receptor dimer.* Molecular cell, 2003. **12**(5): p. 1239-50.

18. Constantinescu, S.N., et al., *The erythropoietin receptor cytosolic juxtamembrane domain contains an essential, precisely oriented, hydrophobic motif.* Molecular cell, 2001. **7**(2): p. 377-85.

19. Livnah, O., et al., *Crystallographic evidence for preformed dimers of erythropoietin receptor before ligand activation.* Science, 1999. **283**(5404): p. 987-90.

20. Livnah, O., et al., *An antagonist peptide-EPO receptor complex suggests that receptor dimerization is not sufficient for activation.* Nature structural biology, 1998. **5**(11): p. 993-1004.

21. Constantinescu, S.N., et al., *Ligand-independent oligomerization of cell-surface erythropoietin receptor is mediated by the transmembrane domain.* Proceedings of the National Academy of Sciences of the United States of America, 2001. **98**(8): p. 4379-84.

22. Kubatzky, K.F., et al., *Self assembly of the transmembrane domain promotes signal transduction through the erythropoietin receptor.* Current biology : CB, 2001. **11**(2): p. 110-5.

23. Lupardus, P.J., et al., *Structural snapshots of full-length Jak1, a transmembrane gp130/IL-6/IL-6Ralpha cytokine receptor complex, and the receptor-Jak1 holocomplex.* Structure, 2011. **19**(1): p. 45-55.

24. Xu, Y., et al., *Crystal structure of the entire ectodomain of gp130: insights into the molecular assembly of the tall cytokine receptor complexes.* The Journal of biological chemistry, 2010. **285**(28): p. 21214-8.

25. Boulanger, M.J., et al., *Hexameric structure and assembly of the interleukin-6/IL-6 alpha-receptor/gp130 complex.* Science, 2003. **300**(5628): p. 2101-4.

26. Krause, C.D. and S. Pestka, *Historical developments in the research of interferon receptors.* Cytokine & growth factor reviews, 2007. **18**(5–6): p. 473-482.

27. Krause, C.D., et al., *Preassembly and ligand-induced restructuring of the chains of the IFN-gamma receptor complex: the roles of Jak kinases, Stat1 and the receptor chains.* Cell research, 2006. **16**(1): p. 55-69.

28. Isaacs, A. and J. Lindenmann, *Virus Interference. I. The interferon.* Proc. Roy. Soc. Lond. Ser. B, 1957. **147**: p. 258-276.

29. Gresser, I. and F. Belardelli, *Endogenous type I interferons as a defense against tumors.* Cytokine & growth factor reviews, 2002. **13**(2): p. 111-8.

30. Santini, S.M., et al., *The natural alliance between type I interferon and dendritic cells and its role in linking innate and adaptive immunity.* Journal of interferon & cytokine research : the official journal of the International Society for Interferon and Cytokine Research, 2002. **22**(11): p. 1071-80.

31. Borden, E.C., et al., *Interferons at age 50: past, current and future impact on biomedicine.* Nature reviews. Drug discovery, 2007. **6**(12): p. 975-90.

32. Uze, G., et al., *The receptor of the type I interferon family.* Current topics in microbiology and immunology, 2007. **316**: p. 71-95.

33. Pestka, S., C.D. Krause, and M.R. Walter, *Interferons, interferon-like cytokines, and their receptors.* Immunological reviews, 2004. **202**: p. 8-32.

34. Pestka, S., *The interferons: 50 years after their discovery, there is much more to learn.* The Journal of biological chemistry, 2007. **282**(28): p. 20047-51.

35. Schindler, C. and C. Plumlee, *Inteferons pen the JAK-STAT pathway.* Seminars in cell & developmental biology, 2008. **19**(4): p. 311-8.

36. van Boxel-Dezaire, A.H., M.R. Rani, and G.R. Stark, *Complex modulation of cell type-specific signaling in response to type I interferons.* Immunity, 2006. **25**(3): p. 361-72.

37. Nguyen, V.P., et al., *Stat2 binding to the interferon-alpha receptor 2 subunit is not required for interferon-alpha signaling.* The Journal of biological chemistry, 2002. **277**(12): p. 9713-21.

38. Li, X., et al., *Functional subdomains of STAT2 required for preassociation with the alpha interferon receptor and for signaling.* Molecular and cellular biology, 1997. **17**(4): p. 2048-56.

39. Yang, C.H., et al., *Interferon alpha /beta promotes cell survival by activating nuclear factor kappa B through phosphatidylinositol 3-kinase and Akt.* The Journal of biological chemistry, 2001. **276**(17): p. 13756-61.

40. Kaur, S., S. Uddin, and L.C. Platanias, *The PI3' kinase pathway in interferon signaling.* Journal of interferon & cytokine research : the official journal of the International Society for Interferon and Cytokine Research, 2005. **25**(12): p. 780-7.

41. Katsoulidis, E., et al., *The p38 mitogen-activated protein kinase pathway in interferon signal transduction.* Journal of interferon & cytokine research : the official journal of the International Society for Interferon and Cytokine Research, 2005. **25**(12): p. 749-56.

42. Platanias, L.C., *Mechanisms of type-I- and type-II-interferon-mediated signalling.* Nature reviews. Immunology, 2005. **5**(5): p. 375-86.

43. Grumbach, I.M., et al., *Activation of the Jak-Stat pathway in cells that exhibit selective sensitivity to the antiviral effects of IFN-beta compared with IFN-alpha.* Journal of

interferon & cytokine research : the official journal of the International Society for Interferon and Cytokine Research, 1999. **19**(7): p. 797-801.

44. Rosenblum, M.G., et al., *Growth inhibitory effects of interferon-beta but not interferon-alpha on human glioma cells: correlation of receptor binding, 2',5'-oligoadenylate synthetase and protein kinase activity.* Journal of interferon research, 1990. **10**(2): p. 141-51.

45. Kalie, E., et al., *An interferon alpha2 mutant optimized by phage display for IFNAR1 binding confers specifically enhanced antitumor activities.* The Journal of biological chemistry, 2007. **282**(15): p. 11602-11.

46. Kalie, E., et al., *The stability of the ternary interferon-receptor complex rather than the affinity to the individual subunits dictates differential biological activities.* The Journal of biological chemistry, 2008. **283**(47): p. 32925-36.

47. Levin, D., D. Harari, and G. Schreiber, *Stochastic receptor expression determines cell fate upon interferon treatment.* Molecular and cellular biology, 2011. **31**(16): p. 3252-66.

48. Mogensen, K.E., et al., *The type I interferon receptor: structure, function, and evolution of a family business.* Journal of interferon & cytokine research : the official journal of the International Society for Interferon and Cytokine Research, 1999. **19**(10): p. 1069-98.

49. Lavoie, T.B., et al., *Binding and activity of all human alpha interferon subtypes.* Cytokine, 2011. **56**(2): p. 282-9.

50. Jaks, E., et al., *Differential receptor subunit affinities of type I interferons govern differential signal activation.* Journal of molecular biology, 2007. **366**(2): p. 525-39.

51. Lamken, P., et al., *Ligand-induced assembling of the type I interferon receptor on supported lipid bilayers.* Journal of molecular biology, 2004. **341**(1): p. 303-18.

52. Gavutis, M., S. Lata, and J. Piehler, *Probing 2-dimensional protein-protein interactions on model membranes.* Nature protocols, 2006. **1**(4): p. 2091-103.

53. Cohen, B., et al., *Ligand-induced association of the type I interferon receptor components.* Molecular and cellular biology, 1995. **15**(8): p. 4208-14.

54. Jaitin, D.A., et al., *Inquiring into the differential action of interferons (IFNs): an IFN-alpha2 mutant with enhanced affinity to IFNAR1 is functionally similar to IFN-beta.* Molecular and cellular biology, 2006. **26**(5): p. 1888-97.

55. Slutzki, M., et al., *Variations in the unstructured C-terminal tail of interferons contribute to differential receptor binding and biological activity.* Journal of molecular biology, 2006. **360**(5): p. 1019-30.

56. Li, Z., et al., *The EM structure of a type I interferon-receptor complex reveals a novel mechanism for cytokine signaling.* Journal of molecular biology, 2008. **377**(3): p. 715-24.

57. Kotenko, S.V. and J.A. Langer, *Full house: 12 receptors for 27 cytokines.* International immunopharmacology, 2004. **4**(5): p. 593-608.

58. Novick, D., B. Cohen, and M. Rubinstein, *The human interferon alpha/beta receptor: characterization and molecular cloning.* Cell, 1994. **77**(3): p. 391-400.

59. Uze, G., G. Lutfalla, and I. Gresser, *Genetic transfer of a functional human interferon alpha receptor into mouse cells: cloning and expression of its cDNA.* Cell, 1990. **60**(2): p. 225-34.

60. Radhakrishnan, R., et al., *Zinc mediated dimer of human interferon-alpha 2b revealed by X-ray crystallography.* Structure, 1996. **4**(12): p. 1453-63.

61. Chill, J.H., et al., *The human type I interferon receptor: NMR structure reveals the molecular basis of ligand binding.* Structure, 2003. **11**(7): p. 791-802.

62. Thomas, C., et al., *Structural linkage between ligand discrimination and receptor activation by type I interferons.* Cell, 2011. **146**(4): p. 621-32.

63. Quadt-Akabayov, S.R., et al., *Determination of the human type I interferon receptor binding site on human interferon-alpha2 by cross saturation and an NMR-based model of the complex.* Protein science : a publication of the Protein Society, 2006. **15**(11): p. 2656-68.

64. Lamken, P., et al., *Functional cartography of the ectodomain of the type I interferon receptor subunit ifnar1.* Journal of molecular biology, 2005. **350**(3): p. 476-88.

65. Kubatzky, K.F., et al., *Structural requirements of the extracellular to transmembrane domain junction for erythropoietin receptor function.* The Journal of biological chemistry, 2005. **280**(15): p. 14844-54.

66. Staerk, J., et al., *Orientation-specific signalling by thrombopoietin receptor dimers.* The EMBO journal, 2011. **30**(21): p. 4398-413.

67. Lopez, A.F., et al., *Molecular basis of cytokine receptor activation.* IUBMB life, 2010. **62**(7): p. 509-18.

68. Lata, S., et al., *High-affinity adaptors for switchable recognition of histidine-tagged proteins.* Journal of the American Chemical Society, 2005. **127**(29): p. 10205-15.

69. Lata, S., et al., *Specific and stable fluorescence labeling of histidine-tagged proteins for dissecting multi-protein complex formation.* Journal of the American Chemical Society, 2006. **128**(7): p. 2365-72.

70. Reichel, A., et al., *Noncovalent, site-specific biotinylation of histidine-tagged proteins.* Analytical chemistry, 2007. **79**(22): p. 8590-600.

71. Lata, S. and J. Piehler, *Stable and functional immobilization of histidine-tagged proteins via multivalent chelator headgroups on a molecular poly(ethylene glycol) brush.* Analytical chemistry, 2005. **77**(4): p. 1096-105.

72. Minnihan, E.C., K. Yokoyama, and J. Stubbe, *Unnatural amino acids: better than the real things?* F1000 biology reports, 2009. **1**: p. 88.

73. Liu, W., et al., *Genetic incorporation of unnatural amino acids into proteins in mammalian cells.* Nat Meth, 2007. **4**(3): p. 239-244.

74. Liu, C.C. and P.G. Schultz, *Adding new chemistries to the genetic code.* Annual review of biochemistry, 2010. **79**: p. 413-44.

75. Wang, L., et al., *A New Functional Suppressor tRNA/Aminoacyl−tRNA Synthetase Pair for the in Vivo Incorporation of Unnatural Amino Acids into Proteins.* Journal of the American Chemical Society, 2000. **122**(20): p. 5010-5011.

76. Wang, L., et al., *Expanding the genetic code of Escherichia coli.* Science, 2001. **292**(5516): p. 498-500.

77. Liu, W., et al., *Genetic incorporation of unnatural amino acids into proteins in mammalian cells.* Nature methods, 2007. **4**(3): p. 239-44.

78. Young, T.S., et al., *Expanding the genetic repertoire of the methylotrophic yeast Pichia pastoris.* Biochemistry, 2009. **48**(12): p. 2643-53.

79. Brustad, E.M., et al., *A general and efficient method for the site-specific dual-labeling of proteins for single molecule fluorescence resonance energy transfer.* Journal of the American Chemical Society, 2008. **130**(52): p. 17664-5.

80. Hahn, M.E. and T.W. Muir, *Manipulating proteins with chemistry: a cross-section of chemical biology.* Trends in biochemical sciences, 2005. **30**(1): p. 26-34.

81. Rabuka, D., *Chemoenzymatic methods for site-specific protein modification.* Current opinion in chemical biology, 2010. **14**(6): p. 790-6.

82. Adams, S.R., et al., *New biarsenical ligands and tetracysteine motifs for protein labeling in vitro and in vivo: synthesis and biological applications.* Journal of the American Chemical Society, 2002. **124**(21): p. 6063-76.

83. Keppler, A., et al., *A general method for the covalent labeling of fusion proteins with small molecules in vivo.* Nature biotechnology, 2003. **21**(1): p. 86-9.

84. Chen, I., et al., *Site-specific labeling of cell surface proteins with biophysical probes using biotin ligase.* Nature methods, 2005. **2**(2): p. 99-104.

85. Fernandez-Suarez, M., et al., *Redirecting lipoic acid ligase for cell surface protein labeling with small-molecule probes.* Nature biotechnology, 2007. **25**(12): p. 1483-7.

86. Los, G.V., et al., *HaloTag: a novel protein labeling technology for cell imaging and protein analysis.* ACS chemical biology, 2008. **3**(6): p. 373-82.

87. Gautier, A., et al., *An engineered protein tag for multiprotein labeling in living cells.* Chemistry & biology, 2008. **15**(2): p. 128-36.

88. Reuter, K., et al., *Crystal structure of the surfactin synthetase-activating enzyme sfp: a prototype of the 4'-phosphopantetheinyl transferase superfamily.* The EMBO journal, 1999. **18**(23): p. 6823-31.

89. Yin, J., et al., *Genetically encoded short peptide tag for versatile protein labeling by Sfp phosphopantetheinyl transferase.* Proceedings of the National Academy of Sciences of the United States of America, 2005. **102**(44): p. 15815-20.

90. Zhou, Z., et al., *Genetically encoded short peptide tags for orthogonal protein labeling by Sfp and AcpS phosphopantetheinyl transferases.* ACS chemical biology, 2007. **2**(5): p. 337-46.

91. Zhou, Z., et al., *An eight residue fragment of an acyl carrier protein suffices for post-translational introduction of fluorescent pantetheinyl arms in protein modification in vitro and in vivo.* Journal of the American Chemical Society, 2008. **130**(30): p. 9925-30.

92. Sunbul, M., et al., *Enzyme catalyzed site-specific protein labeling and cell imaging with quantum dots.* Chemical communications, 2008(45): p. 5927-9.

93. Yin, J., et al., *Site-specific protein labeling by Sfp phosphopantetheinyl transferase.* Nature protocols, 2006. **1**(1): p. 280-5.

94. Wong, L.S., J. Thirlway, and J. Micklefield, *Direct site-selective covalent protein immobilization catalyzed by a phosphopantetheinyl transferase.* Journal of the American Chemical Society, 2008. **130**(37): p. 12456-64.

95. Waichman, S., et al., *Functional immobilization and patterning of proteins by an enzymatic transfer reaction.* Analytical chemistry, 2010. **82**(4): p. 1478-85.

96. Martin, I., E. Goormaghtigh, and J.M. Ruysschaert, *Attenuated total reflection IR spectroscopy as a tool to investigate the orientation and tertiary structure changes in fusion proteins.* Biochimica et biophysica acta, 2003. **1614**(1): p. 97-103.

97. Blum, M.M. and H. John, *Historical perspective and modern applications of Attenuated Total Reflectance-Fourier Transform Infrared Spectroscopy (ATR-FTIR).* Drug testing and analysis, 2012. **4**(3-4): p. 298-302.

98. de Mol, N.J., *Surface plasmon resonance for proteomics.* Methods in molecular biology, 2012. **800**: p. 33-53.

99. Homola, J., *Surface plasmon resonance sensors for detection of chemical and biological species.* Chemical reviews, 2008. **108**(2): p. 462-93.

100. Cooper, M.A., *Optical biosensors in drug discovery.* Nature reviews. Drug discovery, 2002. **1**(7): p. 515-28.

101. Proll, G., et al., *Reflectometric interference spectroscopy.* Methods in molecular biology, 2009. **503**: p. 167-78.

102. Piehler, J. and G. Schreiber, *Fast transient cytokine-receptor interactions monitored in real time by reflectometric interference spectroscopy.* Analytical biochemistry, 2001. **289**(2): p. 173-86.

103. Hanel, C. and G. Gauglitz, *Comparison of reflectometric interference spectroscopy with other instruments for label-free optical detection.* Analytical and bioanalytical chemistry, 2002. **372**(1): p. 91-100.

104. Gavutis, M., et al., *Lateral ligand-receptor interactions on membranes probed by simultaneous fluorescence-interference detection.* Biophysical journal, 2005. **88**(6): p. 4289-302.

105. Weidemann, T. and P. Schwille, *Fluorescence Correlation Spectroscopy in Living Cells*, in *Handbook of Single-Molecule Biophysics*, P. Hinterdorfer and A. Oijen, Editors. 2009, Springer US. p. 217-241.

106. Mütze, J., T. Ohrt, and P. Schwille, *Fluorescence correlation spectroscopy in vivo.* Laser & Photonics Reviews, 2011. **5**(1): p. 52-67.

107. van der Meer, B.W., G. Coker, and S.Y.S. Chen, *Resonance energy transfer: theory and data* 1994: VCH.

108. Lakowicz, J.R., *Principles of Fluorescence Spectroscopy* 2006: Springer.

109. Clegg, R.M., *Chapter 1 Förster resonance energy transfer—FRET what is it, why do it, and how it's done*, in *Laboratory Techniques in Biochemistry and Molecular Biology*, T.W.J. Gadella, Editor 2009, Elsevier. p. 1-57.

2 Covalent protein labelling and surface attachment by enzymatic transfer reaction

2.1 Introduction

Functional protein site-specific modification for in vitro studies is the key prerequisite in producing biologically active material for the studies of protein-protein interactions. For these purposes, simple and generic techniques for biocompatible protein surface tethering and functional attachment of affinity or fluorescent probe to any protein of interest are demanded.

To our experience, fluorescence labelling of type I interferon receptor as well as the different IFNs represents a major challenge. Moreover, no means for the tag-mediated vital surface immobilization of IFNα2 have been implemented so far.

Both, for fluorescence spectroscopy and for further single molecule studies, site-specific covalent modification of the IFN ligand is required. IFNα2-S136C has been used for site-specific attachment of fluorophores and biotin. The challenge in the labelling of IFNα2 proteins by thiol-reactive probes lays in the fact that the interferon polypeptide structure includes two cysteine bridges, one assumed to be a non-essential and connecting Cys1 and Cys98 residue , and the second one, essential, spanning between Cys29 and Cys138 (Figure 2.1) [1]. The disulfide bridges do not properly form with *in vitro* oxidized IFNα2, yielding two differently oxidized subpopulations of interferon. Introduction of the additional cysteine S136C for labelling [2] resulted in poor fraction of the correctly folded protein, and further decreased the yields of single-labelled IFNα2. Moreover, FRET or single molecule studies application of the multiple-labelled species that are produced as a result of non-unique free cysteine reactivity in cysteine-specific labelling, is highly biased. Strikingly, even lower yields have been obtained for mutants IFNα2 such as HEQ and YNS (Figure 2.1 A), which have an increased (~60 fold) affinity towards IFNAR1. These mutants are particularly important for single molecule studies by surface-sensitive detection, super resolution fluorescence microscopy and FCCS. Thus, improved ways for IFN labelling are required as an alternative for cysteine-based chemistry.

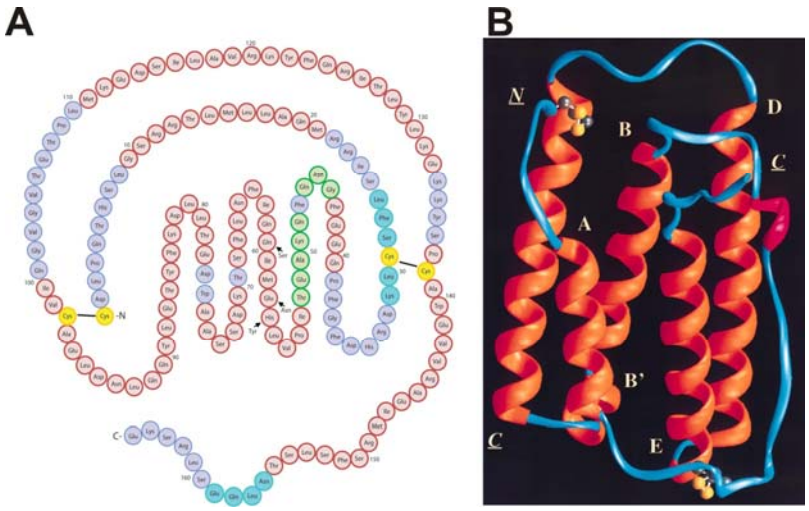

Figure 2.1 Schematic representation of IFNα2-YNS primary structure and IFNα2a NMR ribbon model indicating positions of the disulfide bonds.

A IFNα2-YNS primary structure; colour-coding depicts participation of different sequence regions in helices and loops. Mutation positions encoding for Y, N and S are marked by arrowheads. Disulfide bonds are shown by the cysteines marked as yellow circles connected by black lines. **B** Ribbon display of IFNα2a based on the resolved NMR structure [1]. The α-helices (in orange) are marked with labels A to E close to their N-terminal end. The two disulfide bridges are shown in a ball-and-stick representation with the sulphur atoms in yellow, and the carbon atoms in grey.

The extracellular receptor subunit IFNAR2 with the two fibronectin III (FNIII)-like domain organization contains six internal cysteine residues and is typically produced in a recombinant form as a partly oxidized in *E. coli* and *in vitro* product. Numerous spectroscopic applications require correctly folded IFNAR2-EC labelled material with a single fluorescence reporter. IFNAR2-EC residues S35C, S129C and T169C, far from the contact interface with IFNs have been mutated previously to employ cysteine-based chemistry for FRET analysis by TIRFS/RIf solid phase detection [3] and for distance-dependent quenching in cuvette fluorescence assays [4]. Notably, the same challenges as for IFNαs labelling have been met with the maleimide-based IFNAR2 modifications, resulting in the formation of multiple-labelled species, a fraction of misfolded protein and insufficient degree of labelling. The production of the cysteine mutants in the insect cell expression system can partially resolve these issues however greatly increases costs and time consumption. Thus, introduction of a technique to produce active fluorescence-labelled IFNAR2-EC material is of pivotal interest for the fluorescence spectroscopic studies of the IFN receptor. In particular, tag-specific labelling through phosphopantetheinyl transferases provides promising means for the covalent site-directed one-step modification of both, IFNα2 and IFNAR2 and is explored in the course of this study.

The low affinity extracellular receptor subunit IFNAR1 is the primary protein of interest for introducing the functional site-directed modifications. It is a multi-domain, heavily glycosylated protein comprised of four FN-III-like sub-domains. Insect cell expression system was found to be required for proper IFNAR1 folding and oxidation of the eight internal cysteine residues. These cysteines are essential for structure maintenance and neither can be mutated, nor would tolerate the deleterious reducing conditions for the thiol-reactive chemistry labelling approach through introduction of an additional exposed cysteine. Hence, for the IFNAR1-EC labelling with fluorescence maleimide-probes, several residue positions have been experimentally determined [5] to withstand the mild reducing conditions and modifications with fluorophores. Remarkably, the position N23C on the N-terminal IFNAR1 SD1 has been functionally labelled with various fluorescence thiol-reactive probes of a wide spectral range and structure [4, 5]. Successful labelling of the cysteine residues S147C, N286C and N349C placed on the IFNAR1 SD2-4 has been previously achieved mainly with the dyes of a green spectral range (OG488, AT488 and AF488) [5]. Thereby in that study the ligand-induced conformational change propagation from the membrane distal to the membrane proximal subdomain of IFNAR1-EC has been mapped by site-specific covalent incorporation of green fluorescence-donor probes into different IFNAR1 subdomains [4, 5], efficiently quenched in a distant-dependent manner by the tris-NTA-acceptor conjugates reversibly bound to C-terminal His-tags. Nevertheless for exploring the IFNAR1 conformational dynamics upon ligand binding by FCCS and FRET the covalent dual-colour label attachment to different protein domains is required. It would enable simultaneous monitoring of donor and acceptor fluorescence fluctuations at single molecule concentrations over longer time in comparison to the proteins labelled by the noncovalent, reversible approach such as tris-NTA conjugates. Yet a convenient method for IFNAR1 single-labelling with a selection of fluorophores is in great demand for the general application in surface-sensitive fluorescence assays or dual-colour spectroscopic investigation of ligand-receptor binary and ternary complex architecture, dynamics and distance dependencies. For these purposes, recombinant PPT short peptide tags for enzymatic posttranslational modification can be employed, which enable site-specific incorporation of a fluorescent probe or the controlled dual-colour labelling, orthogonal to the cysteine-specific chemistry, as well as the covalent protein immobilization on surfaces.

To this end, in this section several steps were followed. At first, we wanted to thoroughly explore the methodology of PPTase-catalysed probe incorporation through the short peptide tags fused to proteins of interest, employed in spectroscopic assays in the subsequent sections.

Then, in the course of this section we wanted to characterize the functionality of the labelled proteins through assessment of their binding kinetics in conventional surface assays with reversible protein tethering through their His-tags. Next, the generic approach for the ybbR tag-mediated protein enzymatic immobilization onto CoA-functionalized supports is to be discussed. At last, in this section we aspired to introduce a solid phase binding assay for direct selective surface protein capturing from cell expression supernatants and for rapid assessment of interaction kinetics and affinities of various type I IFNs in label-free and fluorescence binding assays.

2.2 Materials and methods

2.2.1 Materials

Insect cell expression medium Sf-900™ II SFM, penicillin/streptomycin and Pluronic® solutions were purchased from Invitrogen/Gibco, fetal calf serum (FCS) from Biochrom (Biochrom AG, Germany). pBAC-3 vector was obtained from Novagen, BaculoGold transfection kit for baculovirus generation from BD Bioscience. CoA-Biotin, CoA-AT488 and CoA-Dy647 conjugates and phosphopantetheinyl transferase Sfp were purchased from Covalys Bioscience, (Witterrswill, Switzerland), Alexa Fluor C 5 488-maleimide and Alexa Fluor 594-maleimide from Molecular Probes/Invitrogen, Oregon Green 488 maleimide from Molecular Probes. Tris-nitrilotriactic acid (tris-NTA) conjugates with biotin (^{Bt}tris-NTA) [6] and OG488 (^{OG488}tris-NTA) were synthesized and described in the previous study [7]. IFNβ (formulated Rebif 22 μg) was obtained from Serono GmbH, Unterschleißheim/Germany. The anti-human IFNAR1 mouse monoclonal mAb AA3 [8], produced by Biogen, was a gift from our collaborator Erik Mogensen. IFNω1 was a kind gift from Christoph Thomas and K. Christopher Garcia. Quartz fluorescence 120-μL cuvettes were obtained from Hellma (USA) and 561 nm CL 561-200-O 200 mW diode pumped laser - from CrystaLaser, (Reno, USA). All other common biochemicals were purchased from Sigma Aldrich or Carl Roth GmbH.

2.2.2 Construction of vectors

IFNα2, IFNα2-YNS, IFNα2-α8tail, IFNα2-YNS-α8tail, IFNAR2-EC and IFNAR2-EC-H10 carrying an N-terminal ybbR-tag (ybbR-IFNα2, ybbR-IFNα2-YNS, ybbR-IFNα2-α8tail, ybbR-IFNα2-YNS-α8tail, ybbR-IFNAR2 and ybbR-IFNAR2-H10) were cloned by insertion of an oligonucleotide linker coding for the ybbR peptide (DSLEFIASKLA) [9, 10] into the *Nde*I restriction site upstream of the corresponding genes in the plasmids pT72Cα2 and pT72CR2, respectively [11]. For producing IFNAR2-ybbR construct ybbR-peptide-encoding

oligonucleotide was inserted into the *Sal*I restriction site downstream of the corresponding gene in pT72CR2 vector. Site-directed mutagenesis of IFNα2-YNS to IFNα2-YNS-α8tail was carried out, based on the PCR site-directed mutagenesis protocol with a pair of mismatch oligonucleotides obtaining a linear fragment suitable for reclosure, and it was similar to that described elsewhere [12]. YbbR-IFNAR1-H10 and H10-IFNAR1-ybbR were generated by insertion of the ybbR-peptide sequence into the *Nhe*I/*BamH*I or *EcoR*I restriction sites upstream or downstream of the corresponding genes in the vector pBAC-3 (Novagen) or pAcGP67B (BD Pharmingen) respectively. H10-IFNAR1-N23C-ybbR mutant was obtained by cloning the target double-tagged IFNAR1-EC construct into pBluescript II SK(+) transfer vector (Addgene) resulting in a 4.2 kB template. Cysteine mutation was introduced by PCR reaction with a pair of forward and reverse primers with a mismatch on the forward oligonucleotide, and the obtained PCR product was reclosed by ligation. Subsequently, the target gene was cloned from the transfer plasmid by insertion into the *BamHI* and *PstI* restriction sites into pAcGP67B vector (BD Pharmingen) suitable for baculovirus generation. Tagless phosphopantetheinyl transferase (PPT) Sfp was subclonned from the original construct pBAD-Sfp provided by the manufacturer (Covalys Bioscience) by PCR followed by the plasmid reclosure. Control construct for rapid screening assay was based on pBAC-3-IFNAR1-H10 where IFNAR-H10 was exchanged to H6-EGFP by insertion into the *BamH*I and *Pst*I restriction sites downstream of the region encoding gp64 secretion signal peptide.

2.2.3 Cell cultures and transfection

Insect Sf9 cells were cultured according to Invitrogen manual as monolayer or suspension culture in Sf-900™ II SFM medium (Invitrogen/Gibco) supplemented with 1% v/v Pluronic and 5% v/v FCS. For preparation of baculovirus-containing cell supernatants for direct immobilization solid phase assays plasmids pBAC-3 or pAcgp67B harbouring the genes of interest were co-transfected into Sf9 cells with linearized baculoviral DNA (BD Biosciences) using previously applied scale-down protocol [13] with 1/5 of the original amount of DNA, and the baculovirus stocks were produced, according to the Invitrogen manual. In brief, the four generations of baculoviruses from P0 till P3 were produced in increasing medium volume, achieving higher virus titre in each generation. About 2 mL for P0, 4 mL for P1, 14 mL for P2 in monolayer format and 50 mL for P3 as suspension culture were harvested by centrifugation 7-9 days post infection and taken for ligand blotting analysis (with ^{Bt}tris-NTA conjugate) or solid phase binding assays. For protein expression, fresh Sf9 cell cultures (250 mL) were infected with the respective baculovirus and harvested after 4 days.

2.2.4 Protein production, purification and labelling

All IFNα2 and IFNAR2 proteins were expressed and purified by the same protocols established for IFNα2-YNS [14] and wild type IFNAR2-EC [11, 15, 16]. These proteins were expressed in *E. coli*, refolded from inclusion bodies and purified as described previously. YbbR-IFNα2, ybbR-IFNα2-YNS, ybbR-IFNα2-α8tail, ybbR-IFNα2-YNS-α8tail, ybbR-IFNAR2-EC, ybbR-IFNAR2-EC-H10 and IFNAR2-EC-ybbR were labelled by PPTase using CoA-AT488 or CoA-Dy647 and Sfp purchased from Covalys, according to published protocols [9, 10], quenched by addition of 15 mM EDTA and purified by size exclusion chromatography on Superdex^{TM} 75 10/30 column, as we reported recently [17]. Fluorescence non-covalent switchable labelling of His-tagged IFNω1 (Figure 1.10 B) was carried out *in situ*, similarly to the procedure described in [7] by mixing H10-tagged protein with double molar excess of ^{OG488}tris-NTA conjugate and incubating for 5 min prior to running binding assay. Tagless Sfp was produced as a maltose binding protein (MBP) fusion in *E. coli* and purified with amylose resin (New England BioLabs) and by gel filtration. H10-tagged IFNAR1-EC was expressed in *Sf*9 insect cells using baculovirus technology and purified by immobilized metal ion chromatography (IMAC) and gel filtration as described previously [13, 15]. H6-ybbR-EGFP and maltose binding protein with decahistidine tag (MBP-H10) were expressed in *E. coli* and purified by IMAC and size exclusion chromatography (SEC) by standard protocols. N- and C- terminal ybbR-fusions of His-tagged IFNAR1-EC were expressed and purified the same way as IFNAR1-H10. YbbR-IFNAR1-H10 was labelled using CoA-AT488 (Covalys Bioscience), tagless Sfp and Mn^{2+}. Labelling reaction was performed the same way as for interferons and purified using Superdex^{TM} 200 10/30 column. ^{OG488}IFNAR1-N23C-EC-H10 was expressed, purified and labelled with Oregon Green-maleimide (OG488), as described in [5]. The extracellular domain of IFNAR1 cysteine mutant with the C-terminal ybbR-tag fused to an N-terminal decahistidine tag (H10-IFNAR1-N23C-ybbR) was expressed in Sf9 insect cells using baculovirus infection, and purified by immobilized metal-chelating chromatography as previously described [13, 15] for polyhistidine tagged IFNAR1. For obtaining the double-labelled protein at first H10-IFNAR1-N23C-ybbR was reduced after IMAC with 3 mM tricarboxyethylphosphine, reducing agent and aggregates were removed by size exclusion (Superdex^{TM} 200 26/60), then labelled with AF488-maleimide (Molecular Probes) and purified by anion exchange from non-labelled and multiple labelled species, as described earlier for IFNAR1 cysteine mutants [5]. Subsequently, the C-terminal ybbR-tag of the collected protein fraction was coupled with a custom-made CoA-AF594 conjugate by PPTase-mediated transfer reaction the same way as

described above for ybbR-IFNAR1-H10 and reaction was purified by gel filtration with Superdex^{TM} 200 10/30. All relevant fractions of labelled proteins were pooled, purity assayed by 12% SDS-PAGE and protein concentrations were determined by absorption spectroscopy using the extinction coefficients (Table 7.1).

2.2.5 CoA conjugate synthesis

In these studies, commercially available (Covalys Bioscience) small-molecule probe–CoA conjugates did not cover the complete spectral range of needs. CoA-AT488 and CoA-Dy647 conjugates were purchased from the vendor. CoA-AF594 conjugate was synthesized as described in the original protocol [18] by one-step Michael condensation of the maleimide-functionalized small-molecule probe with the free thiol group of CoA at the end of the Ppant arm, resulting in a thioether linkage between the small-molecule probe and CoA [18]. For the synthesis Alexa Fluor 594-maleimide was purchased from Molecular Probes/Invitrogen (Karlsruhe, Germany), CoA trilithium salt is commercially available from Sigma Aldrich.

2.2.6 Absorption and fluorescence spectrophotometry

Absorption spectroscopy measurements (ultraviolet-visible spectrophotometry, UV-Vis) were performed to estimate concentration [19] and degree of labelling (DOL) of produced fluorescence-labelled proteins. UV-vis spectrophotometer (V-650 Spectrophotometer, Jasco) was used to excite a sample in 1 cm quartz cuvette and calculate the concentrations of probed solutions according to the law of Beer-Lambert-Bouguer. Table 7.1 summarizes the molar extinction coefficients used in this study for calculation of purified protein concentration and estimation of DOL.

To obtain a degree of labelling (DOL, dye-to-protein ratio) the following equation was applied:

$$DOL = \frac{A_{dye} / \varepsilon_{dye}}{A_{prot} / \varepsilon_{prot}} = \frac{A_{\max} \cdot \varepsilon_{prot}}{\left(A_{280} - A_{\max} \cdot C_{F280}\right) \cdot \varepsilon_{\max}} \qquad \textbf{Equation 2.1}$$

where A_{prot} – absorbance of the pure protein at 280 nm (absorption maximum of protein), ε_{prot} – molar extinction coefficient (in $M^{-1} \cdot cm^{-1}$) of the pure protein at 280 nm, absorbance A_{max} of the dye at the absorption maximum (λ_{abs}), ε_{max} – molar extinction coefficient (in $M^{-1} \cdot cm^{-1}$) of the dye at its absorbance maximum, CF_{280} – correction factor which depends on the dye's spectral properties.

The relationship given above is valid for the case when the extinction coefficient of the free dye ε_{max} at the absorption maximum is the same as the extinction coefficient of the conjugated dye at this wavelength. The concentration of bound dye is given by Equation 2.2

$$c(dye) = \frac{A_{\max}}{\varepsilon_{\max} \cdot l}$$ **Equation 2.2**

The fluorophores used in this study with respective absorbance maxima and correction factors at 280 nm are listed in the Table 7.2.

Fluorescence spectrophotometry was used to record fluorescence spectra of fluorophores and labelled proteins in fluorescence quenching experiments. Fluorescence spectra were recorded with a FP-6500 (Spectrophotometer, Jasco) using a 120 µL quartz cuvette. A solution of 100 nM labelled protein diluted in Hepes buffered saline (HBS) buffer (20 mM Hepes (pH 7.5), 150 mM NaCl, 0.01% Triton X-100, 50 µM EDTA) was filled into the cuvette, and fluorescence measurement was carried out. Fluorescence spectra were acquired with an excitation of Alexa Fluor 488 at 470 nm and Alexa Fluor 594 at 580 nm (5 nm slit-width) and analysed with the standard software suite Spectra Manager™ (Jasco). For quenching assay, the cuvette containing H10-IFNAR1^{AF488,AF594} protein sample was irradiated by a 561 nm-laser beam, perpendicular to a cuvette window. Illumination time of 15 min and 200 mW laser power were used for maximum bleaching of AF594 probe. Subsequently the sample fluorescence spectra were recorded as described above.

2.2.7 In vitro binding assays by solid phase detection

Ligand binding to IFNAR1 and IFNAR2 ectodomains was probed in real time by using label-free RIf detection in combination with TIRFS (TIRFS/Rif), as described earlier [5, 13]. These measurements were performed with a homebuilt setup, as described earlier, using the 488 nm line of an argon ion laser for the excitation of AT488 and a 633 nm He/Ne laser for excitation of Dy647. Binding assays were performed under continuous flow-through conditions. All measurements were carried out in HBS. For monitoring the interaction with IFNα2 and mutants, IFNAR1-EC and IFNAR2-EC were immobilized onto PEG-modified TIRFS/RIf surfaces using tris-NTA multivalent chelators for stable immobilization, as described in [15, 20]. For the combined-tag immobilization assay surfaces simultaneously modified with tris-NTA and CoA (tris-NTA+CoA) were obtained by reacting a solution of 500 µM tris-NTA-SH [21] and 125 µM CoA in the presence of 10 mM $MgCl_2$ in HBS on the surface for 1 hour at room temperature [22]. Excess coordination sites were blocked with decahistidine-tagged maltose-binding protein (MBP-H10) to avoid non-specific binding and ligand was injected at appropriate concentrations. Spontaneous dissociation was monitored either by washing with

HBS or by chasing with suitable unlabelled IFN in HBS injected during dissociation phase in order to suppress rebinding due to the high association rate constant of some IFNα2 mutants towards IFNAR2-EC.

Sfp–catalysed enzymatic covalent protein immobilization assays were performed as we reported recently in [17]. Maleimide-functionalized TIRFS/RIf transducer slides were equilibrated in HBS and then reacted in flow cell with 1 mM CoA. Prior to protein immobilization, the remaining maleimide groups were blocked by injection of 10 mM 2-mercaptoethanol in HBS. Subsequently, 5 μM of ybbR-IFNα2 or ybbR-IFNα2-YNS in HBS was immobilized in the presence of 1 μM Sfp and 10 mM Mn^{2+} ions. Surface-bound metal ions were removed by an injection of 25 mM EDTA. Then, the activity of the immobilized protein was probed by injecting a suitable interaction partner: IFNAR1-EC or IFNAR2-EC.

For carrying out the IFNAR1-EC direct capturing assay, H6-EGFP or His10-tagged receptor variants were site-specifically immobilized directly from the cell expression supernatants through their C-terminal His-tags onto the surfaces as described for isolated proteins in [15, 20]. PEG/tris-NTA transducers were prepared at medium-density of chelator heads [21] to minimize unspecific adsorption of expression medium components. Excess coordination sites were blocked by injecting 4 μM MBP-H10 to avoid non-specific ligand binding. Subsequently, 150 nM fluorescence-labelled IFNα2-YNS, 500 nM label-free IFNβ or 500 nM *in situ* labelled IFNω were injected, and binding was monitored in real time. For decreasing additional unspecific binding, IFNβ and FNω were mixed with 700 nM tagless IFNAR2 prior to injection. After monitoring the complete ligand dissociation course 50 nM anti-IFNAR1 antibody mAb AA3 was injected to confirm the surface immobilization of IFNAR1.

All binding data were analysed with BIAeval 3.1 (Biacore AB, Uppsala/Sweden) and OriginPro 8 (Microcall Software Inc., Northampton, MA/USA) software, using the standard Langmuir model, or model considering mass transport for fitting kinetic data.

The equilibrium dissociation constant K_D was determined from the fitted rate constants:

$$K_D = \frac{k_d}{k_a} \qquad \textbf{Equation 2.3}$$

2.3 Results and discussion

2.3.1 Site-specific enzymatic labelling of IFNs

In order to obtain biologically active, properly folded IFNs with high degree of fluorescence labelling for the spectroscopic applications, an approach of site-directed covalent labelling of IFNα2s through tag-specific phosphopantetheinyl transferase-mediated enzymatic reaction was devised [9, 10, 18].

To this end the 11-residue ybbR-peptide was fused to the N-terminus of IFNα2 wild type (WT) and high affinity IFNα2 mutants such as IFNα2-YNS and IFNα2-YNS-α8tail and the resulting proteins were expressed and purified according to the protocol developed for tagless IFNα2-YNS [14]. This allowed employing for IFNs an approach of non-reducing refolding and simultaneously minimize the number of chromatographic purification steps (Figure 2.2 A, B and D). The increase of yields has been observed for the ybbR-tagged and tagless IFNs and the highly pure homogeneously oxidized protein was obtained in fewer steps compared to the previously used purification approach [2]. In brief, the combination of column ion exchange (IE) (Figure 2.2, A) and size exclusion (SE) purification (Figure 2.2 B) followed by an additional size exclusion chromatography (SEC) (Figure 2.2, D) was employed to purify non-labelled IFNs to homogenity.

Alternatively, the second purification strategy was followed for obtaining fluorescence-labelled protein material by Sfp-catalised approach. This includes labelling of ybbR-tagged IFNs by standard described enzymatic reaction protocol [18] directly after the preparative IE. Extensive purification steps such as the last IE chromatography can be omitted since the reaction mix has to be cleared out from misfolded/aggregated material, unreacted dye, free CoA, Mn^{2+} co-factor and Sfp enzyme by an additional size-exclusion run (Figure 2.2, C).

This enabled the efficient separation of Sfp enzyme (71 kDa) and IFNα2 (20 kDa) peaks as illustrated in Figure 2.2 (C) for ^{AT488}IFNα2-YNS SEC purification. For each IFN, protein separation as well as homogeneity and attachment of a fluorophore were assayed by non-reducing SDS–PAGE with Coomassie staining and fluorescence detection (Figure 2.2, F).

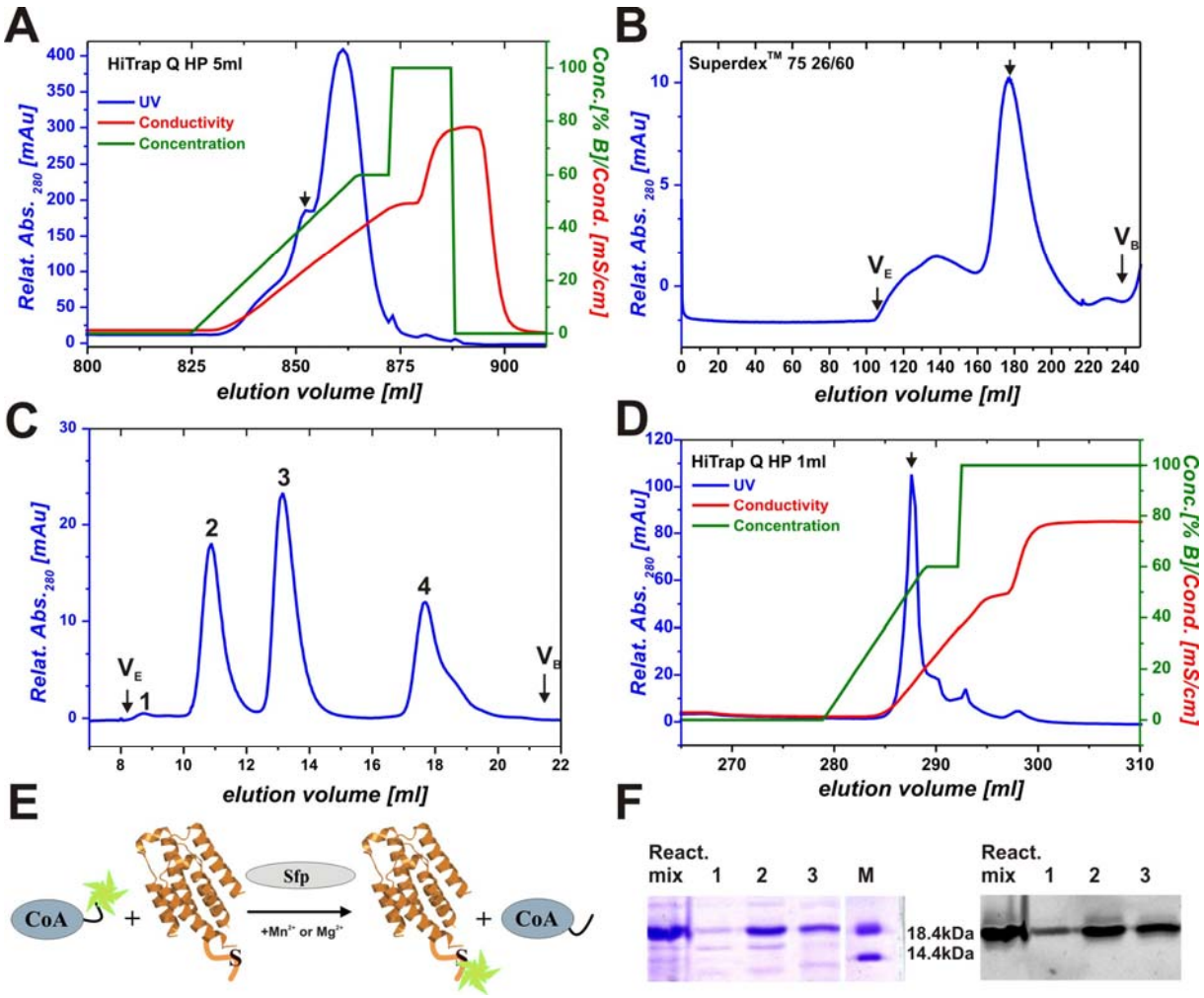

Figure 2.2 Purification and labelling of ybbR-tagged IFNα2 mutants.

A Exemplary purification ion exchange chromatography of ybbR-IFNα2-YNS-α8tail with a 5 ml HiTrap Q HP column. The arrow-indicated peak at 25 $mS \cdot cm^{-1}$ contains the target protein. **B** Size exclusion chromatogram of ybbR-IFNα2-YNS-α8tail obtained with Superdex^{TM} 75 26/60 column. The short arrow at 180 mL points at the main elution peak of monomeric interferon. V_E and V_B indicate exclusion and bed column volume, respectively; **C** Size exclusion chromatography of ybbR-IFNα2-YNS enzymatic labelling reaction with CoA-AT488 conjugate performed with Superdex^{TM} 75 10/30. Peak (1) corresponds to aggregates, peak (2) – Sfp (71 kDa), the main peak (3) at 12.3 mL shows the elution of interferon (20 kDa), peak (4) – the unreacted fluorescent conjugate and free CoA, V_E – exclusion volume, V_B - bed column volume. **D** Ion exchange chromatography (1 ml HiTrap Q HP column) of ybbR-IFNα2-YNS-α8tail after preparative gel filtration. The peak at 13 $mS \cdot cm^{-1}$ indicated with an arrow contains the target protein. **E** The scheme of covalent fluorescent probe attachment to ybbR-tag of IFN by Sfp-mediated phosphopantetheinylation reaction with fluorescent CoA conjugate and in presence of Mn^{2+} or Mg^{2+} as co-factor. **F** The main SEC peak fraction analysis of labelled ^{AT488}IFNα2-YNS with non-reducing SDS-PAGE after Coomassie staining (left) and the corresponding inverted fluorescence image of UV-illuminated SDS-PAGE (right). React. mix: sample with the labelling reaction mix, 1-3: fractionation range, M – protein molecular weight marker.

Typical labelling degrees obtained by this enzymatic reaction approach were 0.75-1 fluorophores per IFNα2 molecule for the purified proteins, making it a powerful technique for achieving highly efficient fluorescent probe transfer. In order to confirm the specificity of the labelling reaction under these conditions, wild type FNα2 without ybbR-fusion peptide for posttranslational labelling was subjected to the same reaction procedure, which did not yield any quantities of labelled protein after purification.

In total 4 variants of IFNα2: ybbR-IFNα2, ybbR-IFNα2-α8tail, ybbR-IFNα2-YNS, ybbR-IFNα2-YNS-α8tail, carrying an N-terminal ybbR-tag, were purified and labelled by same procedure with various CoA conjugates for subsequent different applications.

In the current studies wild type ^{AT488}IFNα2 was used in HPLC SEC assays (section 4.3) to optimize purification conditions of the bis3NTA-stabilized ternary complex by monitoring elution at 490 nm detection channel. Dual-colour FCCS experiments (4.3) were carried out with purified bis3NTA-stabilized ternary complex harbouring wild type ^{Dy647}IFNα2. YbbR-IFNα2 and ybbR-IFNα2-YNS mutants were enzymatically coupled to surfaces in the receptor-cooperativity assays (3.3.2). High affinity mutant ^{AT488}IFNα2-YNS was employed in the screening for hotspot residues on IFNAR1-EC binding site for ligand in 3.3.1. The tightest binding interferon mutant ^{AT488}IFNα2-YNS-α8tail was engaged in the affinity-based stabilization of ternary complex in control experiments in section 4.3.

This small-probe transfer technique via PPTase-mediated conjugation to a specific serine residue on short terminal ybbR peptide tag allows rapid effective production of labelled IFNα2 variants for a broad range of fluorescence spectroscopic applications. In addition this approach allowed to attach small molecule probes from wide selection of different CoA substrates such as biotin, custom-made CoA conjugates with fluorophores and spin labels with resulting molecular degree of IFNα2 labelling close to one.

2.3.2 N- and C- terminal insertion of PPT tags for enzymatic modification of IFNAR2-EC

Following the labelling of N-terminally tagged IFNα2s and to further explore the potency of Sfp-mediated enzymatic probe attachment, short peptide tags, specific for this transferase were fused to the N- or C- termini of IFNAR2 ectodomain and analysed in terms of fluorescence labelling versatility and efficiency. Efficient placement of a green or red fluorescence reporter at the receptor N-terminus is essential for the IFNAR2 label-based spectroscopic detection discussed in the subsequent sections. Whereas exploring the enzymatic recognition efficiency of the C-terminal tag could provide insights for establishing an approach of protein covalent surfaces coupling in oriented manner.

As for IFNα2s, simple, yet efficient covalent labelling of N-terminal tag fused to IFNAR2-EC and IFNAR2-EC-H10 was achieved through enzymatic reaction with CoA-ATTO488 (Figure 2.3). This included, similarly to interferon labelling, the reduction of chromatographic purification steps and good reaction separation from the unreacted conjugates and Sfp (Figure 2.3 B, C). ^{AT488}IFNAR2-EC labelled by this technique was employed for surface binding assays discussed in the frame of this work in 3.3.2. ^{AT488}IFNAR2-EC-H10 carrying C-terminal decahistidine tag for binding to multivalent chelator heads was employed for the calibration of SEC assays in section 4.3.

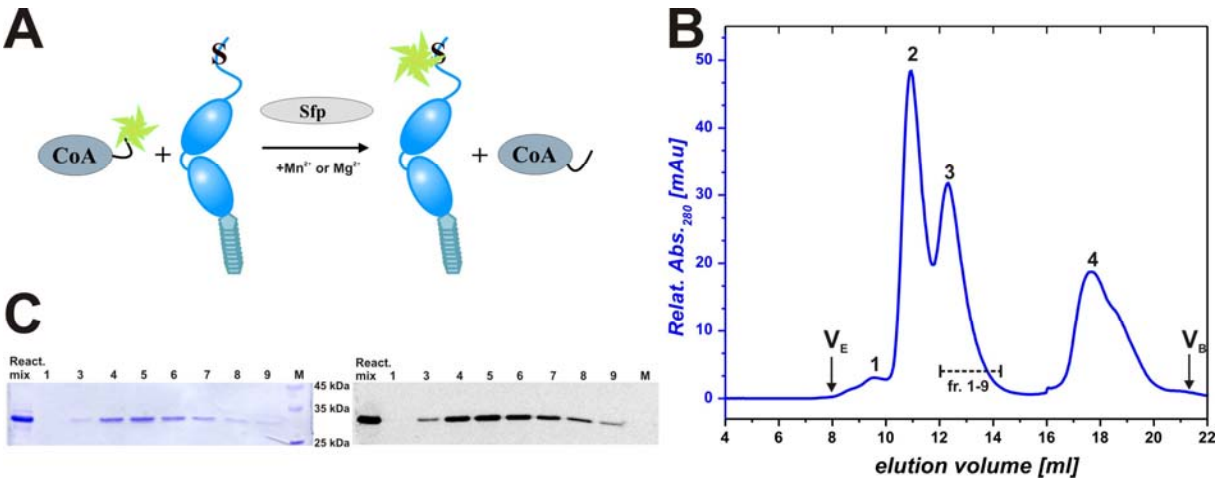

Figure 2.3 Purification and labelling of ybbR-tagged IFNAR2-H10.

A Schematic illustration of covalent fluorescent probe attachment to ybbR-IFNAR2-H10 by the PPTase. **B** Labelling reaction sample with ^{AT488}IFNAR2-H10 was loaded through a 500 µL loop onto a Superdex^{TM} 75 26/60 gel filtration column and monitored at 0.7 ml·min^{-1}. Expected elution volumes are as follows: peak (1) corresponds to aggregates, peak (2) – Sfp (71 kDa), the main peak at 12.3 mL (3) shows the elution of ^{AT488}IFNAR2-H10 (27 kDa), peak (4) – free fluorescent conjugate and CoA; V_E and V_B indicate exclusion and bed column volume, respectively. Fractionation range for analysis is marked with a dashed line. **C** The main SEC peak fraction analysis of the labelling reaction with non-reducing SDS-PAGE after Coomassie staining (left panel) and the corresponding inverted fluorescence image of UV-illuminated SDS-PAGE (right panel). React. mix - sample with the reaction mix after labelling, 1-9: SEC fractionation range, M – protein molecular weight marker.

In vitro PPTase-mediated modification by a series of other fluorescent CoA derivatives led to a set of fluorescent ybbR-IFNAR2-EC proteins with average number of >0.55 (red) or >0.75 (green) fluorophores per IFNAR2 molecule. The same result was observed for labelling of IFNAR2-ybbR (tagged at C-terminus) with CoA-ATTO488 and CoA-Dy647 by PPTase (data not shown), yielding labelling degrees >50%, confirming the integrity of the corresponding ybbR-tags.

Surface binding experiments to IFNα2 (not shown) confirmed that the ligand binding properties of both, N- and C- terminal ybbR tag-fused labelled IFNAR2 proteins were not affected by insertion or labelling.

Out of the scope of current work, in order to explore a potential pair tag for orthogonal PPTase-based modification, the S6-tag, an alternative peptide substrate for Sfp, was tested [17]. Both short peptides, ybbR and S6 were inserted at the receptor C-terminus (IFNAR2-ybbR and IFNAR2-S6) and compared to ybbR-IFNAR2 with respect to enzymatic surface coupling under conditions described for ybbR-IFNα2 and discussed in more details in 2.3.7. In brief, upon tag-mediated surface immobilization of IFNAR2-ybbR relatively low net amount of protein was stably bound on the surface [17]. IFNAR2-S6 yielded much more efficient immobilization than for IFNAR2-ybbR, although it reached only 50% of levels obtained for ybbR-IFNAR2 under the same conditions. This 12 amino acid tag was developed for orthogonal protein labelling by different PPTases (1.3.1) and has even a ~2-fold higher k_{cat}/K_m for modification by Sfp compared to the ybbR-tag [10]. A potentially important difference between S6 and ybbR tags is the additional glycine residue in S6 tag upstream of the shared Asp-Ser-Leu motif containing the serine residue, to which the phosphopantetheinyl moiety is transferred. Met residue was located upstream of the N-terminal ybbR-tag compared to Thr and Phe in case of IFNAR2-ybbR. Though it has been demonstrated that any N-terminal residues upstream of the tag Asp-Ser-Leu recognition motif do not play a significant role for transfer efficiency by Sfp in solution [9], they appear to be critical when protein is being immobilized through the C-terminal tag to surfaces. According to CD-spectra of peptide tags and prediction based on NMR-structures of homological short peptides, the serine residue from the site of phosphopantetheinyl modification is placed at the N-terminal tip of the helical region [9]. It is possible that certain additional residues serve as a spacer between the protein C-terminus and the tag helical motif. They might be essential for preventing sterical hindrance for efficient Sfp enzyme docking at the recognition motif for reacting this tag with CoA moiety on surfaces. Taken together these observations suggest that amino acids flanking the C-terminal ybbR-tag are important for PPT efficiencies and have to be further systematically explored to resolve this issue.

2.3.3 Enzymatic fluorescence labelling of IFNAR1 ectodomain

As the next step, PPTase-based fluorescence labelling was applied to IFNAR1-EC, the most delicate protein in the IFN receptor ternary complex. To explore the enzymatic modification of insect cell-expressed IFNAR1-EC, ybbR tags were fused to N- or C- protein terminus. Optimization of C-terminal IFNAR1-EC labelling would open up prospects for further

development of dual-colour fluorescence labelling strategy discussed in the next subsection. Whereas placement of a donor fluorescence reporter at N-terminus of IFNAR1-EC was required for the fluorescence cross-correlation experiments performed with dual-colour labelled ternary complexes and described in section 4.3.

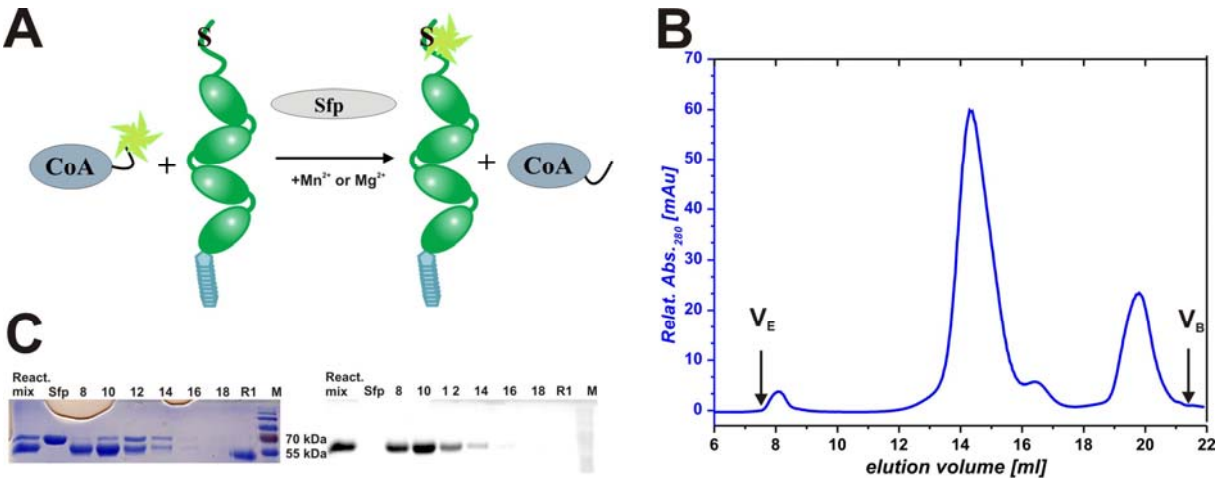

Figure 2.4 Enzymatic covalent labeling of IFNAR1-H10.

A Schematic illustration of ybbR-IFNAR1-H10 labelling with ATTO488-CoA conjugate, catalysed by phosphopantetheinyl transferase Sfp in presence of Mn^{2+} or Mg^{2+}. **B** Purification of ybbR-IFNAR1-H10 labelling reaction by SEC on Superdex^{TM} 200 10/30 column, monitored at 0.7 ml·min^{-1}. Sfp enzyme and IFNAR1 co-elute in a single broadened peak at 14.5 mL. V_E and V_B indicate exclusion and bed column volume, respectively. **C** SDS-PAGE analysis of eluted ^{AT488}IFNAR1-H10 peak fractions after Coomassie staining (left panel). React. mix - sample with the reaction mix after labelling, Sfp and R1 represent the respective enzyme and unlabelled IFNAR1 control samples, M – molecular weight marker. SDS-PAGE analysis of fluorescent proteins under UV-illumination (right panel).

An enzymatic probe attachment to receptor N-terminus was carried out with the construct tagged on the N-terminus with ybbR short peptide for modification by Sfp and on the C-terminus with decahistidine tag utilized for affinity purification or interaction with tris-NTA moieties. PPTase-based posttranslational modification of ybbR-IFNAR1-H10 with the ATTO488-CoA conjugate and the respective purification are illustrated in Figure 2.4. Due to the highly flexible four-subdomain structural organization of IFNAR1-EC and multiple glycosylation at about nine potential sites, the apparent molecular mass as well as apparent hydrodynamic protein radius are substantially increased. Typically receptor ectodomains run on analytical and preparative SEC columns as rather broad asymmetric peak [13] shifted to shorter retention time. Elution of this receptor might overlap with the peak of the Sfp enzyme employed for the ybbR modification. To minimize the effect of potential poor SEC-separation of these two proteins, for the purpose of IFNAR1-EC labelling, Sfp without oligohistidine tag was constructed and employed. Except for that, the protocol for one-step Sfp-catalysed

reaction [18], as described in 2.3.1 for IFNα2s was followed to prepare protein labelling mix with the commercial ATTO488-CoA conjugate and to purify this reaction by size-exclusion chromatography (Figure 2.4). Unlike for IFNs and IFNAR2, for IFNAR1 three major peaks were observed in the course of size exclusion. The first minute peak corresponds to aggregated Sfp and receptor, and the third peak marks the elution of free CoA and excess of a probe conjugate. The middle, highest peak represents the Sfp and the target protein, as assayed by non-reducing SDS–PAGE with fluorescence detection and Coomassie staining (Figure 2.4, C and D). Using the substantially low Sfp molar ratio (1:50) in the labelling reaction, reduces the presence of transferase in the collected peak fractions of labelled ^{AT488}IFNAR1-H10 till trace amounts. Certain spectroscopic studies such as TIRFS/RIf assays or single molecule tracking experiments on tris-NTA-functionalized lipid bilayers involve His-tag mediated tethering of labelled IFNAR1-EC to surface. They are performed in a flow-cell format where the residual contamination of IFNAR1 sample by Sfp without His-tag is efficiently washed off with buffer during rinsing step, and thus can be neglected. If necessary, the enzyme can be efficiently removed from reaction mix after catalysis by an additional semi-purification step with amylose resin, since Sfp is produced as a maltose binding protein (MBP) fusion.

Typical labelling degrees for the transfer reaction of ATTO488 mediated by standard or tagless Sfp enzyme were 0.55-0.75 fluorophores per ^{AT488}IFNAR1-H10 molecule. Labelling of H10-IFNAR1-ybbR with ATTO488-CoA and Dy647-CoA (not shown) yielded a set of fluorescent receptors with labelling degrees over 50%, confirming the utility of the corresponding C-terminal short peptide tag for fluorescent probe attachment.

2.3.4 Orthogonal chemistry for dual-colour covalent labelling

As a next step, we attempted to orthogonally introduce two fluorescent functionalities into a protein of interest in a site-specific controlled manner. To that end, cysteine-based chemistry and PPTase-mediated probe transfer approach were employed to subsequently attach two labels onto IFNAR1-EC receptor subunit. Controlled covalent placement of a donor and acceptor fluorescence reporter onto different IFNAR1-EC subdomains has been in a great demand for monitoring the receptor conformational dynamics in solution by dual-colour FCCS and single molecule FRET.

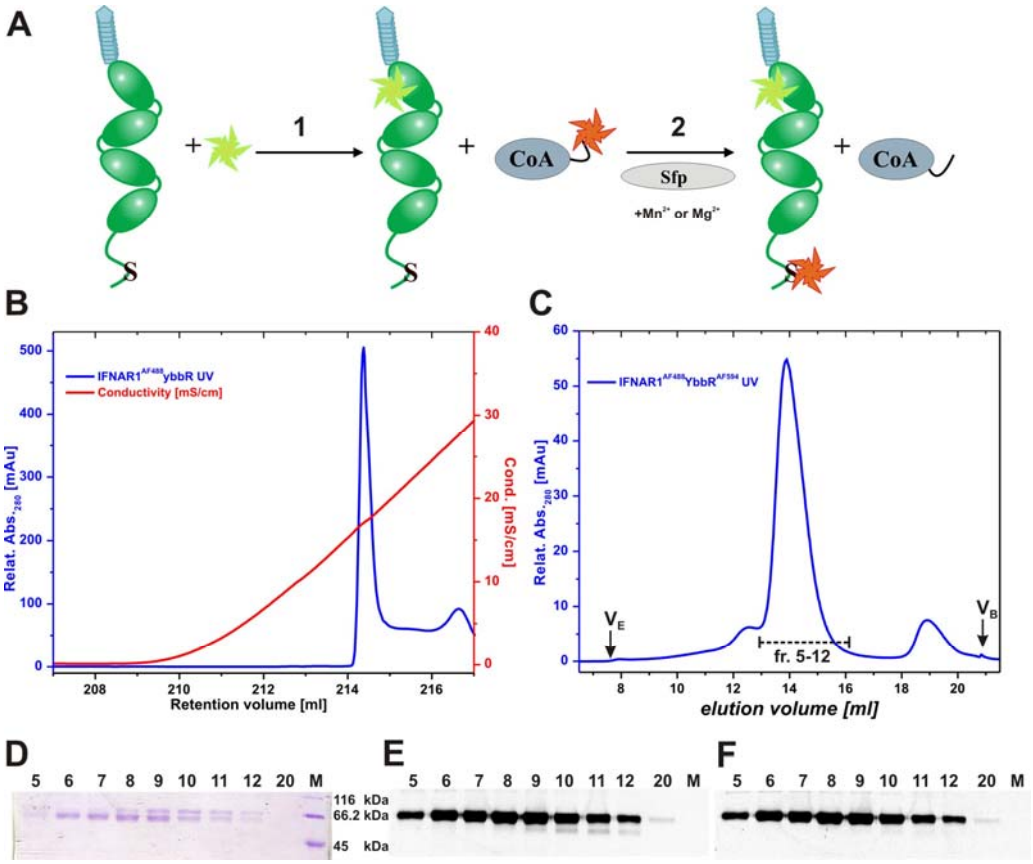

Figure 2.5 Orthogonal dual colour labelling of H10-IFNAR1.

A Schematic cartoon of the two-step covalent labelling strategy. H10-IFNAR1-N23C-ybbR is chemically labelled with Alexa Fluor 488 maleimide (1) and purified on ion exchange column as shown in (B). Subsequently the main peak fraction is orthogonally labelled with Alex Fluor 594-CoA by Sfp enzymatic reaction (2) and purified by SEC (C). **B** Ion exchange chromatography (1 ml HiTrap Q HP column) of H10-IFNAR1-N23C^{AF488}-ybbR after the chemical labelling reaction. The main peak at 17mS·cm^{-1} contains single labelled species. **C** Size exclusion chromatography of H10-IFNAR1-N23C^{AF488}-ybbR^{AF594} after the enzymatic labelling reaction performed with Superdex^{TM} 200 10/30 at flow rate 0.7 ml·min^{-1}. The main peak at 14.5 mL shows the co-elution of Sfp and IFNAR1. V_E and V_B indicate exclusion and bed column volume, respectively. Fractionation range for analysis is marked with a dashed line. **D** The main SEC peak fraction analysis with non-reducing SDS-PAGE after Coomassie staining. Double bands correspond to co-eluted Sfp (upper bands) and IFNAR1 (lower bands), respectively. **E** The corresponding inverted fluorescence image of Blue LED-illuminated SDS-PAGE, AF488 emission collected with 530/28 nm band-pass filter of VersaDoc^{TM} MP 4000 Imaging System (Bio Rad). **F** The corresponding inverted fluorescence image of Green LED-illuminated SDS-PAGE, AF594 emission collected with 605/35 nm band-pass filter.

To resolve this issue, a two-step approach was applied to introduce a fluorescence donor probe through the N23C mutation located at membrane-distal SD1 of H10-IFNAR1-ybbR, followed by PPTase-based acceptor probe conjugation to a C-terminal ybbR-tag (Figure 2.5, A). Chemical labelling of N23C mutant with Alexa Fluor 488-maleimide was carried out by mild reduction of a free cysteine introduced into IFNAR1 [5]. Subsequently, purified

individual single-labelled H10-IFNAR1^{AF488} fractions (Figure 2.5, B) were modified by Sfp (Figure 2.5, C) on the C-terminal tag with AF594-CoA same way as described in details for ybbR-tagged IFNAR1 enzymatic labelling in 2.3.3.

UV absorbance spectra (Figure 2.6, A) confirmed the presence of two fluorescent reporters in the obtained H10-IFNAR1^{AF488,AF594} protein fractions and enabled the estimation of degree of labelling for each attached dye. Taking into account the respective correction factors for the dyes at 280 nm and 490 nm, the average number of fluorophores per protein molecule obtained by the labelling method implemented above was estimated for Alexa Fluor 488 as 0.95 and for Alexa Fluor 594 as 0.75 fluorophores per protein molecule, corroborating the high efficiency of the chosen labelling strategy.

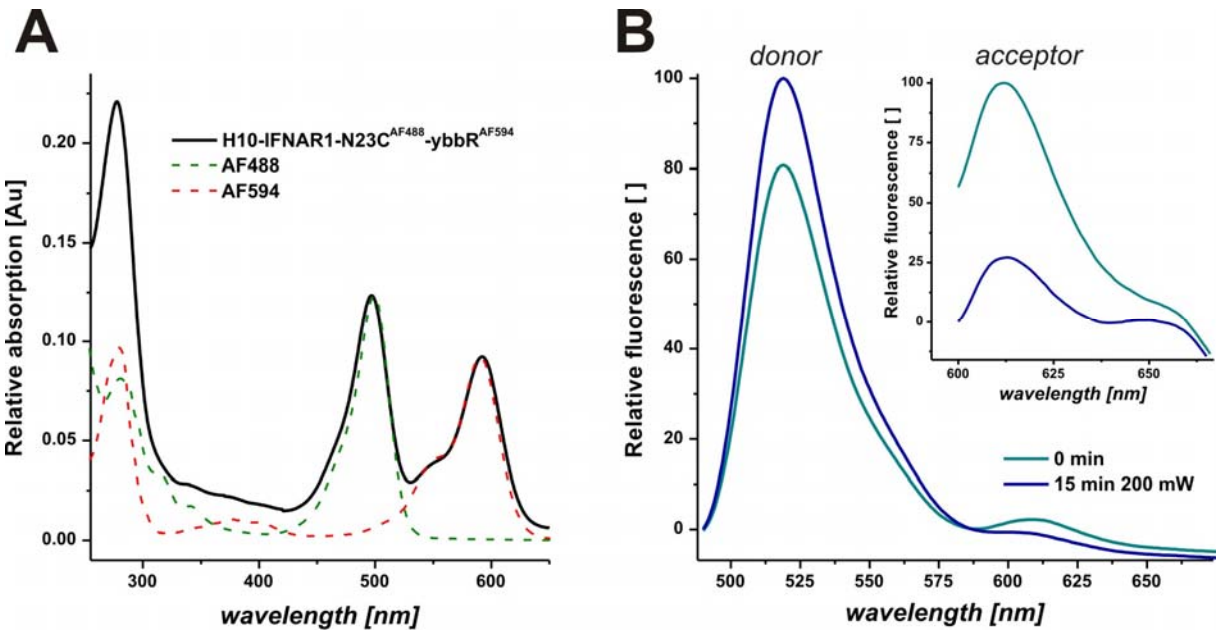

Figure 2.6 Spectra of the double-labelled H10-IFNAR1^{AF488,AF594}.

A Typical absorption spectrum of double-labelled H10-IFNAR1^{AF488,AF594}. For comparison, a dashed line overlay shows the absorption spectra of Alexa Fluor 488 (green) and Alexa Fluor 594 (red) maleimide dyes, normalized for clarity to the absorption maxima of the respective labels attached to protein. **B** H10-IFNAR1^{AF488,AF594} acceptor bleaching course. Relative fluorescence change of H10-IFNAR1^{AF488,AF594} donor spectrum upon dequenching, detected at donor excitation wavelength (470 nm) before (cyan) and after (blue) bleaching for 15 min with 561 nm laser (200 mW). Inset shows the comparison of the relative acceptor bleaching recorded at acceptor excitation wavelength (580 nm) before (cyan) and after (blue) bleaching.

To further confirm the attachment of both, donor and acceptor fluorescence reporters to same protein molecules and to probe the potential utility of the double-labelled IFNAR1 for FRET experiments, the FRET efficiency was probed by acceptor bleaching. Upon illumination of the sample in a cuvette with 561 nm laser, about 20 % of donor fluorescence dequenching was observed (Figure 2.6, B). It was accompanied by a three fold decrease of the acceptor

fluorescence, confirming the FRET-based quenching of the donor molecule. The extent of fluorescence quenching strongly depends on the distance between the inserted dyes. Thus, further FRET-based determination of the intramolecular distances in solution for H10-IFNAR1^{AF488,AF594} can elucidate the receptor conformational dynamics and make an important contribution to the X-ray studies of IFNAR1-EC [23].

Taken together, these results indicate that the two-step orthogonal covalent chemistry for combined cysteine-specific and enzymatic probe incorporation represents a powerful controlled dual-colour labelling strategy for protein studies *in vitro*.

2.3.5 Functional characterization of labelled interferons by TIRFS/RIf

Functional activity of the key IFNα2 mutants and variants after enzymatic fluorescent probe attachment was monitored in real time by probing their interaction with immobilized individual receptor subunits IFNAR1-EC-H10 or IFNAR2-EC-H10 in TIRFS/RIf solid phase detection assays.

A standard course of ^{Dy647}IFNα2 and ^{Dy647}IFNα2-YNS mutant binding to the IFNAR1-EC-H10 immobilized on a PEG polymer brush via tris-NTA is illustrated in Figure 2.7. Typically, an assay consist of surface conditioning (Figure 2.7, A), receptor immobilization via the C-terminal His-tag (10 nM), blocking of the excess of free chelators with MBP-H10 (500 nM) for preventing the unspecific interactions of the bound Ni^{2+}, and a sequence of ligand injections (50 nM) followed their dissociation under constant flow.

For IFNAR1-H10 stable immobilization of about 0.5 nm is detected by the mass channel (Figure 2.7, A), which corresponds to 0.41 ng/mm^2 (8.5 fmol/mm^2) surface concentration of bound protein. Subsequent immobilization of about 1.08 ng/mm^2 (24.1 fmol/mm^2) MBP-H10 ensures sufficient blocking of free chelators heads on surface.

Next, in the experimental course sequential binding of 50 nM ^{Dy647}IFNα2 and ^{Dy647}IFNα2-YNS towards IFNAR1-H10 is probed (Figure 2.7), followed by complete ligand dissociation from receptor at selected experimental conditions. Owing to relatively low protein surface concentration in the assay ligand binding kinetics is monitored on the TIRFS channel (Figure 2.7, B). Binding amplitudes estimated from the mass channel for ^{Dy647}IFNα2-YNS mutant (0.21 ng/mm^2, 10.4 fmol/mm^2) with increased affinity towards IFNAR1 indicate that at least 50% of initially tethered receptor interacts with the ligand.

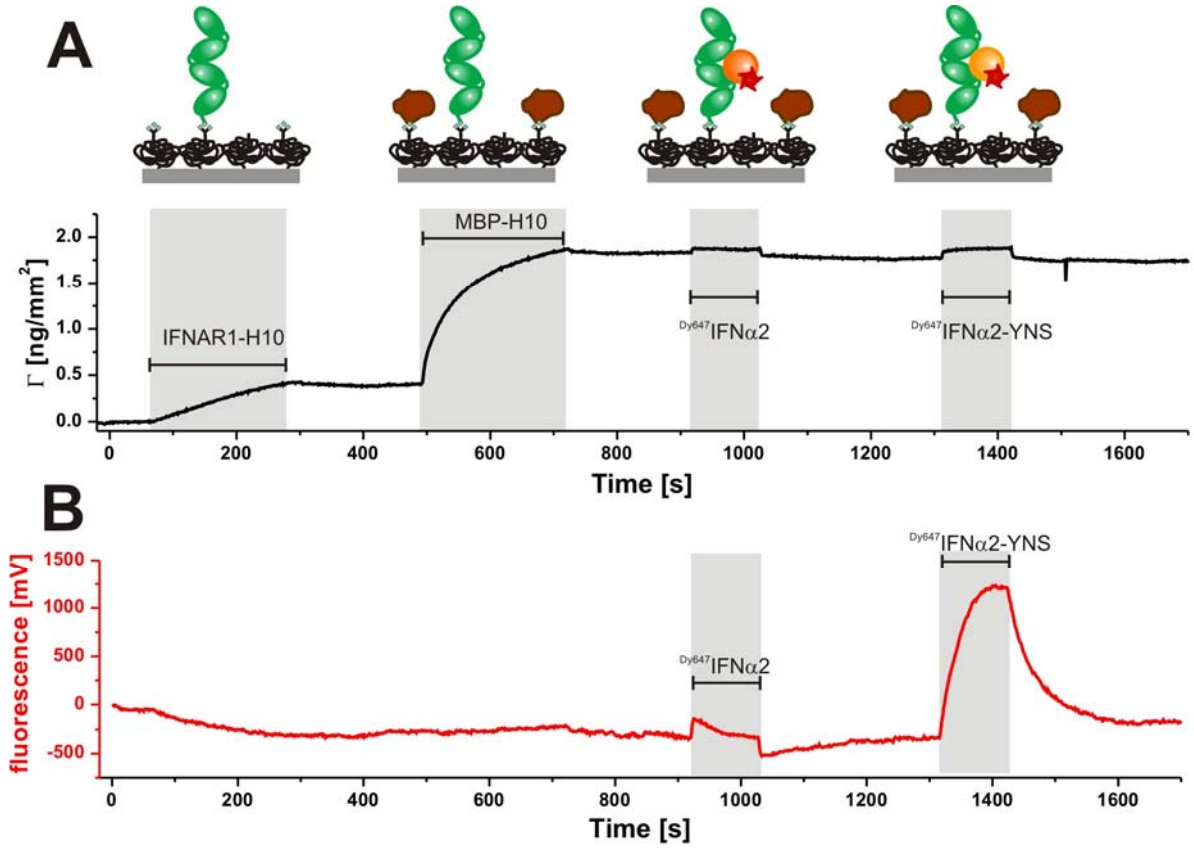

Figure 2.7 Typical TIRFS/RIf binding course of labelled IFNα2 ligands to IFNAR1-H10 immobilized onto high density tris-NTA surface.

Schematic illustration of the assay (upper panel) and RIf mass channel trace (lower panel) with the sequential injection on the following proteins on tris-NTA surface: immobilization of 10 nM IFNAR1-H10, blocking with 500 nM MBP-H10, binding of 50 nM ^{Dy647}IFNα2 and 50 nM ^{Dy647}IFNα2-YNS. **B** The corresponding fluorescence trace of the same injection sequence as detected by TIRF.

In addition, a negative control without immobilized receptor subunits (data not shown) was carried out. Negligible value of the obtained ligand fluorescence amplitude indicates that the binding of fluorescence-labelled ^{Dy647}IFNα2 and ^{Dy647}IFNα2-YNS occurs only in presence of the receptors, and therefore is specific.

Dissociation kinetics (assessment of dissociation rate constant k_d) is the most robust parameter to check for functional integrity of modified proteins. At last, for identifying the interaction rate constants each Dy647-labelled interferon variant was sequentially injected at least three times. Their dissociation from receptor was monitored at TIRFS channel and quantitatively compared (Figure 2.8). Representative fluorescence signals of ^{Dy647}IFNα2 and ^{Dy647}IFNα2-YNS binding to immobilized IFNAR1-H10 are shown as an overlay in Figure 2.8 A. For comparison ligand dissociation is illustrated as normalized curves fitted to standard Langmuir model (Figure 2.8 C). The dissociation rate constants (Table 2.1) obtained by the

fitting an unbiased 1:1 interaction and their values are in a good agreement with the published rate constants [2, 3, 14, 24] for the labelled and label-free ligands. The same good agreement with previously published data was found for interaction of all labelled interferon mutants with immobilized IFNAR1-EC (Table 2.1), confirming thereby functional labelling of these proteins.

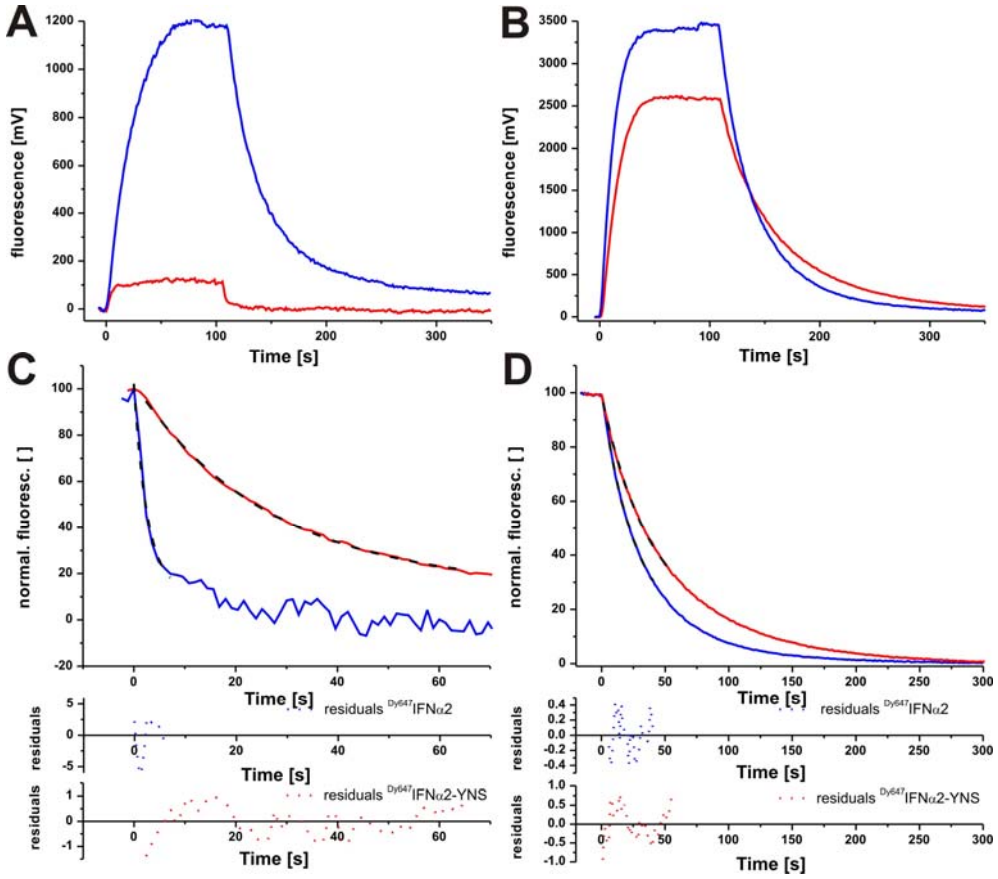

Figure 2.8 Representative IFNAR1 and IFNAR2 binding signals of ^{Dy647}IFNα2 and ^{Dy647}IFNα2-YNS as recorded by the TIRFS channel with receptor subunits being immobilized to the surface.

A Binding of 50 nM ^{Dy647}IFNα2 (blue) and 50 nM ^{Dy647}IFNα2-YNS (red) to 10 nM IFNAR1-H10 tethered to tris-NTA chip. **B** Binding of 50 nM ^{Dy647}IFNα2 (blue) and 50 nM ^{Dy647}IFNα2 YNS (red) to immobilized 20 nM IFNAR2-H10. **C** Comparison of ^{Dy647}IFNα2 (blue) and ^{Dy647}IFNα2-YNS (red) normalized dissociation from binary complex with IFNAR-H10 with respective curve fits (dashed lines) and residuals (lower panels). **D** Comparison of ^{Dy647}IFNα2 (blue) and ^{Dy647}IFNα2-YNS (red) normalized dissociation from binary complex with IFNAR2-H10 with respective curve fits (dashed lines) and residuals (lower panels).

A corresponding assay was carried out for the interaction of labelled IFNs with an extracellular subunit IFNAR2-H10, tethered to a tris-NTA surface. As for the binary complexes with IFNAR1-H10, ligand dissociation kinetics was quantified from binding signals of ^{Dy647}IFNα2 and ^{Dy647}IFNα2-YNS (Figure 2.8 B). For comparison dissociation

curves are normalized and shown with respective fitting results (Figure 2.8 D). Constants obtained by the fits are summarized in the Table 2.1. Again, a good agreement was achieved with literature-reported values [14].

Ligand binary complex formation with either of receptor subunits was probed for the most of ATTO488- and Dy647-labelled IFNα2 mutants with exception for the interaction of ^{AT488}IFNα2WT and ^{AT488}IFNα2-α8tail with IFNAR1-H10. For labelled interferon mutants IFNα2-α8tail and IFNα2-YNS-α8tail with 3 fold higher affinity towards IFNAR2 unlabelled IFNα2-YNS was added during the dissociation phase in order to suppress rebinding to immobilized IFNAR2-H10 receptor. Thus, with the help of a chaser, dissociation rate constants unbiased by rebinding were determined for these mutants. All characterized enzymatically labelled IFNs showed functional binding to both receptor subunits and dissociation behaviour comparable to the previously published results [3, 14, 24, 25].

Table 2.1 Dissociation rate constants of the individual interactions between IFNa2 and the receptor subunits.

IFNα2	Measurement	IFNAR1-H10	IFNAR2-H10
		k_d [s^{-1}]	k_d [s^{-1}]
^{AT488}WT	TIRFS/RIf, tris-NTA chip	-	0.013
^{Dy647}WT	TIRFS/RIf, tris-NTA chip	0.32	0.037
WT	Literature value	1.0	0.0063
^{AT488}YNS	TIRFS/RIf, tris-NTA chip	0.01	0.01
^{Dy647}YNS	TIRFS/RIf, tris-NTA chip	0.039	0.027
YNS	Literature value	0.008	0.0053
^{AT488}α8tail	TIRFS/RIf, tris-NTA chip	-	0.0045
α8tail	Literature value	-	0.002
^{AT488}YNS-α8tail	TIRFS/RIf, tris-NTA chip	0.005	0.003
YNS-α8tail	Literature value	0.008	0.0012
Error %		10	10

Table 2.1 summarizes the dissociation rate constants for all measurements carried out on tris-NTA surfaces as well as the literature values. On average, fluorescence-labelled IFNs

dissociate from receptors approximately 2-3 folds faster than unlabelled ligands, which is consistent with what have been observed previously for chemically labelled IFNα2-WT [2, 15]. This difference can be attributed to the technical discrepancies of the used instrumentation, temperature variations of applied experimental conditions, and method for immobilization of interaction partner onto surfaces under conditions of dense functionalization with PEG-tris-NTA moieties. Additionally minor yet characteristic discrepancies have been observed for dissociation kinetics of IFNs labelled with the dyes differing in spectral range. They were manifested in the slightly faster (~2-3 times) dissociation of the red-labelled ligands owing to the properties of the attached dyes with respect to their charges.

Surface binding assays for interaction between labelled IFNαs and the individual receptor subunits confirmed that the functionality of interferons was not affected by insertion of N-terminal peptide tag as well as by the enzymatic fluorescent probe attachment, thus opening prospects for their application in further measurements.

2.3.6 Functional characterization of ybbR-tagged IFNAR1 on tris-NTA surfaces

In addition to the estimation of labelling efficiency, IFNAR1 fused to N- or C-terminal ybbR tags was functionally characterized by the standard surface-based ligand binding experiments with label-free receptor being immobilized onto tris-NTA-functionalized support.

First to test the functionality of the ybbR-fused receptor ectodomains in individual interactions with ligand, a solid-phase detection binding course was carried out for comparing proteins tethered to transducer via His-tags in the upward orientation. To that end of ybbR-IFNAR1-H10 and untagged FNAR1-H10 were immobilized through C-terminal His-tag in relatively high concentrations (50 nM both) to medium-density PEG 2000/tris-NTA chelating surface (Figure 2.9), similar to the assay described for fluorescent IFNs in 2.3.5. Binding of ^{AT488}IFNα2-YNS to receptor was monitored by TIRFS/RIf (not shown). For comparison, resulting YNS fluorescence binding curves (not shown) were normalized to the respective molar surface concentration (in fmol/mm^2) of the immobilized receptor. Comparison of these normalized ligand binding amplitudes reveals that binding signal for an interaction of ^{AT488}IFNα2-YNS with ybbR-IFNAR1-H10 comprises about 85.3% of the signal obtained for an interaction of ^{AT488}IFNα2-YNS with the wild type IFNAR1-H10. This confirms that the tag-fused receptor retained good activity since frequently IFNAR1-EC, as the most delicate protein in the ternary receptor complex, is prone to denature on the surfaces.

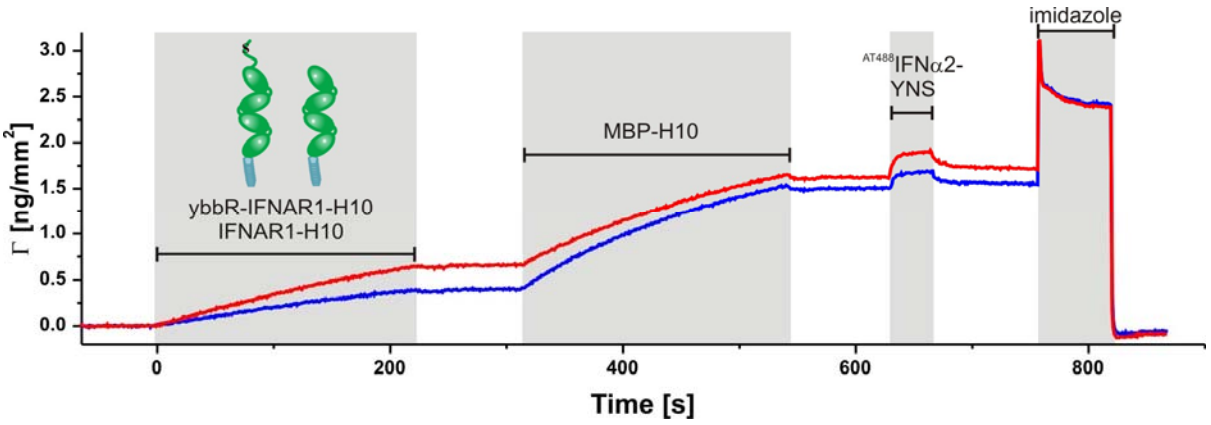

Figure 2.9 Typical binding course of ^{AT488}IFNα2-YNS interaction with ybbR-IFNAR1-H10 and with IFNAR1-H10 immobilized onto tris-NTA surface as monitored by RIf.

RIf mass channel trace with the sequential injection of the following proteins on tris-NTA surface: immobilization of 50 nM IFNAR1-H10 (red) or 50 nM ybbR-IFNAR1-H10 (blue), blocking of free chelators heads with 2 µM MBP-H10, binding of 500 nM ^{AT488}IFNα2-YNS, followed by complete surface regeneration with imidazole injection. The grey bars mark the injection periods.

For an assessment of binding kinetics parameters, due to relatively high surface receptor density, association and dissociation courses were fitted with a model taking into account mass transport limitations. The obtained binding constants are listed in Table 2.2. All fitted rate constants for an interaction of YNS with ybbR-IFNAR1-H10 lie within the range of the values estimated in this assay for the interaction with IFNAR1-H10. They are also in a good agreement with the constants obtained by previous measurements with wild type IFNAR1-H10 receptor on PEG-tris-NTA surfaces, accentuating thereby high integrity of the N-terminal ybbR-tag insertion.

Table 2.2 Binding constants of ^{At488}IFNα2-YNS on His10-tag-immobilized ybbR-IFNAR1-EC-H10 or IFNAR1-EC-H10.

Immobilized receptor	k_a [$s^{-1}\cdot M^{-1}$]	k_d [s^{-1}]	K_D [M]
50 nM ybbR-IFNAR1-EC-H10	3.99×10^{5}	0.033	8.35×10^{-8}
50 nM IFNAR1-EC-H10	5.06×10^{5}	0.027	5.94×10^{-8}
Error %	20	10	

In order to further explore the functionality of ybbR-tagged IFNAR1 ectodomain, the direct comparison of the receptors with N- and with C- terminal tag fusions was carried out in surface interaction experiments with IFNα2-YNS ligand (not shown) in the same manner as in the assay with IFNAR1-H10 described above. About 50 nM of ybbR-IFNAR1-H10 or 50 nM

of H10-IFNAR1-ybbR were immobilized under the same conditions as non-tagged IFNAR1-H10 in the previous assay and receptors were probed with 150 nM ^{AT488}IFNα2-YNS injection.

As before, for comparison fluorescence ligand binding curves were normalized to the molar surface concentrations (fmol/mm^2) of the respective immobilized receptors. Association and dissociation phases were fitted with a model taking into account mass transport limitations and the determined binding parameters are summarized in Table 2.3. The values of equilibrium dissociation constants and rate constants obtained for the interaction with ybbR-IFNAR1-H10 are very close to the once estimated for the H10-IFNAR1-ybbR. These binding constants are also in good agreement with the constants, estimated for the untagged IFNAR1-EC-H10 (Table 2.2).

Comparison of the ^{AT488}IFNα2-YNS relative binding amplitudes shows that ligand binding towards H10-IFNAR1-ybbR represents 84.3% of YNS binding to ybbR-IFNAR1-H10 immobilized in the upwards orientation. As it has been shown previously [13], the orientation of the IFNAR1-EC surface tethering through N- or C- terminal His-tag has no effect on the kinetic parameters of binary complex formation. However the fraction of active protein upon immobilization in different orientations has not been directly compared. Thus the slightly lower extent of YNS binding to H10-IFNAR1-ybbR might be attributed to either the C-terminal insertion of ybbR tag or to the inverted receptor orientation upon histidine tag-mediated surface immobilization.

Table 2.3 Binding constants of ^{At488}IFNα2-YNS on His10-tag-immobilized ybbR-IFNAR1-EC-H10 or H10-IFNAR1-EC-ybbR.

Immobilized receptor	k_a [$s^{-1} \cdot M^{-1}$]	k_d [s^{-1}]	K_D [M]
50 nM ybbR-IFNAR1-EC-H10	9.97×10^5	0.042	4.29×10^{-8}
50 nM H10-IFNAR1-EC-ybbR	7.05×10^5	0.043	6.16×10^{-8}
Error %	20	10	

Taken together, the characterization of IFNAR1-EC interactions with the high affinity mutant YNS on tris-NTA-functionalized surfaces indicates that IFNAR1 ectodomain retained good activity for ligand binding after ybbR-tag fusion to either of receptor termini.

2.3.7 Enzymatic surface immobilization specificity and activity of ybbR-tagged IFNs

In order to explore the potency of N-terminal ybbR-tag for covalent surface attachment and IFN functionality after the tag-mediated coupling, ligand enzymatic immobilization through this tag was tested. Both, wild type ybbR-IFNα2 and ybbR-IFNα2-YNS mutant were readily enzymatically coupled to CoA-functionalized maleimide surfaces in presence of Sfp transferase and their stability as well as binding activity to receptor subunits, were studied. In addition, with the help of this ligand immobilization technique, the influence of one receptor subunit on the binding behaviour of the other receptor subunit was explored in cooperativity assays in the subsequent section of this work 3.3.2.

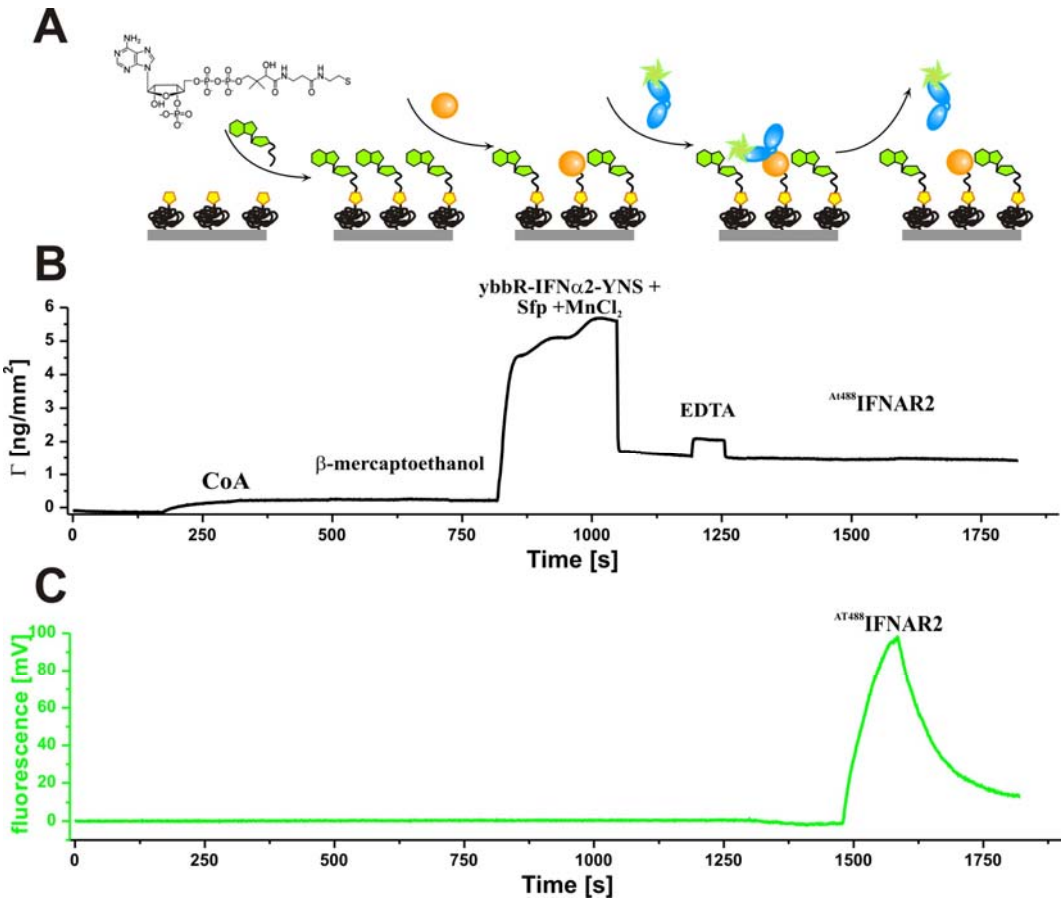

Figure 2.10 Standard binding assay for enzymatic coupling of ybbR-tagged IFNα2-YNS onto CoA-functionalized surface.

A Schematic description of the key reaction steps and binding sequence performed in the flow cell. **B** A typical RIf trace of the experiment. After *in situ* coupling of CoA (100 µM) to a maleimide-functionalized glass substrate, the remaining maleimide groups were saturated by injection of 1 mM β-mercaptoethanol. Subsequently, Sfp (1 µM) mixed with ybbR- FNα2-YNS (5 µM) in buffer containing 10 mM $MnCl_2$ was injected followed by a rinse with 25 mM. Immobilized ligand was probed by the injection of ^{AT488}IFNAR2-EC. **C** TIRF trace of the same injection sequence.

At first, to characterize binary complexes, immobilization specificity and stability of interferon covalent surface attachment were probed. To this end about 5 µM of ybbR-IFNα2 and ybbR-IFNα2-YNS was immobilized (Figure 2.10 B) to CoA-functionalized surface by means of Sfp as we've reported in [17]. A net amount of typically 1.0 ng/mm^2 protein was irreversibly attached by this procedure (Figure 2.10 B). Next, reversible binding of 20 nM ^{AT488}IFNAR2-EC to both ybbR-IFNα2 (Figure 2.10 A) and ybbR-IFNα2-YNS (Figure 2.10 C) was monitored by TIRFS.

Binding specificity was confirmed by a binding inhibition assay (Figure 2.11) with high concentration (500 nM) of free IFNα2 in solution mixed with receptor, reducing binding of ^{AT488}IFNAR2-EC close to the background signal (Figure 2.11 A). In addition, a negative control experiment was carried out with 1 µM Sfp and 10 mM $MnCl_2$ mixed in the absence of ybbR-IFNα2, and reacted to surface in solution. Subsequently it was probed by 20 nM ^{AT488}IFNAR2 injection, resulting in a fluorescence signal as low as background.

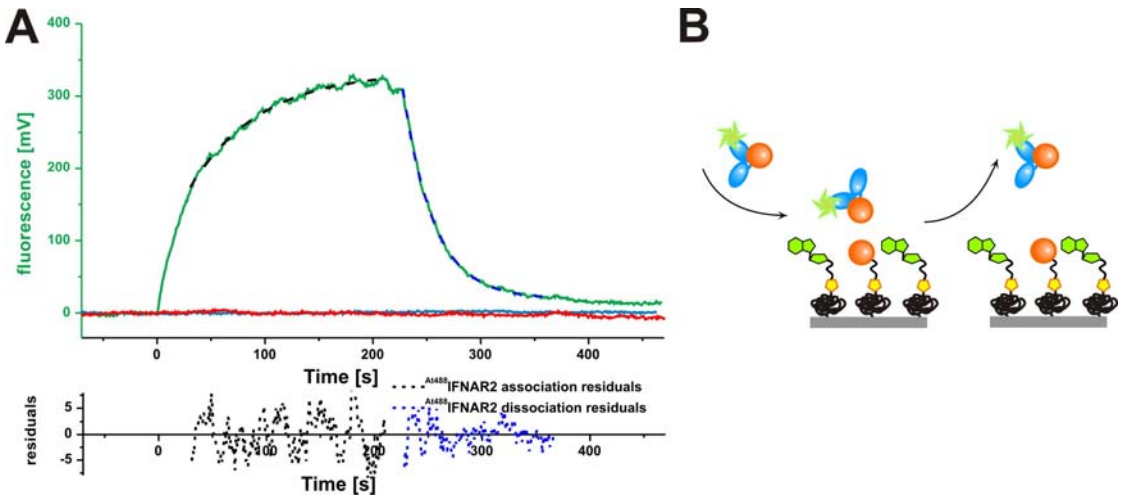

Figure 2.11 Enzymatic coupling of ybbR-tagged IFNα2 onto CoA functionalized surface probed by an interaction with IFNAR2-EC.

A Comparison of the 20 nM ^{AT488}IFNAR2 binding signal (green) to immobilized 5 µM ybbR-IFNα2 and for the negative control, 20 nM ^{AT488}IFNAR2 (cyan) injected after 1 µM Sfp mixed with 10 mM $MnCl_2$ without ybbR-tagged ligand as monitored by TIRFS. Additionally, binding specificity is shown by the inhibition assay (red), where 20 nM ^{AT488}IFNAR2 was directly mixed in solution with 500 nM IFNα2 and injected. ^{AT488}IFNAR2 association (black) and dissociation (blue) fits are shown as dashed lines with respective residuals in the lower panel. **D** Schematic illustration of the inhibition assay.

The stability of the immobilized IFNs was analysed with surface-coupled ybbR-IFNα2-YNS in a time period over 21 hour. Strikingly, nearly unchanged binding constants of 20 nM ^{At488}IFNAR2-EC binding (Table 2.4) were obtained 21 h after standard PPT-mediated coupling of 5 µM ybbR-IFNα2 (not shown) to transducer. The binding amplitude comparison

reveals that only about 42% of immobilized protein was active after 21 hour. However, all estimated rate constants are within the range of the once obtained for YNS/IFNAR2 interaction by other measurements on PEG/tris-NTA surfaces and in good agreement with the published literature values, highlighting the highly biocompatible enzymatic immobilization conditions. For immobilized ybbR-IFNα2-YNS mutant, which has an increased binding affinity towards IFNAR1, specific binding of ^{OG488}IFNAR1-EC to immobilized YNS ligand was observed (illustrated in Figure 3.6 C), confirming functional protein immobilization.

Table 2.4 Binding constants of 20 nM ^{AT488}IFNAR2-EC on 5 µM PPT-immobilized ybbR-IFNα2-YNS at time point 0 h and 21 h after immobilization.

Injection time course	k_a [$s^{-1} \cdot M^{-1}$]	k_d [s^{-1}]	K_D [M]
20 nM ^{AT488}IFNAR2, 0 h	5.82×10^5	0.022	3.84×10^{-8}
20 nM ^{AT488}IFNAR2, 21 h	7.33×10^5	0.027	3.66×10^{-8}
Error %	20	10	

Therefore these observations indicate that stable covalent highly biocompatible surface tethering of IFNαs through ybbR-tag fused to N-termini was achieved in an enzymatic reaction assay. By these means for the first time functional and durable binding activity of surface-immobilized interferons was retained over extended period of several hours after immobilization.

2.3.8 Combining peptide tags for functional surface coupling of ybbR-tagged IFNAR1-EC

The standard solid phase assays confirmed the ligand binding activity of His-tethered IFNAR1 ectodomains fused to N- or C-terminal ybbR tags. Tris-NTA-mediated protein anchoring is reversible and also not suitable for surface assays where the orthogonality to His-tag chemistry is required. Additionally, tris-NTA loading with Ni^{2+} ions creates potential sites for unspecific protein interaction with charged surfaces. In contrast, Sfp-mediated tethering provides an irreversible covalent chemistry though it suffers from rather slow reaction kinetics requiring relatively large protein concentrations for surface immobilization. To overcome these limitations an elegant approach of combined peptide tags was employed for highly efficient stable enzymatic surface immobilization of these receptor variants for subsequent probing their functionality by interactions with YNS ligand. YbbR-IFNAR1-H10 and H10-IFNAR1-ybbR receptor proteins were readily enzymatically coupled to

tris-NTA/CoA-functionalized chip by the novel two-step combined His-ybbR tag immobilization assay. This recently devised surface assay [22] was employed in order to overcome limitations of poor enzymatic immobilization efficiencies observed for IFANR2-EC with ybbR and S6 tags inserted at C-terminus [17]. It is based on subsequent rapid capturing of double-tagged protein through His-tag to surface. Then it is followed by more efficient Sfp transfer reaction for ybbR peptide covalent coupling owing to significantly increased effective local peptide tag concentration and thus the rate of the reaction.

To illustrate the two-step assay principle, EGFP carrying a tandem N-terminal hexahistidine tag followed by ybbR-tag (H6-ybbR-EGFP) was used in a control experiment (Figure 2.12 A) and monitored by TIRFS. Injection of 200 nM H6-ybbR-EGFP onto Ni^{2+} loaded surface resulted in 840 pm binding amplitude of His-tag-anchored EGFP. Subsequently a mix of 1 μM Sfp with 10 mM Mn^{2+} was injected to catalyse the reaction of the ybbR tag to neighbouring CoA moieties on surface. Upon rinsing injection of 250 mM imidazole with 250 mM EDTA equal amount (840 pm) of EGFP remained stably bound, confirming high efficiency of the employed immobilization approach.

In comparison to the control experiment, His-ybbR-tagged IFNAR1 ectodomains carry tags on the opposite termini. As it has been shown, binding constants obtained for binary complexes with IFNAR1-EC variants tagged on N and C-termini with H10-tag were unaffected by receptor surface tethering through double-decahistidine tag [13]. In this study ligand interaction with the receptor is probed after the His-tag and tris-NTA interaction is disrupted by Ni^{2+} elimination with rinse. After removal of the non-covalently bound fraction with imidazole/EDTA, receptor ectodomains ybbR-IFNAR1-H10 and H10-IFNAR1-ybbR remain stably captured to surface by means of ybbR tag, either in upward or inverse orientation. As illustrated on example of ybbR-IFNAR1-H10 (Figure 2.12 B), more than 750 pm of protein was anchored by His-tag when 100 nM protein was injected at the 1st step and after the enzymatic reaction and His-tag binding disruption during washing step, more than a half, about 410 pm of protein remained stably reacted to the surface. Under similar conditions, 290 pm and 250 pm respective amplitudes for His-tag and ybbR-tag immobilization of 100 nM H10-IFNAR1-ybbR were obtained on average, demonstrating even higher enzymatic immobilization efficiency by the combined-tag tethering strategy. In the same experiment no binding at all occurred after additional control injection of 3 μM H6-EGFP (not shown), confirming that all coordination interaction sites on surface were non-functionalized for His-tag capturing.

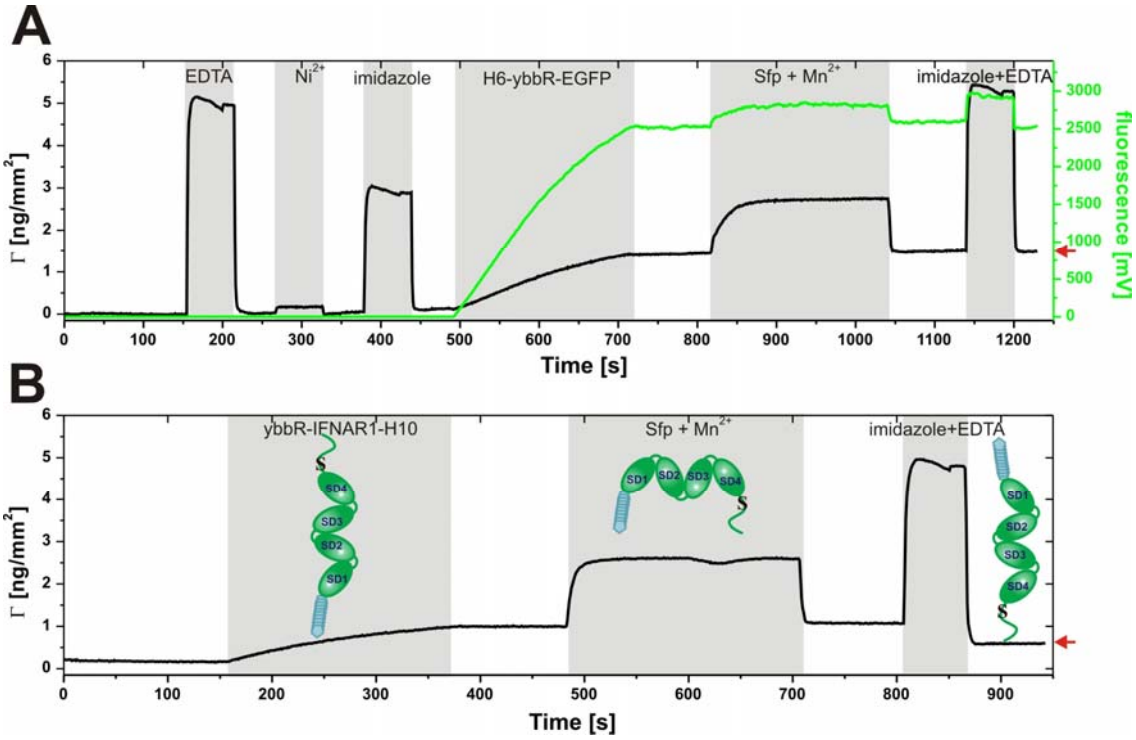

Figure 2.12 Two-step immobilization of His-ybbR tagged IFNAR1-EC monitored by TIRFS/RIf.

A Principle of the two step His-ybbR assay illustrated with His-ybbR-EGPF. Surface functionalized with tris-NTA and CoA groups is conditioned and loaded with metal ions by sequential injections of EDTA, Ni^{2+} and imidazole (black). His-tag immobilization of 200 nM H6-ybbR-EGFP followed by injection of 1 µM Sfp with 10 mM Mn^{2+}. Then His-tag interaction with chelators on surface is disrupted by an imidazole/EDTA (250 mM) rinsing step. The corresponding fluorescence TIRFS trace is shown in green. **B** RIf mass channel trace depicting binding of 100 nM ybbR-IFNAR1-H10 to Ni^{2+} loaded tris-NTA followed by the enzymatic covalent transfer reaction to CoA moieties on surface in presence of 1 µM Sfp with 10 mM Mn^{2+} with subsequent Ni^{2+} removal by an imidazole/EDTA injection. The arrows indicate the protein levels after wash with imidazole and EDTA. The grey bars mark the injection periods.

Then immobilized receptors were probed by a series of 150 nM ^{AT488}IFNα2-YNS injections and monitored by TIRFS/RIf. Resulting binging curves were fitted to the model taking into account mass transport limitations and the average binding constants values are summarized in Table 2.5. The dissociation rate constant estimated for YNS interaction (0.044 s^{-1}) with H10-IFNAR1-ybbR was identical to the constants derived for ligand binding to His-tag immobilized H10-IFNAR1-ybbR and ybbR-IFNAR1-H10 (Table 2.3), suggesting that the formation of the binary complex was not affected by the enzymatic receptor tethering through the C-terminal ybbR-tag. For the subunit ybbR-IFNAR1-H10 only slightly faster dissociation (0.034 s^{-1}) was observed compared to the dissociation from H10-IFNAR1-ybbR, however, this difference lies within the standard error for individual interactions measured for H10-IFNAR1-ybbR (Table 2.5).

Table 2.5 Binding constants of ^{AT488}IFNα2-YNS on ybbR-tag-immobilized ybbR-IFNAR1-EC-H10 or H10-IFNAR1-EC-ybbR.

Immobilized receptor	k_a [$s^{-1} \cdot M^{-1}$]	k_d [s^{-1}]	K_D [M]
100 nM ybbR-IFNAR1-EC-H10	8.30×10^5	0.034	4.09×10^{-8}
100 nM H10-IFNAR1-EC-ybbR	9.74×10^5	0.044	9.52×10^{-8}
Error %	20	10	

All equilibrium dissociation constants and association rate constants obtained for IFNα2-YNS interaction with ybbR-immobilized receptors were also in agreement with the values observed for His-tag captured proteins, corroborating toward that IFNAR1 ectodomain retains functionality after N- or C- terminal ybbR-tag-mediated surface coupling. Thus the approach to immobilize IFNAR1-EC carrying combined His-ybbR tags enabled not only to increase the efficiency of protein capture to surface. It also showed the utility of tags placed at different receptor termini for covalent immobilization and confirmed protein activity in quantitative receptor-ligand interaction assays.

2.3.9 Direct protein capturing assay from cell supernatants

A possibility to quickly analyse activity of proteins with introduced genetic modifications through their interaction with suitable binding partner without the need of prior purification would make this approach highly attractive. It can be especially beneficial for exploring recombinant proteins requiring multiple purification chromatographic steps such as IFNAR1 ectodomain isolated in soluble form from insect cell supernatants and taken here as a model protein. This assay should combine high throughput for direct selective surface capturing of IFNAR1-EC variants, enable quantification of their relative immobilized surface amount as well as encompass certain degree of chemical orthogonality to probe interactions with ligands labelled by different methods.

To fulfil those requirements, at first the wild type IFNAR1-EC and ybbR-tagged variants were generated as terminal decahistidine tag fusions, co-transfected into *Sf9* cells to produce baculovirus supernatants from generation P0 to P3 whereto expressed proteins are secreted in a soluble form. Subsequently viral expression supernatants of each generation were tested for specific His-tag-mediated protein binding to surface tris-NTA chelating moieties, followed by confirmation of receptor immobilization by an interaction with fluorescence-labelled high affinity YNS ligand and an injection of anti-IFNAR1 mAb. In addition, mAb provided means for quantification of the receptor surface loading levels.

A control binding course was carried out to confirm that detected surface signals upon direct immobilization from expression supernatants are unbiased of the unspecific interactions of other medium components (Figure 2.13). Previous observations have indicated the ability of some Sf-900™ II SFM (Invitrogen/Gibco) expression medium components to compete unspecifically with protein His-tags for interaction with nitrilotriacetic acid (NTA) moieties. To rule these out, the P1 IFNAR1-H10 expression supernatant diluted ~5 fold with HBS running buffer was injected onto a protein-repellent PEG polymer brush-supported surface, functionalized with tris-NTA multivalent chelating heads (MCHs) at medium density before and after (Figure 2.13 A) they were loaded with Ni^{2+} for selective His-tag capturing.

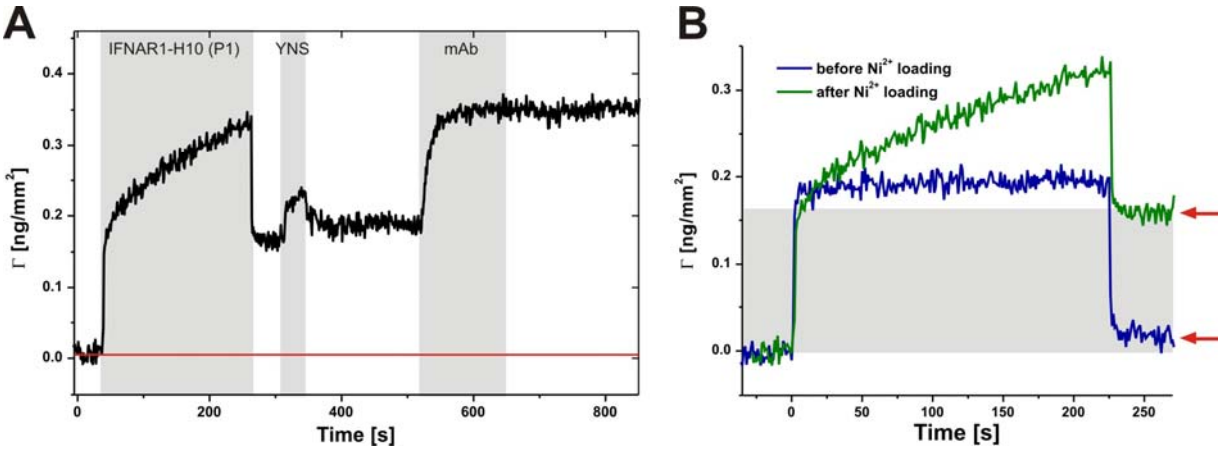

Figure 2.13 Selective His-tag-mediated direct surface capturing of IFNAR1 from cell supernatants.

A RIf binding course of specific IFNAR1-H10 surface immobilization from P1 cell expression supernatant. Supernatant containing expressed IFNAR1-H10 (diluted 5 × fold in HBS) is injected onto the conditioned surface tris-NTA groups preloaded with Ni^{2+} ions. Immobilized receptor is subsequently probed by the interaction with IFNα2-YNS ligand and mAb AA3 antibody. The surface amplitude after the Ni^{2+} loading and prior to the protein tethering is indicated by the red line. The grey bars mark the injection periods. **B** Specificity of the His-tag direct surface capturing by Ni^{2+}-loaded tris-NTA groups. Binding of IFNAR1-H10 from P1 supernatant to tris-NTA before (blue) and after functionalization with Ni^{2+} ions (green). The arrows indicate the protein levels with and without Ni^{2+}-loading. The grey box indicates the surface level of the specifically immobilized IFNAR1-H10. Note that during injection of medium-containing samples, a high transient background signal is observed due to change in the refractive index.

Comparison of the resulting immobilized protein levels reveals (Figure 2.13 B) significantly higher mass channel amplitudes obtained after the surface loading with Ni^{2+} and nearly a background level of the unspecific binding obtained without the loading. Typically during injection of medium-containing samples a high transient background signal was observed due to change in the refractive index. Additionally, specific immobilization of IFNAR1 onto tris-NTA/ Ni^{2+} chelators was probed by subsequent injections of IFNα2-YNS ligand and mAb

AA3 anti-IFNAR1 antibody (Figure 2.13 A), confirming thereby that the obtained mass signal is due to the receptor immobilization. For comparison YNS and mAb AA3 were injected after the supernatant injection onto the surface without prior Ni^{2+} loading, resulting in the same binding amplitudes as the background level (not shown).

In an additional specificity control experiment H6-EGFP from expression supernatant was directly captured via His-tag only after the MCHs were loaded with Ni^{2+} and fluorescence signal resulting from H6-EGFP immobilization was detected at TIRFS channel (not shown). Finally, for negative control, undiluted Sf-900™ II medium was injected directly onto functionalized transducer before and after Ni^{2+} loading resulting in each case in a minute increase of the binding amplitude close to the background level. This indicates markedly low unspecific interaction of medium components with Ni^{2+} ions on this type of surfaces.

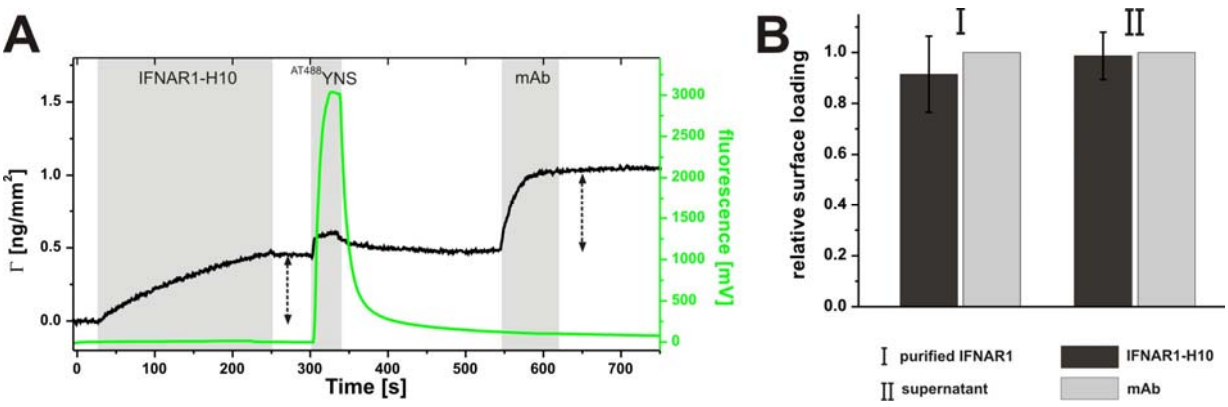

Figure 2.14 IFNAR1-H10 surface quantification by anti-IFNAR1 mAb AA3 antibody.

A Typical binding course of IFNAR1-H10 surface amount quantification. As example, recombinant IFNAR1-H10 (20 nM) is specifically anchored to tris-NTA surface and subsequently probed by ^{AT488}IFNα2-YNS (100 nM) and mAb AA3 antibody (30 nM). For illustration, respective fluorescence TIRFS trace is shown in green. The amplitudes of immobilized IFNAR1-H10 and bound mAb AA3 are indicated by the arrows. The grey bars mark the injection periods. **B** Correlation of protein surface amount and antibody amplitudes obtained for purified IFNAR1-H10 (I) and for direct IFNAR1-H10 capturing from P2 cell supernatant (II). Mass signals are normalized to respective mAb AA3 antibody amplitudes.

Concentration of soluble IFNAR1-EC in the cell supernatants can not be assessed by direct methods prior to the surface immobilization. Next, by calibrating the assay with purified IFNAR1-H10 we can demonstrate the receptor surface amount quantification with mAb AA3 antibody. Wild type IFNAR1-H10 was immobilized at different concentrations onto Ni^{2+}-loaded tris-NTA surface and subsequently probed by the injections of ^{AT488}IFNα2-YNS and AA3 antibody (Figure 2.14). Under the applied experimental conditions the correlation of mass amplitudes for the tethered receptor and bound AA3 mAb antibody corresponded to slightly less than one-to-one binding signals (Figure 2.14). Taking into account molecular

weight of the antibody and ~55 kDa for the IFNAR1 glycosylated form, this observation implies that one Ig molecule binds 2 receptors on average.

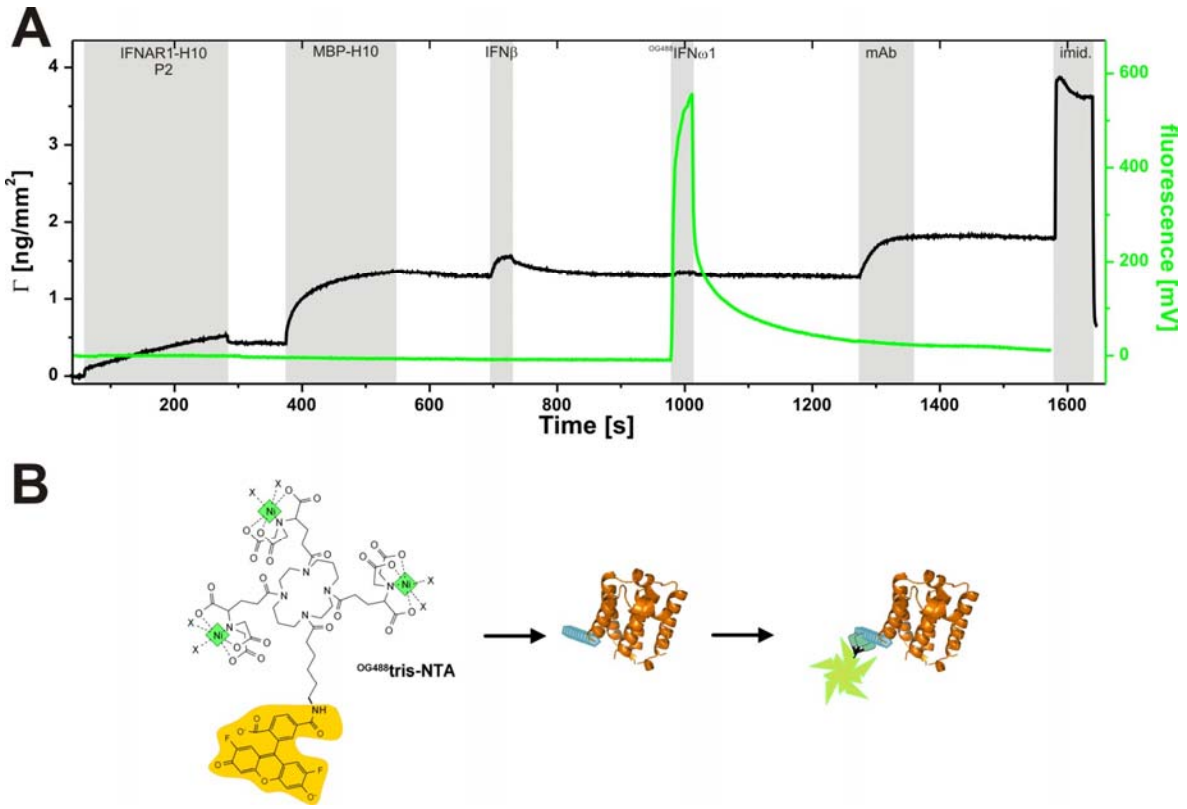

Figure 2.15 IFNAR1 direct immobilization and interaction with various type I IFNs.

A Typical binding course of IFNAR1 interaction assay with various type I IFNs as detected by TIRFS/RIf. As example, wild type IFNAR1-H10 P2 baculovirus supernatant (x5 fold dilution in HBS) is specifically anchored to tris-NTA surface and subsequently probed by IFNβ (500 nM), ^{OG488}IFNω (500 nM) and mAb AA3 antibody (50 nM), followed by surface regeneration with imidazole. For illustration, respective fluorescence TIRFS trace is shown in green. The grey bars mark the injection periods. **B** Chemical structure of ^{OG488}tris-NTA and schematic drowsing of its multivalent interaction with the histidine tag of IFNω.

The same good correlation for the surface amplitudes was achieved in the assays, carried out with 5-10 nM IFNAR1-H10 premixed with the expression medium (not shown) and with IFNAR1-H10 cell supernatant from P2 baculovirus generation (Figure 2.14), confirming that the devised approach can be used for the relative quantification of immobilized receptor amount. Interestingly, low unspecific binding enables to estimated relative immobilization from direct protein capturing demonstrating that an antibody is not even required for quantification by this technique. Moreover, as an extension of this assay, protein quantification was also possible for cell supernatants containing ybbR-tagged and single-point mutants of IFNAR1 confirming thereby the generic applicability of this approach.

Having this direct capturing assay in hands, receptor interaction can be explored with various IFN ligands in label-free as well as in fluorescence assays. In addition to the binding of ybbR-IFNα2-YNS enzymatically labelled with ATTO488 (Figure 2.14) receptors were probed by injections of IFNβ (Figure 2.15) and H8-IFNω reversibly labelled by ^{OG488}tris-NTA incorporated *in situ* through the His-tag [7]. However this assay on PEG/ Ni^{2+}-tris-NTA surface lacks the full orthogonality due to the His-tag-mediated labelling chemistry of IFNω. To overcome this limitation the excess of free functionalized chelator groups on surface was fully blocked with MBP-H10 prior to the ligand injections and thus no significant non-specific binding of IFNβ or IFNω was detectable. Further, full orthogonality can be achieved by devising a direct coupling of ybbR-tagged receptors from expression supernatants through covalent enzymatic surface immobilization chemistry.

This established rapid method of direct protein immobilization from cell supernatants showed simplicity and working efficiency. We can quantify the relative receptor loading on the surface as well as to probe binding of IFNAR1 by different type I IFNs in label-free and fluorescence assays.

2.4 Conclusions

Site-specific protein labelling with small molecule probes and covalent biocompatible surface immobilization is highly demanded for numerous analytical and biotechnological applications. Although several strategies are currently available for functional protein labelling through chemical modification of the exposed residues or through affinity groups, very generic approach is needed for efficient irreversible single-labelling of any protein of interest in the study. As demonstrated here, PPTase-based probe transfer is very simple and robust method to achieve this aim. One-step enzymatic probe conjugation to a short peptide tag inserted at protein termini was performed in order to modify proteins with a variety of small-molecule probes. Under physiological conditions, the transfer of phosphopantetheinyl moiety from CoA-small-probe conjugate to a specific serine of a short 11-residue ybbR tag fused to different proteins was achieved with more than 75% average efficiency. The generic nature of this labelling approach was demonstrated by using it to efficiently attach divers small molecule probes, including biotin and various fluorophores from custom-made CoA conjugates with AF568, ATTO565, AF594, and ATTO655. Moreover, this high efficiency of reaction was achieved for modifying peptide tags inserted at both, N- or C- protein termini. This labelling method is chemically orthogonal to the cysteine-based approach and can be successfully employed for dual-colour fluorescence protein labelling. Labelled proteins were

confirmed to be active by studying their interactions in ligand-receptor binary complexes. In addition, protein tagging with short peptides for posttranslational enzymatic modification provided means for biocompatible protein surface immobilization in a covalent manner. In a devised bottom-up assay with IFNs stably immobilized to surface their biological functionality was confirmed by probing interaction with each of receptor ectodomains. The combination of His-tag with ybbR-tag was reported to provide enzymatic surface covalent immobilization of fusion receptor proteins with much higher efficiency than the individual reactive recombinant peptide tags. Finally, rapid immobilization solid phase assay have been devised to efficiently and selectively capture receptor proteins directly from cell expression supernatants and to quantify their relative surface amount as well as to explore subsequently interaction of IFNAR1 with various IFNs in fluorescence assays. This assay can be further extended to achieve full orthogonality to His-tag chemistry by enzymatic immobilization of ybbR- or His/ybbR-tagged proteins directly from expression supernatants.

2.5 Summary

We presented a generic technique for posttranslational modification of short recombinant peptide tags fused to proteins using enzymatic transfer reaction. Small-molecule probes or functionalized surfaces coupled through a phosphopantetheinyl linker to CoA moiety serve as substrates in this reaction. Interaction assays between IFN and individual receptor subunits confirmed the high degree of activity of enzymatically labelled and surface-attached proteins. Direct surface protein immobilization assay for selective His-tag capturing from cell supernatants enabled rapid quantitative tethering of receptors and probing their interaction with various IFNs labelled by different fluorescent approaches.

2.6 References

1. Klaus, W., et al., *The three-dimensional high resolution structure of human interferon alpha-2a determined by heteronuclear NMR spectroscopy in solution.* Journal of molecular biology, 1997. **274**(4): p. 661-75.

2. Jaks, E., et al., *Differential receptor subunit affinities of type I interferons govern differential signal activation.* Journal of molecular biology, 2007. **366**(2): p. 525-39.

3. Gavutis, M., et al., *Determination of the two-dimensional interaction rate constants of a cytokine receptor complex.* Biophysical journal, 2006. **90**(9): p. 3345-55.

4. Strunk, J.J., et al., *Probing protein conformations by in situ non-covalent fluorescence labeling.* Bioconjugate chemistry, 2009. **20**(1): p. 41-6.

5. Strunk, J.J., et al., *Ligand binding induces a conformational change in ifnar1 that is propagated to its membrane-proximal domain.* Journal of molecular biology, 2008. **377**(3): p. 725-39.

6. Reichel, A., et al., *Noncovalent, site-specific biotinylation of histidine-tagged proteins.* Analytical chemistry, 2007. **79**(22): p. 8590-600.

7. Lata, S., et al., *High-affinity adaptors for switchable recognition of histidine-tagged proteins.* Journal of the American Chemical Society, 2005. **127**(29): p. 10205-15.

8. Goldman, L.A., et al., *Characterization of antihuman IFNAR-1 monoclonal antibodies: epitope localization and functional analysis.* Journal of interferon & cytokine research : the official journal of the International Society for Interferon and Cytokine Research, 1999. **19**(1): p. 15-26.

9. Yin, J., et al., *Genetically encoded short peptide tag for versatile protein labeling by Sfp phosphopantetheinyl transferase.* Proceedings of the National Academy of Sciences of the United States of America, 2005. **102**(44): p. 15815-20.

10. Zhou, Z., et al., *Genetically encoded short peptide tags for orthogonal protein labeling by Sfp and AcpS phosphopantetheinyl transferases.* ACS chemical biology, 2007. **2**(5): p. 337-46.

11. Piehler, J. and G. Schreiber, *Biophysical analysis of the interaction of human ifnar2 expressed in E. coli with IFNalpha2.* Journal of molecular biology, 1999. **289**(1): p. 57-67.

12. Griffin, A.M. and H.G. Griffin, *Molecular Biology: Current Innovations and Future Trends* 1997, Norfolk, UK Horizon Scientific Press. 176.

13. Lamken, P., et al., *Functional cartography of the ectodomain of the type I interferon receptor subunit ifnar1.* Journal of molecular biology, 2005. **350**(3): p. 476-88.

14. Kalie, E., et al., *An interferon alpha2 mutant optimized by phage display for IFNAR1 binding confers specifically enhanced antitumor activities.* The Journal of biological chemistry, 2007. **282**(15): p. 11602-11.

15. Lamken, P., et al., *Ligand-induced assembling of the type I interferon receptor on supported lipid bilayers.* Journal of molecular biology, 2004. **341**(1): p. 303-18.

16. Piehler, J. and G. Schreiber, *Mutational and structural analysis of the binding interface between type I interferons and their receptor Ifnar2.* Journal of molecular biology, 1999. **294**(1): p. 223-37.

17. Waichman, S., et al., *Functional immobilization and patterning of proteins by an enzymatic transfer reaction.* Analytical chemistry, 2010. **82**(4): p. 1478-85.

18. Yin, J., et al., *Site-specific protein labeling by Sfp phosphopantetheinyl transferase.* Nature protocols, 2006. **1**(1): p. 280-5.

19. Grimsley, G.R. and C.N. Pace, *Spectrophotometric determination of protein concentration.* Current protocols in protein science / editorial board, John E. Coligan et al., 2004. **Chapter 3**: p. Unit 3 1.

20. Lata, S. and J. Piehler, *Stable and functional immobilization of histidine-tagged proteins via multivalent chelator headgroups on a molecular poly(ethylene glycol) brush.* Analytical chemistry, 2005. **77**(4): p. 1096-105.

21. You, C., et al., *Self-controlled monofunctionalization of quantum dots for multiplexed protein tracking in live cells.* Angewandte Chemie, 2010. **49**(24): p. 4108-12.

22. Bhagawati, M., *Photolithographic surface functionalization for spatio-temporal control over protein immobilization*, 2011, University of Osnabrueck: Osnabrueck.

23. Thomas, C., et al., *Structural linkage between ligand discrimination and receptor activation by type I interferons.* Cell, 2011. **146**(4): p. 621-32.

24. Levin, D., D. Harari, and G. Schreiber, *Stochastic receptor expression determines cell fate upon interferon treatment.* Molecular and cellular biology, 2011. **31**(16): p. 3252-66.

25. Slutzki, M., et al., *Variations in the unstructured C-terminal tail of interferons contribute to differential receptor binding and biological activity.* Journal of molecular biology, 2006. **360**(5): p. 1019-30.

3 Energetics of the interferon/IFNAR1-EC binding

3.1 Introduction

Sixteen type I interferons initiate signalling through a shared extracellular receptor complex comprised of IFNAR1 and IFNAR2 subunits. Ternary complex assembly represents a sophisticated interplay of a three-body interaction involving a conformational change within two non-preassembled ectodomains and apparent fine-tuned communication with intracellular domains to relay signals from binding of various IFN subtypes for activation of different cellular responses. Various instances of differential activities of IFNs have been reported [1-3]. Generally all IFN subtypes differ only quantitatively in their potencies to induce Jak/STAT signalling cascade and antiviral responses, but some members show strongly different gene expression patterns and elicit further cellular responses much more potently than others. Few possible mechanisms conveying the IFN differential signalling have been speculated. Initially, specific, additional components of the receptor have been suspected to be responsible, but they have never been found. Lately the differential signalling was proposed to be governed by the subtle variations in the interaction mode of IFN subtypes with their receptor subunits IFNAR1 and IFNAR2. These differences can be manifested through the variations in general architecture of the signalling complexes, affinities towards individual receptor chains, in particular towards IFNAR1 [4], allosteric interactions as well as trough ligand binding site recognition chemistries.

The initial insights into the general architecture of the extracellular IFN/IFNAR1/IFNAR2 complexes with various ligands were provided by single particle negative stain electron microscopy imaging [5]. The low resolution structures of the ternary complexes (Figure 1.7) harboured two different interferon subtypes: HEQ, mutant of IFNα2 with increased affinity towards IFNAR1, and IFNβ. These images demonstrated strikingly similar structural arrangement of the complexes with these two IFNs. These findings corroborated that in both complexes the ligand interacts independently [6] with IFNAR1 and IFNAR2 on the opposite sites, forming with the three subdomains SD1-SD3 of IFNAR1-EC a broad binding interface, atypical for short cytokine receptors. Also in these two complexes the membrane-proximal domains of both receptor ectodomains, SD4 of IFNAR1 and D2 of IFNAR2 respectively, were shown to be very close, suggesting similar mechanism for bringing cytoplasmic kinases in proximity for their activation.

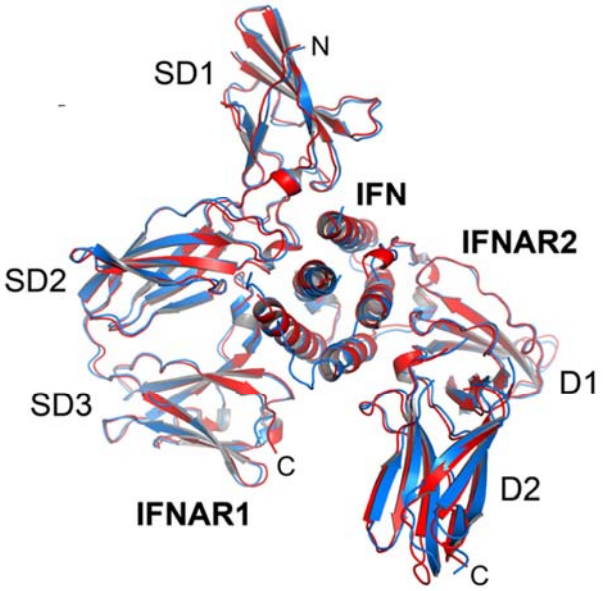

Figure 3.1 Architectures of the ternary complex observed for different type I IFNs.
Structures of type I IFN complexes: the IFN molecules of the IFNω (blue) and IFNα2-YNS (red) ternary complex X-ray structures are superimposed and shown in side view [7].

Recently the X-ray structures of two ternary extracellular complexes containing IFNω1 and IFNα2-YNS mutant [8], which binds IFNAR1 even tighter than HEQ, have been determined at good resolution [7]. Interestingly, despite the different physiological activities of the two ligands, the heterotrimeric receptor-ligand complexes share the same overall architecture (Figure 3.1). Upon superimposition of these two structures, the root-mean-square deviation (RMSD) of α-carbon atoms is 0.9 Å. However the membrane-proximal subdomain SD4 of IFNAR1-EC was not visible in the X-ray structures and its relative position in the complexes remained unresolved. IFANR1 binding mode and the relative orientation of its subdomains in the complexes represent a particular interest in the line with the hypothesis of the different roles of the two receptor subunits IFNAR1 and IFNAR2 in differential signalling. One of the proposed models poses that differential ligand affinities towards IFNAR1 result in differential stabilities of the ternary complex [4].

In all type I interferons, the binding affinity to the IFNAR1 receptor is much weaker (up to 1000-fold) compared with the binding affinity to IFNAR2 [1]. The large, energetically flat recognition interface of IFNAR1 enables the ligands to realize a broad range of binding affinities from 50 nM (IFNβ) to 5 μM (IFNα2) [1]. This raised the possibility that IFNAR1 has a special role in differential signalling by modulating the binding affinities of IFN subtypes. This hypothesis has been tested by changing the IFNα2 affinities towards individual receptor subunits [4, 8-10]. For this purpose, a panel of IFN muteins targeting either the IFNAR1 or IFNAR2 independent binding sites has been generated. This resulted in IFNAR1-

to-IFNAR2 binding affinity ratios ranging from 1:1000 to 1000:1. Interestingly, observations suggested that the differential cellular activity of interferons is related to the integral ternary complex binding affinity and not to the affinity towards individual receptor components [9, 10].

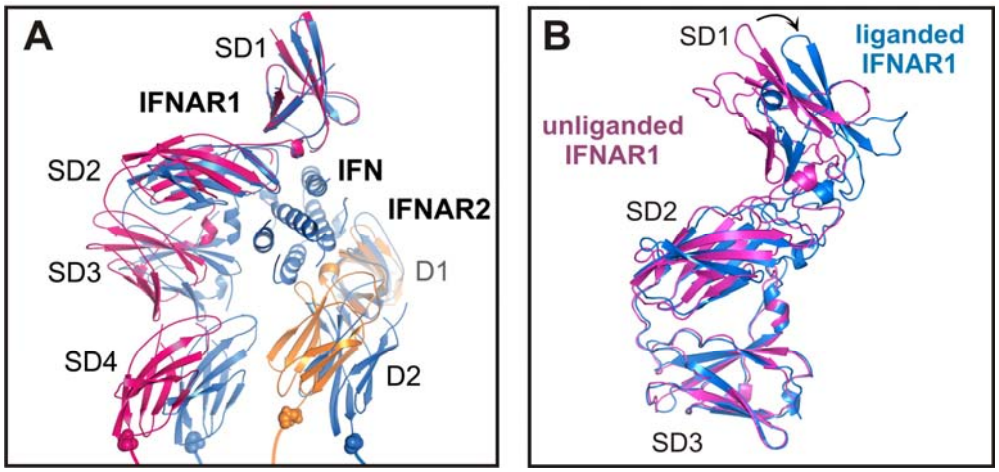

Figure 3.2 Ligand-induced conformational changes of IFNAR based on a comparison of unliganded and liganded structures.

A Overlay of the unbound (magenta and yellow) and bound (blue) X-ray ternary complex structures. SD4 of IFNAR1 was not visible in the X-ray structures and was modelled for clarity. **B** Conformational change in IFNAR1 upon IFN binding. Unliganded IFNAR1ΔSD4 (magenta) was superimposed onto subdomains 3 (SD3) of IFNAR1 (blue) from the X-ray ternary complex structure with YNS mutant. The difference in the position of the SD1 domain is depicted as an arrow.

Since the large and energetically weak ligand binding site of IFNAR1 does not play a role in the simple affinity-based modulation of cellular responses, it appears to be designed for the adoption of different conformations upon binding of different type I IFNs, which could be responsible for the differential activation of IFN-dependent signalling pathways.

Ligand-induced conformational change of IFNAR1 ectodomain was first demonstrated by FRET measurements [11, 12]. More recently the comparison of the X-ray structures of free IFNAR1ΔSD4 and in liganded ternary complex corroborated this conformational change of IFNAR1 occurring upon an interaction with a ligand (Figure 3.2). The superimposition of these two structures shows the movement of the N-terminal portion of the SD1 toward the ligand by nearly ~17 Å (Figure 3.2 B) and the relative SD2-SD3 conformational rearrangement which is propagated to the membrane-proximal subdomain SD4 (Figure 3.2 A). Since SD4 of IFNAR1 was not resolved in the X-ray structures it was modelled in accordance with the notion of SD1–SD2 homology to SD3–SD4 due to gene duplication. For some type I cytokine receptors membrane-proximal receptor domains have been shown to participate in the transfer of ligand-induced conformational change required for the activation

of cytoplasmic kinases. The key importance of SD4 of IFNAR1 in signalling was also shown by the inability of a chimeric IFNAR1 with SD4 being replaced with the corresponding domains of other class II cytokine receptors to form a ternary complex and to activate an IFN response [1]. The invisibility of the SD4 in the electron density maps of the ternary complexes indicates its flexible connection, thus implying that this subdomain potentially can have a role in the conformation-dependent activation of the type I IFN signalling complex.

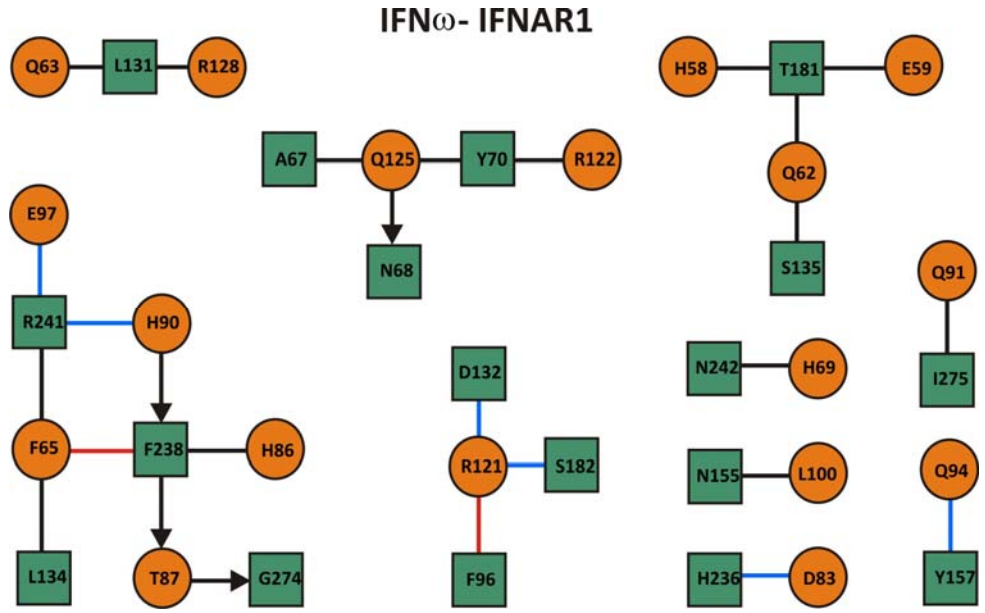

Figure 3.3 Two-dimensional interaction map of the IFNω-IFNAR1 interface in the IFNω ternary complex.

Amino acids are depicted as nodes in the interaction map (rectangles: IFNAR1: ellipses: IFNω). Solid lines represent side-chain/ side-chain interactions, backbone to side-chain interactions are represented by an arrow pointing towards the backbone. Black is for hydrophobic contacts, blue for H-bonds and red for aromatic interactions. Modified from [7].

As the observed type I IFN receptor complexes share similar general architecture and the conformation-dependent receptor activation upon binding various ligands is still speculative, thus, differential recognition of IFNs by the receptor subunits IFNAR1 and IFNAR2 must be responsible for differential activity. Initially, to obtain a thorough biophysical understanding of the relations between sequence, energetics and function, the interfaces of IFNα2, IFNω (and some other IFNs) for IFNAR1 and IFNAR2 were subjected to systematic alanine scanning mutagenesis, and the binding affinities and biological activities of the muteins were determined [7, 13, 14]. The high affinity IFNα2/IFNAR2 interface has been shown to contain a strong hotspot residue surrounded by a ring of residues contributing less. Conversely, only a single hotspot (R120) residue [15] was found on the binding site for IFNAR1, indicating the fragmented distribution of binding energies over large interface which may explain the low

affinity of IFNs towards IFNAR1. In particular, weak chemistry of the IFN/IFNAR1 binding interface could be responsible for the modulation of differential ligand discrimination and fine-tuning of the intracellular signalling responses. Several residues on the IFNAR1 binding site for ligand were proposed to be potentially involved in the differential recognition of IFN subtypes. This prediction was based on the two-dimensional interaction map (Figure 3.3) created by AquaProt server [16].

Thus, if functional discrepancy between IFNs in differential response is linked to their respective receptor recognition chemistries in concert with a ligand-induced conformational change in IFNAR1, it requires a comprehensive understanding of the structure, the energetics and the dynamics of the IFN/receptor interactions, explored on atomic level. This may offer new insights into the novel activation mechanism of distinct signalling pathways by a single receptor.

3.2 Materials and methods

3.2.1 Materials

Synthetic stearoyl-oleoyl phosphatidylcholine (SOPC) lipids were purchased from Avanti Polar Lipids (Alabaster, AL, USA). Chelator lipid analogues based on a bis-NTA chelator head group [17] and tris-NTA conjugate with OG488 (^{OG488}tris-NTA) [18] were revisited from the previous studies. IFNβ (formulated Rebif 22 μg) was obtained from Serono GmbH, Unterschleißheim/Germany. IFNω1 was a kind gift from Christoph Thomas and K. Christopher Garcia, YNS-30A, YNS-33A, YNS-148A, YNS-153A mutants of IFNα2-YNS were provided by Gideon Schreiber and anti-human IFNAR1 mouse monoclonal mAb AA3 (Biogen) [19] by Erik Mogensen. Other common chemicals were purchased from Sigma Aldrich.

3.2.2 Construction of vectors

IFNα2, IFNα2-YNS and IFNAR2 carrying an N-terminal ybbR-tag (ybbR-IFNα2, ybbR-IFNα2-YNS and ybbR-IFNAR2) were cloned by insertion of an oligonucleotide linker coding for the ybbR peptide (DSLEFIASKLA) into the *Nde*I restriction site upstream of the corresponding gene in the plasmid pT72Cα2 as described in 2.2.2. Alanine site-directed mutagenesis of IFNAR1-H10 was carried out in pBAC-3 (Novagen) vector based on the common PCR site-directed mutagenesis protocol [20] with a pair of forward and reverse primers with a mismatch on either of oligonucleotides, and the obtained full vector length PCR products were reclosed by ligation. Control construct for rapid screening assay was

based on pBAC-3-IFNAR1-H10 where IFNAR-H10 was exchanged to H6-EGFP by insertion into *BamH*I and *Pst*I restriction sites downstream of the region encoding gp64 secretion signal peptide.

3.2.3 Protein production, purification and labelling

YbbR-IFNα2, ybbR-IFNα2-YNS, ybbR-IFNAR2 and tagless IFNα2-YNS and IFNAR2 proteins were expressed and purified by the same protocols established for IFNα2-YNS [8] and wild-type IFNAR2-EC [6, 21, 22]. These proteins were expressed in *E. coli*, refolded from inclusion bodies and purified by anion exchange and size exclusion chromatography as described previously [21]. Maltose Binding Protein with tag (MBP-H10) was expressed as a soluble fraction in *E. coli* and purified as described previously [18]. H10-tagged IFNAR1-EC and K113A mutant were expressed in *Sf*9 insect cells and purified by IMAC and gel filtration as described in [6]. Mutant receptor proteins IFNAR1-E111A-H10, IFNAR1-N155T-H10 and IFNAR1-N349C^{AT655}-H10 were revisited from the earlier studies [5, 11]. Subfragment of ectodomain IFNAR1-EC construct containing the three N-terminal fibronectin-like domains fused to a N-terminal H10-tag (SD123) was generated, as reported in [23] and tag-less IFNAR1-EC without H10-tag (IFNAR1-tl,) as in [11], respectively. YbbR-IFNα2-YNS and ybbR-IFNAR2 were labelled by PPT using CoA-AT488 and Sfp purchased from Covalys, according to the methodology established in 2.3.1 and in 2.3.2. Fluorescence non-covalent switchable labelling of His-tagged IFNω1 was carried out *in situ*, similarly to the procedure described in [18] by mixing H10-tagged protein with double molar excess of ^{OG488}tris-NTA conjugate and incubating for 5 min prior to running binding assay. ^{OG488}IFNAR1-N23C-EC-H10 was expressed, purified and labelled with Oregon Green-maleimide (OG488), as described in [11].

3.2.4 In vitro binding assays by solid phase detection

Binding assays on tris-NTA surfaces. Ligand binding to IFNAR1-EC mutants was probed in real time by using label-free RIf detection in combination with TIRFS as reported previously [11, 23]. These measurements were performed with a homebuilt setup as described earlier using continuous flow-through conditions and the 488-nm line of an Argon ion laser for the excitation of EGFP and AT488. All measurements were carried out in HBS (20 mM Hepes (pH 7.5), 150 mM NaCl, 0.01% Triton X-100, 50 μM EDTA).

For comparing the interaction of different type I IFNs, wild-type IFNAR1-EC, mutants and control EGFP were site specifically immobilized directly from the expression supernatants through their C-terminal His-tags onto the surfaces as described for isolated proteins in [6,

24]. PEG-modified tris-NTA transducers were prepared at medium-density of chelator heads [25] to minimize unspecific adsorption of expression medium components. Excess coordination sites were blocked by injecting 4 μM decahistidine-tagged maltose binding protein (MBP-H10) to avoid non-specific binding. Subsequently, 150 nM fluorescence-labelled IFNα2-YNS, 500 nM unlabelled IFNβ or *in situ* labelled 500 nM IFNω1 were injected in triplets, and binding was monitored in real time. For decreasing additional unspecific binding, IFNβ and FNω1 were mixed with 700 nM tagless IFNAR2 and injected. After monitoring the complete ligand dissociation course 100 nM anti-IFNAR1 antibody mAb AA3 was injected to quantify wild type IFNAR1 and mutants surface loading. Surfaces were regenerated by an injection of 500 mM imidazole in HBS to remove the protein, and subsequently, next immobilization and ligand binding experimental course was carried out.

Ternary complex assembly on lipid bilayers. Binding of IFNα2 to IFNAR1-EC and IFNAR2-EC tethered onto artificial membranes was monitored in real time by simultaneous TIRFS/RIf detection as described previously [26, 27]. Continuous membranes were obtained by fusing lipid vesicles (stearoyl-oleoyl phosphatidylcholine), which were doped with ~5 % lipids carrying tris-NTA head groups for tethering the receptor subunits [17] onto clean silica transducer slides. Ternary complex formation was probed via the ligand-induced conformational change of IFNAR1 [11]. For this purpose, IFNAR1-N349C-H10 was cysteine-specifically labelled with ATTO-655 (^{AT655}IFNAR1-H10), which is quenched by the proximal Trp347. Upon ligand binding, the accessibility of Trp347 is substantially reduced, leading to dequenching of the dye [11]. ATTO-655 was excited by a helium-neon laser (excitation power ~150 μW). For comparing different combined IFNα2 mutants targeting IFNAR1 and IFNAR2 binding, IFNAR2-H10 (~3.5 fmol/mm^2) and ^{AT655}IFNAR1-H10 (~2.5 fmol/mm2) were sequentially tethered onto the membrane. Subsequently, the ligand was injected (100–500 nM), and its dissociation was monitored under constant flow, followed by an injection of imidazole (500 nM) for removing all proteins from the surface prior to the next experiment.

Protein interaction probed on CoA-functionalized supports. For exploring the cooperativity of receptor subunits IFNAR1-EC and IFNAR2-EC about 5 μM of ybbR-IFNα2-WT or ybbR-IFNα2-YNS was covalently tethered in presence of Sfp and MnCl2 to CoA-functionalized surface as described in 2.2.7 and in [28]. Then, to explore the receptor subunit cooperativity, since YNS mutant binds both receptors with relatively high affinity, ybbR-IFNα2-YNS was probed with 20 nM injection of 20 nM ^{AT488}ybbR-IFNAR2-EC or 100 nM ^{OG488}IFNAR1-EC-H10, and their spontaneous dissociation was monitored under

constant flow or by rapid injection of buffer in negative control experiment. Alternatively, to explore the influence of different chasers on ^{AT488}ybbR-IFNAR2-EC dissociation, 500 µM IFNα2-WT alone was injected to suppress receptor rebinding or it was mixed with non-labelled receptor subunits: 3 µM IFNAR1-EC-H10, 3 µM IFNAR1-EC-tl or SD123 to investigate the effect of cooperativity, role of H10-tag or membrane-proximal SD4 respectively. To confirm positive cooperativity, dissociation of ^{OG488}IFNAR1-EC-H10 was probed by injection of buffer or in presence of 2 µM IFNAR2-EC-H10. In addition, cooperativity on immobilized wild type ybbR-IFNα2 was probed by binding 20 nM ^{AT488}ybbR-IFNAR2-EC and chasing with buffer injection, 500 µM IFNα2-WT or with 10 µM IFNAR1-EC-H10. The carried out chasing experiments, as well as the examined effects for each case, are summarized in Table 7.3.

3.2.5 Data evaluation

Ligand binding to individual receptor subunits was analysed with BIAeval 3.1 software, using the standard Langmuir models for fitting kinetic data. For comparison of binding affinities of IFN variants, binding signals from IFNβ were normalized to the amount of receptor loaded onto the surface. Dissociation constants K_D were determined from the rate constants according to Equation 3.1

$$K_D = \frac{k_d}{k_a} \qquad \textbf{Equation 3.1}$$

Where k_d – dissociation rate constant and k_a - association rate constant.

For analysing ternary complex kinetic data, the curves were drift-corrected by blank run subtraction, and the dissociation curves were fitted by a two-step dissociation model considering the two equilibria of the binary complexes IFNα2/IFNAR1 and IFN/IFNAR2 with the ternary IFNα2/IFNAR1/IFNAR2 complex [26]. The differential equations describing the two-step dissociation were fitted using Berkeley Madonna 8.0.1. The parameters for the interaction with IFNAR1 were kept constant for all IFNα2 mutants, and only the two-dimensional dissociation constant for the interaction with IFNAR2 on the membrane was varied. For the control assay probing the binary complex between ^{AT655}IFNAR1-H10 and the IFNα2 mutants, the dissociation curves were fitted by a monoexponential decay using BIAeval 3.1 software.

3.3 Results and discussion

3.3.1 Differential recognition of interferon/IFNAR1 binding interface by various type I IFNS

An attractive explanation of differential activation caused by different interferons would be their mode of binding to receptor ectodomains, which would be translated into differential intracellular activation. Since binding interface on IFNAR2 is rather conserved and consists of a few anchor spots overlapping for the most of IFNs, IFNAR1 is proposed to be the subunit performing the fine-tuned ligand discrimination. In order to obtain a comprehensive biophysical understanding of the relations between sequence, three-dimensional structure, energetics and function, we mapped the binding site for type I IFNs on IFNAR1-EC. The ligand-receptor interface was subjected to systematic alanine scanning mutagenesis by replacing single residues from the IFNAR1-IFN interaction interface and few residues in the contact between SD2-SD3 and by determining the binding affinities of obtained single mutants for interaction with IFNα/β/ω variants.

The selection of mutation positions on IFNAR1 was based on the two-dimensional interaction map prediction (Figure 3.3) for IFNω/IFNAR1 identified by AquaProt server [16], the first X-ray structural insights into the ternary complexes formed with IFNα2-YNS and IFNω, and on previously measured affinities for binding to IFNα2 [5, 11]. In total 15 residues from the ligand binding pocket and 2 positions on the contact between FNIII-like subdomains SD2-3 have been mutated (Figure 3.4 and Table 3.1).

Screening of the mutants required to establish a high throughput approach for identifying the key hotspot residues for the interaction with various IFNs. To probe the complex formation kinetics and assess relative binding affinities we employed TIRFS/RIf spectroscopy and direct surface capturing assay from cell supernatants devised in 2.3.9. IFNAR1-EC mutants carrying individual amino acid mutations were directly immobilized onto tris-NTA chelating surface from baculovirus P2 cell supernatants and binding was assessed for IFNβ, IFNω, and IFNα2-YNS, a triple mutant of IFNα2 (H57Y, E58N, and Q61S) that binds to IFNAR1 50-fold tighter than the wild type [8]. Interaction behaviour was monitored for IFNβ by label-free detection at RIf channel, and for fluorescence-labelled ^{AT488}IFNα2-YNS and ^{OG488}IFNω at fluorescence TIRFS channel as established in 2.3.9 and methodologically described in 3.2.4. The energetic contributions of amino acid residues in the binding interfaces of IFNAR1 and IFNs employed in the study are summarized in Table 3.1.

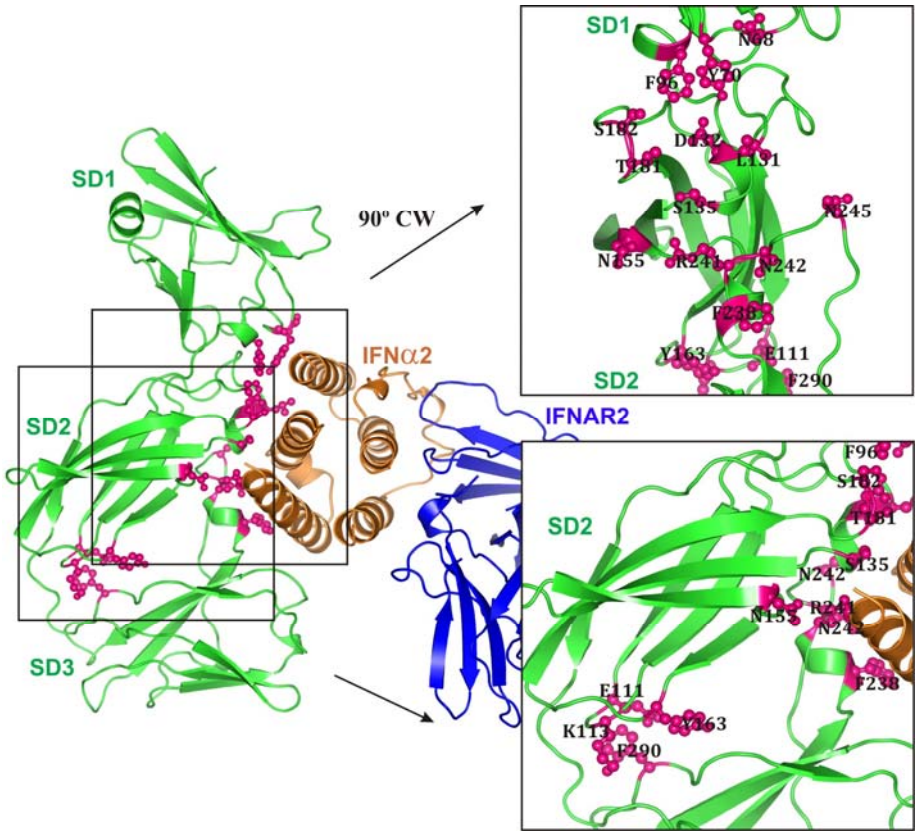

Figure 3.4 Mutagenesis of the IFN-IFNAR1 binding interface.

Illustration of the IFN-IFNAR1 interaction interface in the IFNα2-YNS ternary complex. Three FNIII-like subdomains of IFNAR1 (green) resolved by X-ray studies are designated as SD1-SD3, IFNα2-YNS is in orange, IFNAR2 is shown in blue. Mutated amino acids are depicted in pink. Upper right panel: close-up front view of the contact between SD1 of IFNAR1 and IFN. For clarity IFNα2 and IFNAR2 are not shown. Lower right panel: close-up side view of the contact between SD2-SD3 of IFNAR1 and IFN binding interface.

Analysis of IFNAR1 mutagenesis data shows a weak, broad overlapping interaction surface for the explored IFNα/β/ω variants which is diffused over the three membrane-distal subdomains SD1-SD3 (Figure 3.4). Though the N-terminal SD1 does not seem to form many contacts with ligand it has been demonstrated alone with the SD2 and SD3 to be necessary and sufficient for ligand binding [23], and that the SD1 segment spanning residues 62–70 is crucial for ligand binding and biological activity [29]. According to the superimposed X-ray structures of unliganded IFNAR1ΔSD4 and IFNAR1ΔSD4 of the ternary complexes it is apparent that the N-terminal SD1 domain and the SD2-SD3 portion of IFNAR1 move relative to each other upon IFN binding (Figure 3.2 A), allowing all three subdomains of IFNAR1 to contact the ligand.

Table 3.1 Influence of mutations in IFNAR1 receptor chain on binding affinity.

IFNAR1	IFNα2-YNS relative affinity[1]	IFNβ relative affinity[2]	IFNω relative affinity[3]	Int[4] IFNAR1
WT	1.0	1.0	1.0	
N68A	1.8	ND[5]	ND	+
Y70A	0.08	<0.1	<0.1	+
F96A	0.5	ND	ND	+
E111A	0.3	<0.1	ND	-
K113A	0.08	ND	ND	-
L131A	1.0	1.0	0.8	+
D132A	0.4	1.0	0.8	+
***S135A**	0.4	1.5	1.0	+
***N155A**	0.8	7.5	0.5	+
Y163A	0.5	0.6	1.6	-
T181A	1.3	1	2.5	+
S182A	1.5	-[6]	-	+
F238A	0.08	<0.1	<0.1	+
R241A	0.5	0.6	0.6	+
***N242A**	0.4	1,5	1	+
N245A	0.7	0.3	0.6	-
F290A	1.0	-	0.7	-

[1,2,3]Relative binding affinities (K_D mutant/ K_D WT) of IFNAR1 mutants towards IFNα2-YNS[1], IFNβ[2] and IFNω[3], respectively

[4]Interacting IFNAR1 residues located in the interface with IFNα2-YNS, IFNβ or IFNω are denoted with a "+" sign

[5]Binding not determined

[6]Binding not explored

*Mutations in IFNAR1 that differentially affect IFNα, IFNβ and IFNω

The SD1 domain shifts by about 17 Å down towards the ligand (Figure 3.2 B), bringing a hydrophobic patch containing Asn68^{R1}, Tyr70^{R1} and Phe96^{R1} in contact with helix D of the IFN ligand. Knocking off the Tyr70^{R1} results in a dramatic reduction of binding by more than >12 fold for IFNα2 (Table 3.1) and an abrogated binding for IFNβ and IFNω, clearly confirming this residue to be an interaction hotspot. Interestingly, for the mutations of Asn68^{R1} binding to IFNα2 was increased by almost 2-fold and for Phe96^{R1} reduced by 2-fold, whereas no interaction was detected for these mutants with other two IFNs. The aromatic rings of these two residues together with the side chain of Leu131^{R1} form a hydrophobic patch that packs against the ligand. However substitution of Leu131^{R1} does not change the receptor affinity to either of IFNs employed in the study. Phe238^{R1} located at SD2 of receptor appears to be another most important residue for the interaction of three IFNs with IFNAR1, stabilizing a hydrophobic interaction with the phenylalanine in the ligands. Replacing Phe238^{R1} in IFNAR1 results in 10 to 12-fold decreased binding for every of explored IFNs. As another example Lys113^{R1} is crucial for receptor interaction with all IFNs. Substituting Lys113^{R1} by alanine destabilizes binding more than any other mutation in IFNAR1, resulting in a high micromolar range affinity for the ligands. Though this critical residue is located far from the ligand binding site (Figure 3.4) at the contact interface of SD2 and SD3 of IFNAR1, mutagenesis clearly confirms its significance in stabilizing the overall ectodomain architecture and the hinge between these subdomains for forming the ligand binding pocket. Thus, these two hotspot residues, Tyr70^{R1}, Phe238^{R1} together with Lys113^{R1} are the only critical, shared anchor points for the ligand-binding on IFNAR1, representing its relatively energetically flat landscape compared to IFNAR2 binding surface and mediating IFN cross-reactivity.

In contrast, the mechanism of fine-tuned ligand discrimination by IFNAR1 appears to derive in large part from differential recognition of shared contact positions among the different IFNs. Comparison of the relative binding affinities revealed a number of residues that upon mutation differently affect binding to IFN subtypes (Figure 3.5). Most notable is Asn155Thr^{R1} that has no effect on binding of IFNα2 or IFNω, but increases the affinity towards IFNβ by 8-fold (resulting in a nanomolar-affinity interaction between these two proteins) [11]. Conversely, the IFNAR1 mutant Glu111Ala reduces the affinity towards IFNα2 by 3-fold and to IFNβ by >10-fold. A third residue is Asn242^{R1}, which, upon mutation into Ala, reduces the affinity to IFNα2 by two-fold, but increases the affinity to IFNβ by 50% and does not change the affinity towards IFNω. This difference may arise from the variation in chemical environments of Asn242^{R1}, participating in IFNω-IFNAR1 complex in a hydrophobic interaction with His71$^{\omega}$ which is replaced with a serine in IFNα2. Thus it appears that these

specific amino acids Asn155, Glu111 and Asn242 on the receptor confer different energetic contributions towards different IFN subtypes.

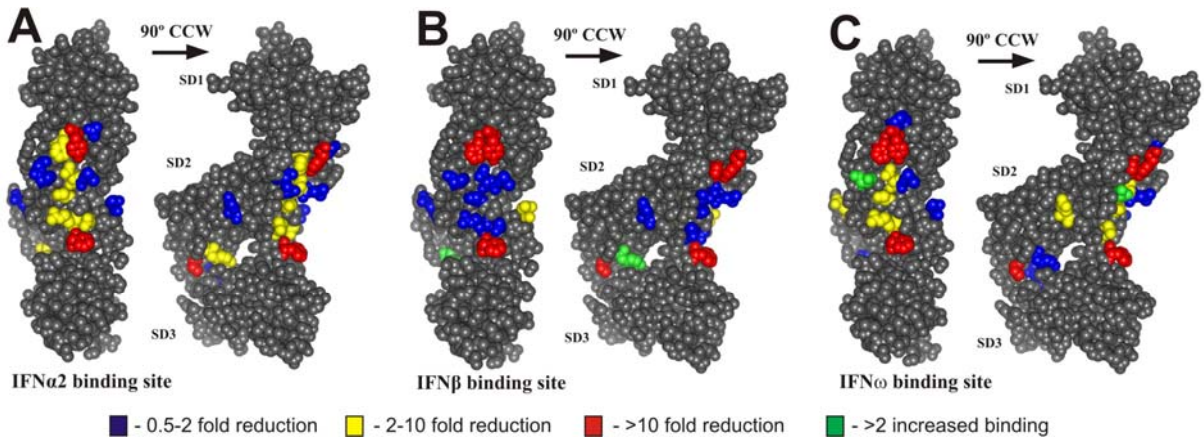

Figure 3.5 Type I IFNs bind competitive to the same functional interface on IFNAR1 but with distinct binding chemistries.

Alanine scanning of IFNAR1 binding site for IFNs. Residues involved in the interaction with different type I IFNS were mutated to alanine with an exception for N155T and schematically depicted on IFNAR1 X-ray structure. **A** Binding interface (left) and side-view (right) for IFNα2-YNS. **B** Binding interface (left) and side-view (right) for IFNβ. **C** Binding interface (left) and side-view (right) for IFNω. The two IFNAR1 representations are rotated by 90° contraclockwise with respect to each other. SD1-SD3 indicate three of four FNIII-like domains of IFNAR1-EC resolved by X-ray crystallography. Side chain colour-coding indicates relative (K_D mutant/ K_D WT) changes in the binding affinities upon mutation of residues.

All other substituted IFNAR1 residues were found to display minor role towards mediating the specific ligand-receptor interaction points and differential discrimination of ligand subtypes (Table 3.1).

The insights from mutagenesis data for IFNAR1 enable to elucidate the most prominent specificities of IFN/IFNAR1 binding. This interaction is conserved across type I IFNs through few critical ‘‘anchor points’’, identified on SD1-3, forming a diffuse and broad interface with the ligands. This fragmented distribution of binding energies may suggest that weak binding of IFNs to the IFNAR1 receptor chain is of biological importance, as it is conserved between the different ligand subtypes. Moreover, the observation that several IFNAR1 mutations to alanine differentially affect IFNα2, IFNβ and IFNω binding demonstrates that the specific ligand discrimination by IFNAR1 is related to differential recognition chemistries of shared contact residues on the IFN binding interface. Apparently it is evolved mechanism for optimizing binding affinities towards various IFN subtypes.

Overall, the mutagenesis data complement the structural findings and substantiate a hypothesis that the relatively large binding interface of IFNAR1 for IFNs involving 3 FNIII-

like subdomains mediates IFN cross-reactivity through conservation of interactions and in addition provides versatile means for fine-tuning the binding affinity towards different IFN subtypes for tailoring differential cellular response patterns.

3.3.2 Receptor binding cooperativity

Cooperativity is a phenomenon applied for receptors with multiple binding sites, where the affinity of the binding sites for a ligand is influenced upon ligand binding. Unlike for other cytokine ligand/receptor interactions including interleukin-6 gp130/IL-6/IL-6Rα hexameric complex [30] and interleukin-13 IL-13/IL-13Rα1/IL-4Rα1 signalling complex [31-33], cooperative binding for IFNα2/IFNAR1/IFNAR2 heterotrimeric complex had not been reported previously. Cooperativity would have far-going consequences for the signal transduction process since it would change the complex stability and therefore affect differential signalling. The non-overlapping independent interaction for IFNAR1 and IFNAR2 receptor subunits with interferon ligands is suggested by binding studies [6, 26, 34], EM imaging [5] and crystallography [7]. Subdomains on IFNAR2-EC designated as D1 and D2 and subdomains SD1-SD3 of IFNAR1-EC are involved and are essential for interaction with the ligands [5, 7, 23]. However the role of membrane-proximal SD4 of IFNAR1 is not uncovered by crystallography studies [7] since it was not visible in the electron density maps. Interestingly, in the negative stain EM-model reconstruction of the ternary complexes formed with IFNβ and high affinity interferon alpha 2 mutant HEQ (Figure 1.7), the membrane-proximal subdomains of the respective receptor subunits D2 and SD4 are shown to be in close proximity [5], so they potentially could participate in cooperative binding.

Based on the approach of functional covalent PPTase-mediated protein immobilization, an assay to quantitatively probe simultaneous binding of both IFNAR1-EC and IFNAR2-EC by TIRFS/RIf was devised. With this assay in hands, the influence of one receptor subunit on the binding behaviour of the other receptor subunit and possible role of receptor subdomains in it could be explored in order to elucidate receptor cooperative properties.

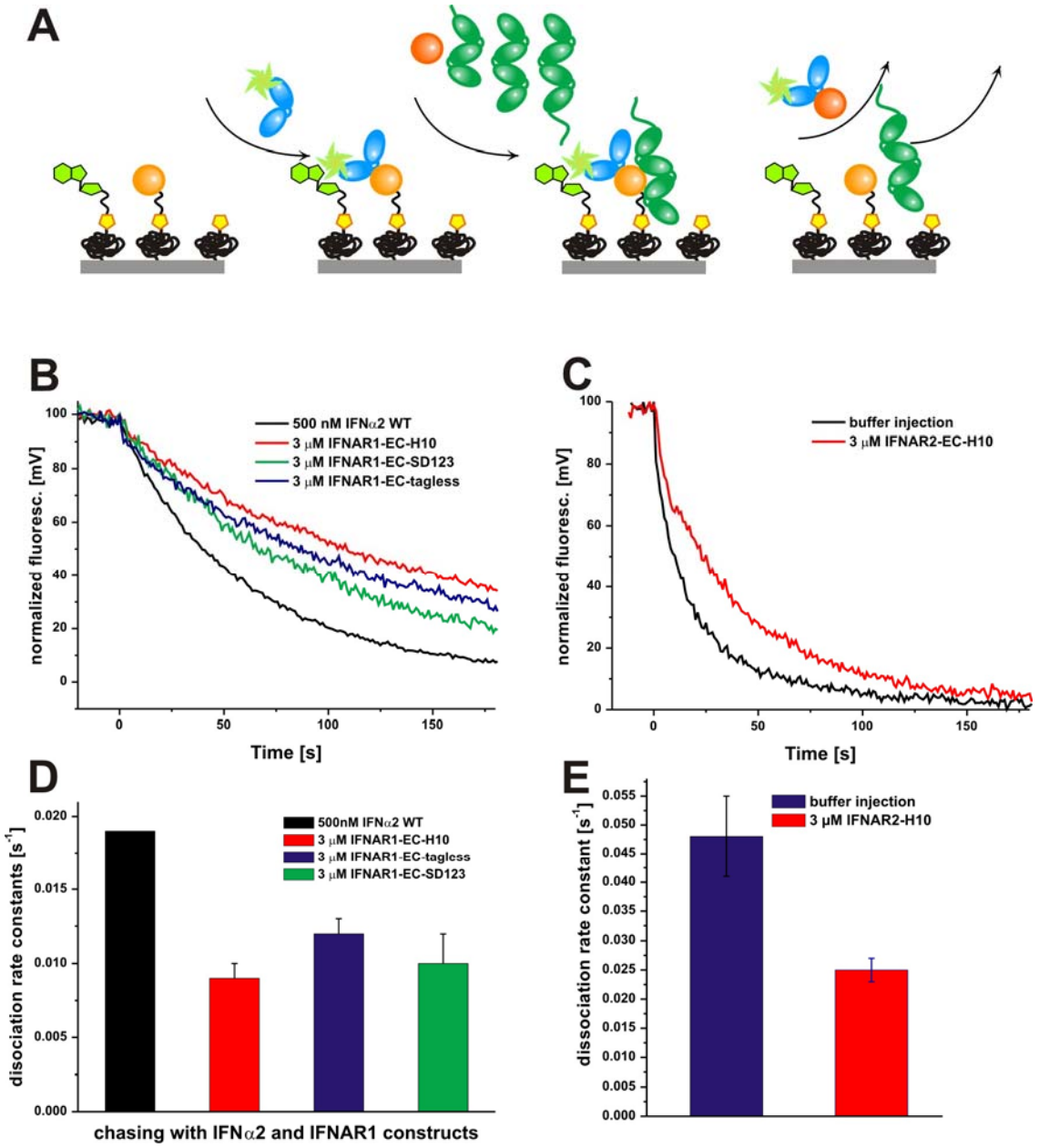

Figure 3.6 Binding cooperativity of IFNAR2 EC or IFNAR1 EC on ybbR-IFNα2 YNS.

A Cartoon representation of the ^{AT488}IFNAR2 chasing assay with different IFNAR-EC constructs. **B** Chasing of ^{AT488}IFNAR2. Normalized dissociation curves for chasing experiments of 20 nM ^{AT488}IFNAR2 bound to 5 μM ybbR-IFNα2-YNS followed by different chasers. **C** Chasing of ^{OG488}IFNAR1-H10. Normalized dissociation curves for chasing experiments of 100 nM ^{OG488}IFNAR1-H10 followed by injection of buffer (black) and IFNAR2-H10 (red). **D** Comparison of ^{AT488}IFNAR2 dissociation rate constants for different chasing experiments. **E** Comparison of ^{OG488}IFNAR1-H10 dissociation rate constants for chasing with buffer and IFNAR2-H10.

To this end we probed simultaneous binding of both receptors IFNAR2-EC and IFNAR1-EC to the PPT-mediated surface-coupled ligand by means of TIRFS/RIf.

Binding of fluorescence-labelled 20 nM ^{AT488}IFNAR2-EC to ybbR-IFNα2-YNS and dissociation were selectively detected by TIRFS similar to the surface enzymatic functional

immobilization assays (2.3.7). For probing ternary complex formation, dissociation of ^{AT488}IFNAR2-EC in presence and in absence of unlabeled IFNAR1-EC variants was measured (Figure 3.6 B). Relatively low surface concentration of immobilized ybbR-IFNα2-YNS was used and free, unlabelled IFNα2 wild type was added to suppress rebinding. Additionally, wild type interferon was mixed and injected during spontaneous dissociation phase with the full-length label-free IFNAR1-EC-H10 (Figure 3.6 B) or tagless IFNAR1-EC to exclude the possible artefact introduced by His10-tag on the observed effect. Furthermore, interferon with an IFNAR1-EC sub-fragment containing the three N-terminal fibronectin III (FN-III)-like subdomains SD123, which was previously shown to be required and sufficient for ligand recognition, was probed in the same manner. Comparison of ^{AT488}IFNAR2-EC dissociation with and without IFNα2 WT chasing yielded very similar values for constant (data not shown), therefore assuming that rebinding effect hardly took place. Dissociation rate constants obtained by fitting a standard Langmuir model to the dissociation curves, display significant changes (Figure 3.6 B and D), indicating that simultaneous binding of the second receptor subunit results in nearly two times (47%) tighter binging of ^{At488}IFNAR2-EC (Figure 3.6 D). The resulting change in k_d by a factor of 1.5- 2 was consistent for all tested IFNAR1-EC variants: IFNAR1-EC-H10, IFNAR1-EC-tl, IFNAR1-SD123, demonstrating that the observed cooperativity effect is not due to the artefact interaction with H10-tag or by contact with membrane-proximal subdomain SD4. Thus by employing in this analysis the C-terminally truncated IFNAR1-SD123 version, the role of SD4 in the ternary complex was additionally elucidated. The comparison of the fitted dissociation rate constants with standard deviations is summarized in the bar plot in Figure 3.6 D.

To examine whether the observed cooperativity effect is unilateral and was caused only by chasing ^{OG488}IFNAR2-EC with IFNAR1 constructs, the corresponding measurements by chasing ^{OG488}IFNAR1-H10 with IRNAR2 were carried out. Taking into account the lower association rate constant of IFNAR1 to IFNα2-YNS, the possibility of rebinding effect was considered to be low, and the measurements were carried out without presence of WT interferon in the chasing mix. Figure 3.6 C displays representative dissociation curves with chasing ^{OG488}IFNAR1-H10 on immobilized ybbR-IFNα2-YNS, chased with buffer injection or by unlabelled tagless IRNAR2. All dissociation rate constants are summarizes in Figure 3.6 E, demonstrating that ^{OG488}IFNAR-H10 dissociates from YNS ligand almost 1.8-2 times (46%) slower in presence of IRNAR2. The difference between obtained values lies within the range of the experimental error. In comparison with the measurements taken on IFNAR2 (Figure 3.6 E) it is evident that the observed cooperativity effect is interchangeable. Thus,

these little, but significant changes in the dissociation kinetics indicate that immobilized ybbR-IFNα2-YNS can simultaneously interact with IFNAR1-EC and IFNAR2-EC in a slightly cooperative manner.

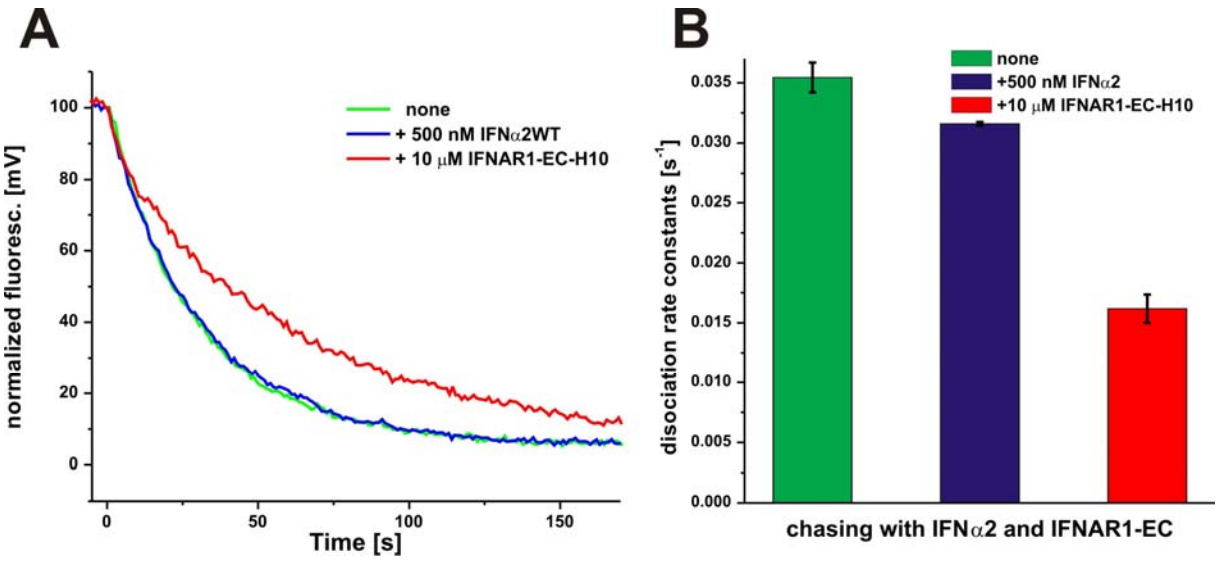

Figure 3.7 Binding cooperativity of IFNAR2-EC and IFNAR1-EC on IFNα2 WT.

A Chasing of ^{AT488}IFNAR2. Normalized dissociation curves for chasing experiments of 20 nM ^{AT488}IFNAR2 bound to 5 μM ybbR-IFNα2 followed by different chasers. **B** Comparison of ^{AT488}IFNAR2 dissociation rate constants for different chasing experiments.

Very similar results were obtained in the assay when wild type ybbR-IFNα2 was coupled by Sfp-enzyme transfer reaction to CoA-functionalized surface (Figure 3.7). YbbR-IFNα2 was immobilized the same way as shown in Figure 2.10 B, and dissociation of 20 nM ^{AT488}IFNAR2 was monitored in the absence and presence of 500 nM IFNα2 to suppress rebinding. Nevertheless, little to no rebinding took place. The binding affinity of wild type IFNα2 towards IFNAR1 lies within the micromolar range (~5 μM), so 10 μM unlabelled IFNAR1-EC-H10 was employed for ^{AT488}IFNAR2 chasing to probe cooperativity. In 4 independent chasing measurements nearly two fold k_d reduction from 0.0354 s^{-1} to 0.016 s^{-1} was detected (Figure 3.7 B), illustrating that small but significant cooperative complex stabilization is found for the WT ternary complex as well. This observation suggests that cooperative binding is not uniquely attributed to the ternary complex formed with YNS mutant, and hence, possibly, is not entirely influenced by ligand mutagenesis at positions His57Tyr, Glu58Asn, Gln61Ser.

Moreover, since the stabilization of the type I interferon ternary complex is not due to the interaction of the membrane-proximal subdomains of IFNAR1-EC and IFNAR2-EC, and no other contacts are shown in EM-based structural model and X-ray structure, we conclude that the receptor subunit cooperativity is mediated through the ligand. It appears that upon receptor

recruitment on the one side of ligand/receptor binding interface, small conformational rearrangement is propagated to the adjacent independent binding site for the second receptor subunit. Recent NMR study showed that IFNAR1 binding to the binary IFNα2/IFNAR2 complex affected IFNα2 residues contained in two large patches on the binding interface for IFNAR1 and in a third patch located on the face containing the IFNAR2 binding site [35], pointing towards the cross-communication between the binding sites for the two receptors upon ternary complex formation. Thus, the devised surface assay revealed ligand-mediated allosteric binding of two receptor ectodomains resulting in a change of complex stability which may have relevance for induced downstream signalling.

3.3.3 IFNAR1 conformational change

For the most of the IFNs the binding affinity to IFNAR2 is much higher (up to 1000-fold) compared with the binding affinity to IFNAR1. The overall affinity towards the ternary complex has been proposed to dictate the pattern of antiviral and antiproliferative cellular responses evoked by various type I IFNs [9]. To examine whether the IFN binding to individual receptors have differential role in signalling, a panel of Ala mutations targeting the IFNAR2 binding site has been generated in accordance with the notion of independent IFNAR1/2 binding sites on IFN. IFNα2-YNS mutant, which increases the affinity to IFNAR1 by 60-fold was used as a background to create four mutants on the IFNAR2 binding interface, including Leu^{30}, Arg^{33}, Met^{148}, and Leu^{153}. The cellular responses induced by these mutants are correlated with binding to the receptor measured *in situ* as well as with the affinities obtained *in vitro* for ternary complexes. To these ends ligand-induced conformational change of IFNAR1 was exploited as a readout of ternary complex formation on artificial membranes. We probed ternary complex assembly with combined IFNAR1/2 interferon mutants on lipid bilayers by simultaneous total internal reflection fluorescence spectroscopy-reflectance interference detection (TIRFS/RIf). IFNAR1-EC and IFNAR2-EC were tethered to the membrane via their C-terminal His10 tags, which were selectively captured by tris-NTA moieties embedded into the membrane, enabling lateral diffusion and ligand-induced ternary complex formation [6, 17, 26]. IFNAR1-EC N349C cysteine-specifically labelled with ATTO 655 (^{AT655}IFNAR1-H10) was used for probing binding. The ligand-induced conformational change of IFNAR1-EC strongly reduces the accessibility of Trp^{347}, leading to dequenching of the dye [11, 12].

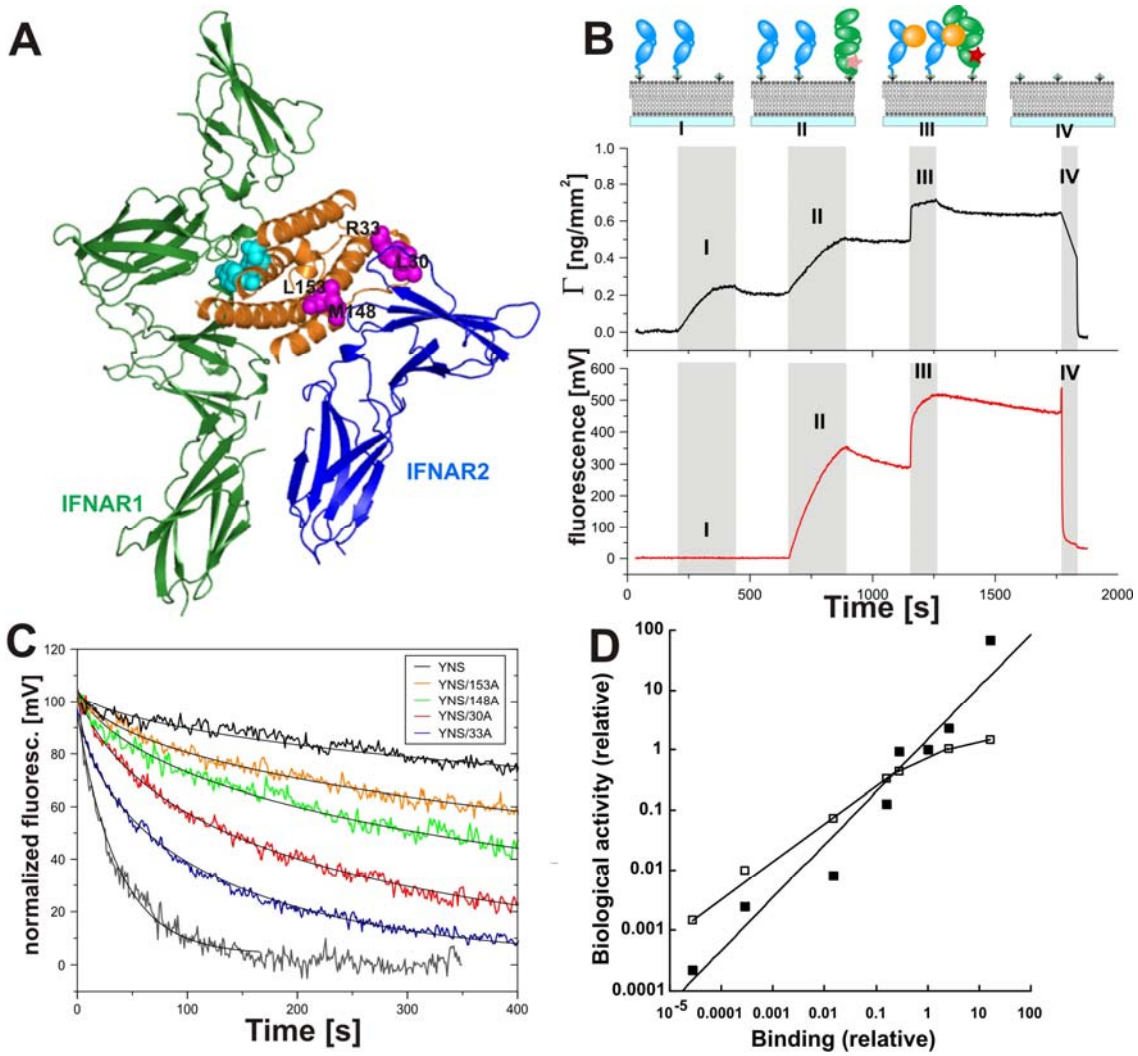

Figure 3.8 Ternary complex assembly and binding affinities.

A Structure of the YNS-IFNAR1-IFNAR2 ternary complex. Mutations facing IFNAR1 (YNS residues) are marked in cyan and mutations facing IFNAR2 are marked in magenta. **B** Typical binding course as detected by RIFs channel (black) and TIRFS channel (red). (I) tethering of IFNAR2-H10, (II) tethering of ^{AT655}IFNAR1-H10, (III) binding of IFNα2-YNS, (IV) removal of the proteins by imidazole. The grey bars mark the injection periods. **C** Ternary complex dissociation of IFNα2-YNS bearing mutations at the IFNAR2 binding site in comparison with the dissociation from IFNAR1-H10 alone. All experiments were carried out with ~2.5 fmol/mm^2 ^{AT655}IFNAR1-H10 and ~3.5 fmol/mm^2 IFNAR2-H10. Black lines correspond to the best fit by a two-step dissociation model. For comparison, dissociation of IFNα2-YNS/33A from ^{AT655}IFNAR1-H10 alone measured under the same conditions is shown in grey. **D** Correlation of affinities and activities of IFN mutants: relative biological potency measured in WISH cells *versus* relative *in situ* affinity of IFNα2 mutants. X axis, *in situ* binding affinity relative to wild type IFNα2. Y axis, antiproliferative (black squares) and antiviral (open squares) potency of combined IFNα2 mutants relative to wild type.

A typical assay is shown in Figure 3.8 B; after sequential tethering of IFNAR2-EC and IFNAR1-EC, the ligand is injected and detected by the increase in fluorescence of ^{AT655}IFNAR1-H10 undergoing conformational change. Whereas on the RIf channel, all ligand

binding to the receptor subunits on the membrane is detected, the fluorescence channel selectively detects binding to IFNAR1.

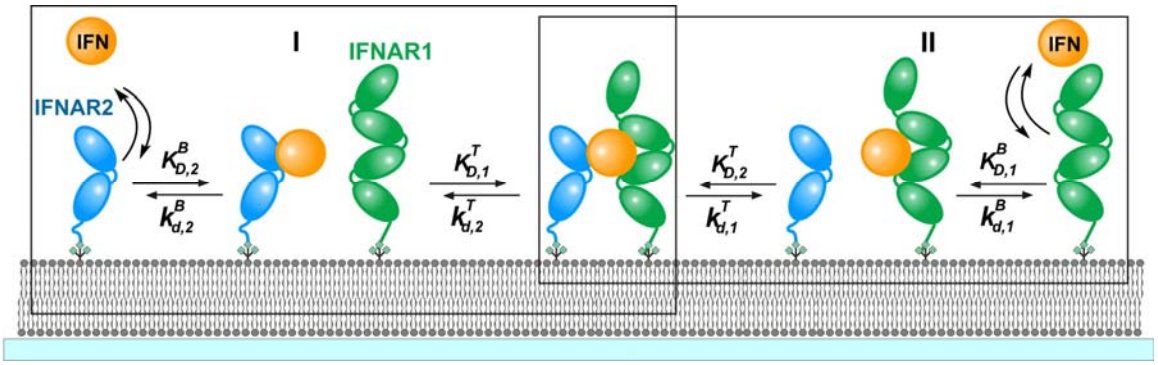

Figure 3.9 Dynamic equilibrium of IFN-YNS-induced ternary complex on artificial membranes. Schematic drawing of the IFN-YNS-induced assembly of the ternary complex, leading to a dynamic equilibrium between the binary IFN-IFNAR1 and IFN-IFNAR2 and the ternary IFN-IFNAR1-IFNAR2 complexes. The dynamics of the exchange of subunits is determined by the two-dimensional rate constants $k^T_{d,1}$ and $k^T_{d,2}$ [27]. The total binding affinity is determined by binary complex equilibrium constants $K^B_{D,1}$ and $K^B_{D,2}$ as well as the equilibrium between binary and ternary complex, which is determined by $K^T_{D,1}$ and $K^T_{D,2}$ and the receptor surface concentrations. Altering the binding affinities towards the receptor subunits will affect not only the total binding affinity towards the ligand but also the equilibria between ternary and binary complexes and the dynamics of the exchange. Two pathways are outlined by rectangles.

Fitting of the binding data assumed two-step dissociation model, considering the two equilibria (Figure 3.9) of the binary complexes IFNα2/IFNAR1 and IFNα2/IFNAR2 with the ternary IFNα2/IFNAR1/IFNAR2 complex [26]. The dissociation curves for different IFNα2 mutants from the ternary complex are compared in Figure 3.8 C. With decreasing affinity towards IFNAR2, faster dissociation from IFNAR1 in the presence of IFNAR2 is observed. On the contrary, in the absence of IFNAR2 on the surface, very similar dissociation from IFNAR1-EC was confirmed for all IFNα2-YNS mutants (not shown). Substantial stabilization of ligand binding by the presence of IFNAR2 was observed even for IFNα2-YNS/R33A (blue versus grey in Figure 3.8 C). Although the quenching of ^{AT655}IFNAR1-H10 is not directly related to the half-life of the ternary complex (since it is a measure of IFN-IFNAR1 binding), it is qualitatively related. Thus, the half-life extracted from the dissociation curves of the different mutants (Table 3.2) provides a measure of the stability of the ternary complex. Complex half-life and two-dimensional dissociation rate constants of an interferon-receptor interaction depend on the surface concentration of tethered receptors. A schematic representation of the dynamic stabilization of the ternary complex is presented in Figure 3.9.

Table 3.2 Stability of ternary complex formed with IFNAR1/2 combined mutants.

IFNα2	$t_{1/2}$ [s] (ternary complex)	Ratio[1] $t_{1/2}$ (mutant/WT)	IFNAR2	
			K_D [μM]	Ratio[1] (mutant/WT)
WT	400	1	0.002	1
YNS	1600	4.1	0.0014	1.4
YNS/L153A	600	1.5	0.019	0.11
YNS/M148A	310	0.79	0.087	0.023
YNS/L30A	140	0.35	1.8	0.0011
YNS/R33A	64	0.16	29	0.00007

[1] Ratios are relative to wild type IFNα2 (given in the first row).

SPR was used to explore *in vitro* the interaction of interferon mutants with each receptor individually [9]. It verified that the engineered panel of IFNα2-YNS-based mutants targeted IFNAR2 binding interface with the change in affinities in the range of ~1:10000 keeping the affinity to IFNAR1 unaffected. The relevance of the in *vitro* data was compared with the *in situ* binding of the various interferon mutants toward receptor on the cell surface using ^{125}I-labeled interferon. Relating the affinity values measured *in situ* on the cell surface to the affinities of IFNs to two receptors bound on artificial membranes (Figure 3.8 and Table 3.2) showed a good correlation between the data. The EC_{50} values also correlated well with the theoretically estimated affinity from the contribution of each receptor subunit (R1 × R2) to the additive affinity, corroborating independent ligand binding sites on IFNAR1 and IFNAR2.

The biological activity of different IFN mutants was tested in WISH cells in order to investigate the relations between affinities and the differential cellular responses. A very strict linear correlation between relative binding and antiproliferative potency (Figure 3.8 D) suggests that antiproliferative activity is foremost determined by the total ligand affinity, but not the particular affinity towards one of the receptor subunits. Thus, a simple additivity, rather than cooperativity in the binding of the two receptors takes place on the cell surface. Though we have previously observed slightly cooperative (1.5-2 fold change in k_d) interaction of receptor subunits on solid supports (3.3.2), apparently it is not relevant for cellular activity assays. In contrast, the antiviral activity correlates with the integral affinity only for low binding affinities (Figure 3.8 D). Several observations indicate that a mechanism more

complex than the sole factor of binding affinity dictates the antiviral cellular response. In general, biological potency of IFNs is proposed to be encoded by the dynamics of signalling complex formation which is a function of ligand affinity towards both receptors and concentration of all components at cell surface. Thus, a ternary complex stability on artificial membranes assessed through ligand-induced conformational change of IFNAR1 corroborated to the general model of various IFNs affinity-activity relation.

3.4 Conclusions

Through these experiments different aspects of the type I IFN receptor complex assembly were explored *in vitro* on solid supports. The formation of IFN/IFNAR1/IFNAR2 ternary complex is a dynamic interaction of three bodies, including differential energetics of IFN recognition by the two receptor subunits, ligand-mediated receptor-receptor cross-talk as well as the substantial conformational change upon the assembly. A detailed analysis of the residues involved in the IFNAR1 interaction with IFNα2, IFNβ and IFNω subtypes highlighted the complexity of IFN recognition. Unlike the IFN/IFNAR2 binding mediated through several strong conservative anchor points, IFNAR1 forms a more diffuse and weak interface with the IFNs. All interferons share similar mode of binding through two main critical conservative interaction hotspots on the IFNAR1 binding site for ligands, conferring subtype cross-reactivity. While the mechanism of ligand discrimination appears to derive from differential energetics of shared contact points. This likely reflects the fact that the IFN differential recognition chemistry by their receptor controls signal initiation and differential cellular response pattern. Kinetic investigation of the simultaneous binding of both receptor subunits to the ligand revealed small cooperative complex stabilization. This allosteric interaction appears to be not due to the stem-stem receptor contacts but mediated by the ligand conformational change and binding sites communication upon the ternary complex assembly. Apparently the observed little cooperativity is not relevant for cellular activity assays. Ligand-induced conformational change of IFNAR1 was taken as a reporter to probe the formation of ternary complex on artificial membranes. The explored stability of complexes with combined interferon mutants affecting binding to IFNAR1 and IFNAR2 suggested that the differential activity of IFNs is related to the total ternary complex affinity and not to affinity towards individual receptor subunits. This sophisticated mechanism of ligand recognition and receptor activation, involving IFN cross-reactivity versus differential discrimination and conformational change accentuate the complexity and uniqueness of IFN interaction with its receptor among other cytokines.

3.5 Summary

This section presented insights into the type I IFNs interaction with their cell surface receptor subunits IFNAR1 and IFNAR2. We elucidated binding chemistries of IFNAR1 that are conserved across IFN subtypes (i.e., "anchor points") versus those that would be ligand-specific. Differential energetics of interactions "tunes" the relative IFN binding affinities, serving as an apparent extracellular "ligand proofreading" mechanism that might modulate biological activity pattern. Formation of IFN/IFNAR1/IFNAR2 ternary complex involves conformational changes and a cooperative interaction of receptor subunits mediated through ligand binding sites cross-talk. Ligand binding-induced conformational change of IFNAR1 taken as a reporter enabled to assess ternary complex life times on artificial membranes. Exploring the stability of ternary complexes with IFNα2 combined IFNAR1/2 mutants *in vitro* corroborated to the suggestion that the total binding affinity of both receptors to interferon rather than affinity to individual subunits defines the pattern of cellular responses.

3.6 References

1. Jaks, E., et al., *Differential receptor subunit affinities of type I interferons govern differential signal activation.* Journal of molecular biology, 2007. **366**(2): p. 525-39.

2. Severa, M., et al., *Differential responsiveness to IFN-alpha and IFN-beta of human mature DC through modulation of IFNAR expression.* Journal of leukocyte biology, 2006. **79**(6): p. 1286-94.

3. Langer, J.A., *Interferon at 50: new molecules, new potential, new (and old) questions.* Science's STKE : signal transduction knowledge environment, 2007. **2007**(405): p. pe53.

4. Jaitin, D.A., et al., *Inquiring into the differential action of interferons (IFNs): an IFN-alpha2 mutant with enhanced affinity to IFNAR1 is functionally similar to IFN-beta.* Molecular and cellular biology, 2006. **26**(5): p. 1888-97.

5. Li, Z., et al., *The EM structure of a type I interferon-receptor complex reveals a novel mechanism for cytokine signaling.* Journal of molecular biology, 2008. **377**(3): p. 715-24.

6. Lamken, P., et al., *Ligand-induced assembling of the type I interferon receptor on supported lipid bilayers.* Journal of molecular biology, 2004. **341**(1): p. 303-18.

7. Thomas, C., et al., *Structural linkage between ligand discrimination and receptor activation by type I interferons.* Cell, 2011. **146**(4): p. 621-32.

8. Kalie, E., et al., *An interferon alpha2 mutant optimized by phage display for IFNAR1 binding confers specifically enhanced antitumor activities.* The Journal of biological chemistry, 2007. **282**(15): p. 11602-11.

9. Kalie, E., et al., *The stability of the ternary interferon-receptor complex rather than the affinity to the individual subunits dictates differential biological activities.* The Journal of biological chemistry, 2008. **283**(47): p. 32925-36.

10. Levin, D., D. Harari, and G. Schreiber, *Stochastic receptor expression determines cell fate upon interferon treatment.* Molecular and cellular biology, 2011. **31**(16): p. 3252-66.

11. Strunk, J.J., et al., *Ligand binding induces a conformational change in ifnar1 that is propagated to its membrane-proximal domain.* Journal of molecular biology, 2008. **377**(3): p. 725-39.

12. Strunk, J.J., et al., *Probing protein conformations by in situ non-covalent fluorescence labeling.* Bioconjugate chemistry, 2009. **20**(1): p. 41-6.

13. Yamamoto, K., et al., *Creation of interferon-alpha8 mutants with amino acid substitutions against interferon-alpha receptor-2 binding sites using phage display system and evaluation of their biologic properties.* Journal of interferon & cytokine research : the official journal of the International Society for Interferon and Cytokine Research, 2009. **29**(3): p. 161-70.

14. Runkel, L., et al., *Systematic mutational mapping of sites on human interferon-beta-1a that are important for receptor binding and functional activity.* Biochemistry, 2000. **39**(10): p. 2538-51.

15. Pan, M., et al., *Mutation of the IFNAR-1 receptor binding site of human IFN-alpha2 generates type I IFN competitive antagonists.* Biochemistry, 2008. **47**(46): p. 12018-27.

16. Reichmann, D., et al., *Binding hot spots in the TEM1-BLIP interface in light of its modular architecture.* Journal of Molecular Biology, 2007. **365**(3): p. 663-79.

17. Lata, S., M. Gavutis, and J. Piehler, *Monitoring the dynamics of ligand-receptor complexes on model membranes.* Journal of the American Chemical Society, 2006. **128**(1): p. 6-7.

18. Lata, S., et al., *High-affinity adaptors for switchable recognition of histidine-tagged proteins.* Journal of the American Chemical Society, 2005. **127**(29): p. 10205-15.

19. Goldman, L.A., et al., *Characterization of antihuman IFNAR-1 monoclonal antibodies: epitope localization and functional analysis.* Journal of interferon & cytokine research : the official journal of the International Society for Interferon and Cytokine Research, 1999. **19**(1): p. 15-26.

20. Griffin, A.M. and H.G. Griffin, *Molecular Biology: Current Innovations and Future Trends* 1997, Norfolk, UK Horizon Scientific Press. 176.

21. Piehler, J. and G. Schreiber, *Biophysical analysis of the interaction of human ifnar2 expressed in E. coli with IFNalpha2.* Journal of molecular biology, 1999. **289**(1): p. 57-67.

22. Piehler, J. and G. Schreiber, *Mutational and structural analysis of the binding interface between type I interferons and their receptor Ifnar2.* Journal of molecular biology, 1999. **294**(1): p. 223-37.

23. Lamken, P., et al., *Functional cartography of the ectodomain of the type I interferon receptor subunit ifnar1.* Journal of molecular biology, 2005. **350**(3): p. 476-88.

24. Lata, S. and J. Piehler, *Stable and functional immobilization of histidine-tagged proteins via multivalent chelator headgroups on a molecular poly(ethylene glycol) brush.* Analytical chemistry, 2005. **77**(4): p. 1096-105.

25. You, C., et al., *Self-controlled monofunctionalization of quantum dots for multiplexed protein tracking in live cells.* Angewandte Chemie, 2010. **49**(24): p. 4108-12.

26. Gavutis, M., et al., *Lateral ligand-receptor interactions on membranes probed by simultaneous fluorescence-interference detection.* Biophysical journal, 2005. **88**(6): p. 4289-302.

27. Gavutis, M., et al., *Determination of the two-dimensional interaction rate constants of a cytokine receptor complex.* Biophysical journal, 2006. **90**(9): p. 3345-55.

28. Waichman, S., et al., *Functional immobilization and patterning of proteins by an enzymatic transfer reaction.* Analytical chemistry, 2010. **82**(4): p. 1478-85.

29. Cajean-Feroldi, C., et al., *Identification of residues of the IFNAR1 chain of the type I human interferon receptor critical for ligand binding and biological activity.* Biochemistry, 2004. **43**(39): p. 12498-512.

30. Boulanger, M.J., et al., *Hexameric structure and assembly of the interleukin-6/IL-6 alpha-receptor/gp130 complex.* Science, 2003. **300**(5628): p. 2101-4.

31. Andrews, A.L., et al., *Kinetic analysis of the interleukin-13 receptor complex.* The Journal of biological chemistry, 2002. **277**(48): p. 46073-8.

32. Kuznetsov, V.A. and R.K. Puri, *Kinetic analysis of high affinity forms of interleukin (IL)-13 receptors: suppression of IL-13 binding by IL-2 receptor gamma chain.* Biophysical Journal, 1999. **77**(1): p. 154-72.

33. LaPorte, S.L., et al., *Molecular and structural basis of cytokine receptor pleiotropy in the interleukin-4/13 system.* Cell, 2008. **132**(2): p. 259-72.

34. Roisman, L.C., et al., *Mutational analysis of the IFNAR1 binding site on IFNalpha2 reveals the architecture of a weak ligand-receptor binding-site.* Journal of molecular biology, 2005. **353**(2): p. 271-81.

35. Akabayov, S.R., et al., *NMR mapping of the IFNAR1-EC binding site on IFNalpha2 reveals allosteric changes in the IFNAR2-EC binding site.* Biochemistry, 2010. **49**(4): p. 687-95.

4 Ternary complex stabilization by entropic clamps

4.1 Introduction

The last section of the previous chapter described an examination of ligand-receptor interaction in the ternary IFNα2/IFNAR1/IFNAR2 complex on artificial membranes exploiting ligand-induced IFNAR1 receptor conformational change. Ternary complex formation occurs as a sequential process, with IFN first interacting with the higher affinity IFNAR2 subunit followed by IFNAR1 recruitment through at independent binding site and involves a substantial movement in the receptor orientation and the outward movement of IFN upon the assembly (Figure 1.9) revealed by the comparison of unbound and bound X-ray structures [1]. The large conformational rearrangement of IFNAR1 accompanying the signalling complex assembly can be readily detected and studied by the approaches employed in the previous sections. However the assessment of dynamics of this process, protein conformational flexibility has to be addressed by markedly different methods. To evaluate the complex conformational dynamics in solution we would turn to fluorescence cross-correlation spectroscopy (FCCS) and single molecule Förster resonance energy transfer (smFRET). These are very powerful techniques which can monitor dynamic protein interactions in real time, but are generally limited to strong interacting pairs because of the low concentrations ($<10^{-9}$ M) needed for single molecule detection. Thus the key challenges for employing FCCS technique are the site-specific placement of two suitable fluorescence reporters and stabilization of low affinity multi-protein complexes. The generic method of site-specific covalent protein labelling presented in the chapter 2.3 is readily applicable for fluorescence probe incorporation for FCCS studies as well. As demonstrated by solid-phase techniques on artificial membranes, stability of individual ternary complexes formed with IFNα2 is below 10 s [2, 3]. Taking into account an affinity in the micromolar range, even purified at high concentrations, ternary complex falls apart quickly upon dilution. Monitoring this complex in solution diluted to nanomolar concentrations requires particular means for stabilizing the intrinsic low affinity-based protein complexation.

Many biophysical, chemical and biochemical methods can be used to force proteins into complexes. Encapsulation into lipid unilamellar liposomes or “nanovesicle trapping” is one of the approaches to bring weak interaction partners together at high effective concentrations as high as tens of micromolar to facilitate their complexation [4]. This approach suffers from the limitations imposed by the need of high initial concentration (tens of micromolar) of fluorescence-labelled proteins for encapsulation, little statistical occupancy of nanocontainers

with double-labelled protein complexes as well as from the relatively harsh vesicle preparation conditions.

Chemical crosslinking is the process of joining two or more proteins or regions in a protein by a covalent bond which is formed between the end reactive groups of crosslinkers and the functional groups of proteins [5, 6]. The application of the most widely used homobifunctional reagents targeting primary amine groups such as glutaraldehyde [7], disuccinimidyl suberate (DSS), and bis(sulfosuccinimidyl) suberate (BS^3) [5] is impaired by the low specificity of the reagents, which can chemically bridge any two amines that are close in space. Chemical orthogonality of a reaction for targeted, non-random conjugation of protein heterocomplexes can be enabled through heterobifunctional reagents which may incorporate two different reactive groups, e.g. Lys- and Cys-reactive, protected [8] and photoreactive groups [9, 10]. Another extension of the chemical conjugation, native chemical ligation (NCL) [11, 12], is a concept for joining of two or more unprotected polypeptide segments by *in situ* transthioesterification resulting in amide bond. However, the latter approaches pose potential difficulties since they require site-specific modification of proteins with additional functional groups and intermediate reaction purification steps and they are not suitable for oxidized proteins and generally limited to proteins available in large quantities.

Biochemical techniques for crosslinking include genetic protein fusions to peptide motifs such as encoding for intein for protein linkage through naturally occurring NCL-analogy [13-15] and E/K peptides of the self-heterodimerizing ($K_D=3.5\cdot10^{-9}$ M) coiled-coil tag system [16, 17]. As an alternative to the dimerizing adapters, recombinant bispecific diabodies, with a binding capacity to two antigens, can be employed to recruit two diverse interacting molecules [18, 19]. However, the use of genetic adapter fusions imposes various disadvantages [20-22] as well as difficulties in the generation of bispecific diabodies limit their practical application. A more simple stabilization approach based on crosslinking of receptor terminal His-tags with an anti-His mAb introduces additional constraints due to low heterodimerization selectivity and significant material loss upon purification of crosslinked ternary complexes.

So far the most of the chemical and biochemical crosslinking techniques impose a significant disadvantage of low selectivity for the recognition of protein complex formation. These crosslinkers do not specifically sense and selectively bridge the proteins which naturally interact, resulting in an undesirable non-specific crosslinking.

To overcome these limitations, we aimed to employ a crosslinker sensitive to the assembly of IFNα2/IFNAR1/IFNAR2 heterotrimeric complex by an intrinsic affinity, selectively

exploiting the feature of this preference to join naturally interacting proteins. We try to address the following challenge: how can one *in vitro* stably zip together in a single-step mode the receptor termini of preassembled ternary complex, using little amount of available labelled proteins. The simplicity of the devised procedure ideally should enable *in situ* complex stabilization in a fluorescence cuvette or on a microscope stage. Thus, a high affinity crosslinker is required for working at high dilutions with proteins interacting at low affinity. Moreover, new crosslinking strategy would not require additional elaborate genetic manipulations with proteins, exploiting the available already introduced side-directed modifications such as the His-tag.

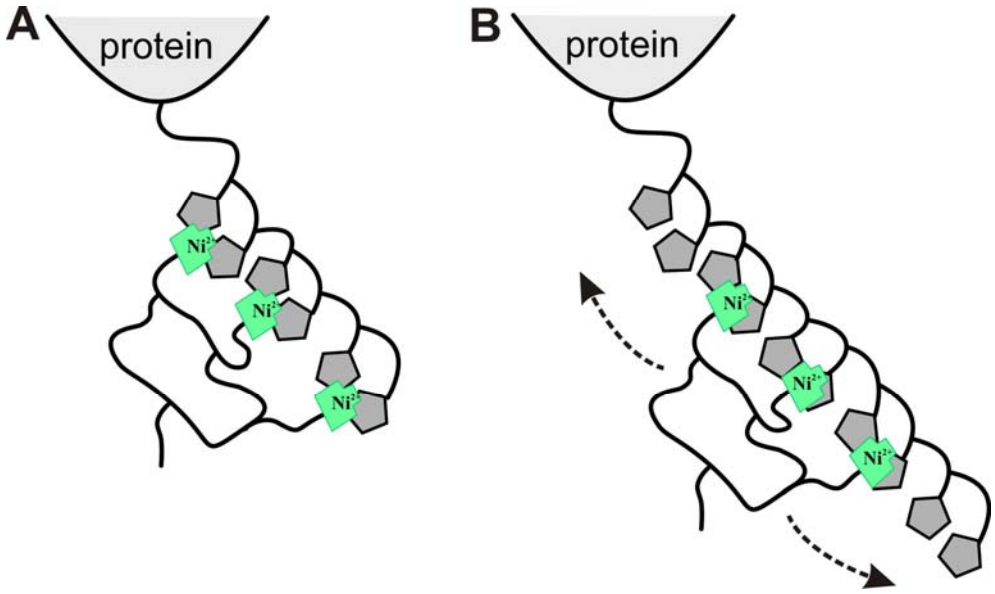

Figure 4.1 Multivalent interaction of tris-NTA moieties with H6- and H10- tags.

Schematic of different scenarios of multivalency and redundancy. **A** Schematic representation of multivalent non-redundant interaction of tris-NTA moiety with H6-tag. Each tris-NTA moiety complexes three Ni^{2+} ions (green) and potentially coordinates six histidines, providing high multivalency and low redundancy. **B** Redundancy in histidine moieties of H10-tag provides additional degrees of freedom for docking of tris-NTA.

To this end we employed the features of reversible interaction of high affinity multivalent chelator head (MCH) adaptors with oligohistidine peptide tags (which is well-studied and readily available for in-house application) [23-26]. A single trivalent MCH entity, tris(nitrilotriacetic acid) (tris-NTA) loaded with Ni^{2+}, reversibly binds a hexahistidine peptide tag with about 2 nM and decahistidine tag with ~0.2 nM affinity [24, 26] and forms complexes with 1:1 stoichiometry (Figure 4.1 A, B). Its greater binding affinity to the H10-tag at the same stoichiometry can be ascribed to a gain in entropy at high redundancy compared to multivalent but highly confined, non-redundant tris-NTA/H6 interaction. Thus, one-to-one tris-NTA/H10 stoichiometry can be preferred due to a significant increase in free energy [27].

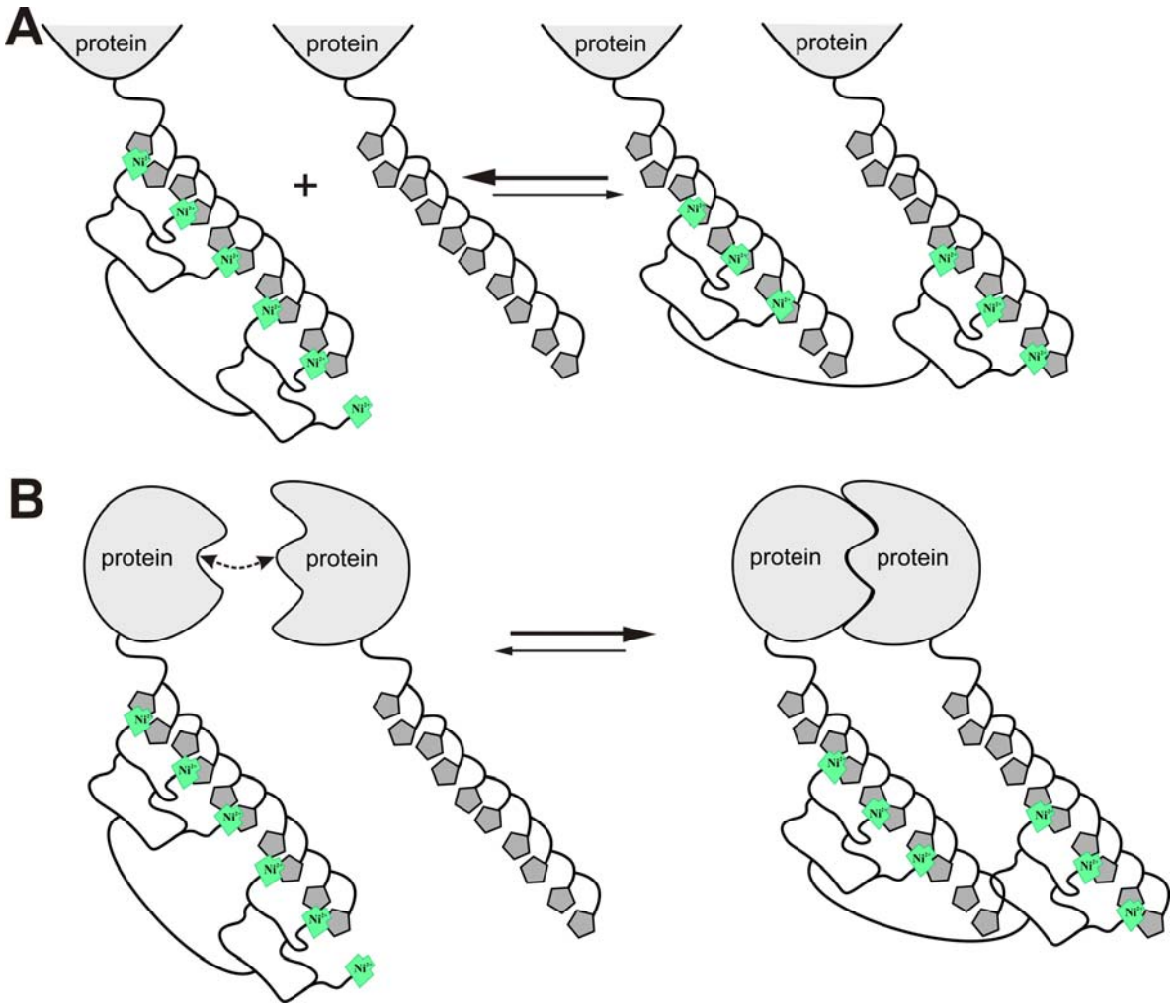

Figure 4.2 Equilibria at entropic selectivity of bis3NTA clamp for crosslinking H10-tagged proteins in solution.

A For non-interacting proteins under condition of redundancy in chelator groups one-to-one bis3NTA/H10 binding stoichiometry is preferred rather than crosslinking due to the gain in energy and entropy and at expense of enthalpy. **B** Bis3NTA gains the maximum energy and enthalpy by selectively crosslinking H10-tagged proteins in complexes formed by intrinsic affinity.

A recently devised multivalent chelator head based on tris-NTA is built of two single tris-NTA moieties connected through a PEG-thiol linker (Figure 4.2 A and Figure 4.3 A) and termed bis3NTA [25]. As for tris-NTA, for bis3NTA similar 1:1 stoichiometry at binding H10-tag is preferred. Compared to tris-NTA, at this stoichiometry bis3NTA gains more energy due to additive increase in $\Delta G°$ and $\Delta H°$ at the expenses of entropy with lesser redundancy and upon loosing conformational flexibility with the multiple coordination bonds being formed (Figure 4.2 A).

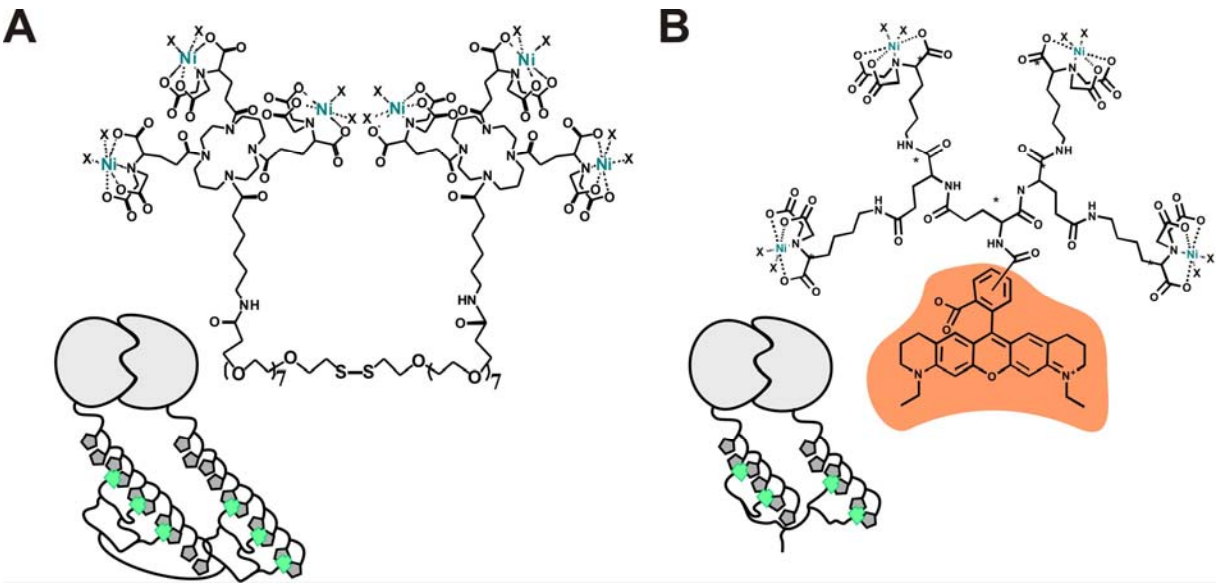

Figure 4.3 Chemical structures of tris-NTA-EG7-disulfide (bis3NTA) and tetrakis-NTA (4NTA) multivalent clamps loaded with Ni2+ ions and schematic illustrations of their interaction with His-tagged protein complexes.

A Bis3NTA structure comprised of two single tris (nitrilotriacetic) acid (tris-NTA) moieties connected by a flexible (polyethylene glycol) PEG linker indicated by ( )7 where n=7 stands for 7 number of PEG units connected by a thiol linker. Coordinated nickel is shown as cyan characters. **B** Chemical structure of ^{AT565}tetrakis-NTA (^{AT565}4NTA). Tetrakis-NTA is conjugated to ATTO565-maleimide and loaded with Ni^{2+} ions shown as cyan characters. Conjugated fluorophore is outlined in orange. Inset figures are the schematic illustrations of His-tag crosslinking by entropic clamps in assembled protein complexes: (A) -bis3NTA/H10 crosslinking and (B) - 4NTA/H6 crosslinking.

We envisioned exploiting bis3NTA as a potential crosslinker, a homobifunctional clamp with entropic selectivity feature. Under conditions of redundancy, formation of 1:1 bis3NTA/H10-tag complex by multi-coordinated interaction with cumulated histidines even at expense of enthalpy would be energetically favourable compared to the binding of two individual non-interacting H10-tagged proteins (Figure 4.2 A). However in a protein complex assembled by intrinsic affinity, two H10-tags in a close proximity form a high cumulation of redundant histidines for recognition by NTA moieties. The bis3NTA clamp can gain more free energy and enthalpy but at expense of entropy by crosslinking the second neighbouring H10-tag than in a 1:1 interaction with H10 shifting the equilibrium towards complex stabilization (Figure 4.2 B). Therefore bis3NTA can serve as an entropic clamp with entropic selectivity for crosslinking protein complexes having intrinsic affinity and not crosslinking proteins which do not interact.

Another synthesized multivalent chelator head clamp, tetrakis-NTA (4NTA) contains four functional NTA moieties (~40 nM 4NTA/H6 and 1 nM 4NTA/H10 affinity) connected in a dendrimer-like structure (Figure 4.3 B) [24] and coupled via the primary amino group to

ATTO565 dye. Conjugation of tetrakis-NTA with fluorescence probes in the original study followed two purposes: creating an adaptor for reversible fluorescence reporter incorporation into His-tagged proteins and the simplification of the MCH purification by increasing its molar absorption coefficient. Similarly to bis3NTA/H10 crosslinking, 4NTA may display entropic selectivity for stabilizing H6- (as well as H10-) tagged protein complexes (Figure 4.3 B). The tetrakis-NTA clamp can be employed for zipping up His-tags spaced in complexes by a relatively short distance due to about 3.8 nm span between the end coordination groups. Consiquently, crosslinking H10-tags over much longer distances needs bis3NTA clamp with 12.0 nm between the end NTA moieties, making it a more generic tool.

We envisaged that the two vacant receptor H10-tags transiently brought into proximity upon IFNα2/IFNAR1/IFNAR2 complex assembly can be fixed together by bis3NTA entropic clamp in a controlled, distance-dependent manner. Thus, in this project validating bis3NTA as a suitable mean for the interferon receptor complex stabilization would pave the way for probing conformational crosstalk of the ternary complex by FCCS and FRET.

4.2 Materials and methods

4.2.1 Materials

CoA-AT488 and CoA-Dy647 conjugates and phosphopantetheinyl transferase Sfp were purchased from Covalys Bioscience, Witterrswill/Switzerland, Alexa Fluor C 5 488-maleimide from Molecular Probes, ATTO 655-maleimide from ATTO-TEC GmbH, Standard Probe for FCCS from IBA Gmbh, Goettingen/Germany. All other chemicals were purchased from Sigma Aldrich.

4.2.2 Construction of vectors

IFNα2, IFNα2-YNS and IFNAR2-EC-H10 carrying an N-terminal ybbR-tag (ybbR-IFNα2, ybbR-IFN2-YNS, ybbR-IFNα2-YNS-α8tail and ybbR-IFNAR2-H10) were cloned by insertion of an oligonucleotide linker coding for the ybbR peptide (DSLEFIASKLA) [28, 29] into the *Nde*I restriction site upstream of the corresponding genes in the plasmids pT72Cα2 and pT72CR2, respectively [30]. Site-directed mutagenesis of IFNα to IFNα-R120A and IFNα-YNS to IFNα2-YNS-α8tail was carried out by PCR site-directed mutagenesis protocol with a pair of mismatch oligonucleotides obtaining a linear fragment, suitable for reclosure and was similar to that described elsewhere [31]. IFNAR1-H6 was subcloned from IFNAR1-H10 construct by PCR-based placement of stop-codon at the C-terminus. YbbR-IFNAR1-H10-EC and H10-IFNAR1-ybbR-EC were generated by insertion of ybbR peptide

into *Nhe*I and *BamH*I or *Eco*RI restriction sites upstream or downstream of the corresponding genes in the vector pBAC-3 (Novagen) or pAcGP67B (BD Pharmingen) respectively. Tagless phosphopantetheinyl transferase (PPT) Sfp was generated from original construct pBAD-Sfp provided by the manufacturer (Covalys Bioscience) by PCR-based removal of H15-tag downstream of the maltose binding protein fusion and upstream of PPT.

4.2.3 Protein production, purification and labelling

Maltose binding protein with hexa- and decahistidine tag (MBP-H6 and MBP-H10), all interferon α2 and IFNAR2 proteins were expressed in *E. coli* and purified by the same protocols established for MBP [24], IFNα2-YNS [32] and wild-type IFNAR2-EC [3, 30, 33] respectively. YbbR-IFNα2, ybbR-IFNα2-YNS, ybbR-IFNα2-YNS-α8tail were labelled by PPTase using CoA-Dy647, and ybbR-IFNAR2-H10 using CoA-AT488 purchased from Covalys and Sfp and purified by size exclusion chromatography on Superdex^{TM} 75 10/30 column as described in section 2.3.1 and 2.3.2 and reported recently [34]. Tagless Sfp was produced as an MBP fusion protein in *E. coli* and purified with amylose resin (New England BioLabs) and by SEC. H6- and H10-tagged IFNAR1 were expressed in *Sf*9 insect cells and purified by IMAC and gel filtration as described previously [3]. YbbR-fusion of His-tagged IFNAR1-EC proteins were expressed and purified the same way as IFNAR1-H10, and ybbR-IFNAR1-H10 was posttranslationally labelled using CoA-AT488 (Covalys Bioscience) and tagless Sfp and purified according to the procedure established in 2.3.3.

4.2.4 Synthesis and conjugation of entropic clamps

The synthesis of tris-NTA-EG_7-disulfide (bis3NTA), loading with Ni(II) ions and purification was done according to the recently described protocol [25]. Tetrakis-NTA chelator heads were conjugated to ATTO-565 NHS-ester and Ni(II) loaded similarly to the standard conjugation procedure [24].

4.2.5 Size exclusion chromatography

Analytical size-exclusion chromatography (SEC) was employed to examine in-solution binding of MCHs to hexa- and decahistidine tagged maltose binding protein or IFNAR1 (MBP-H6, MBP-H10, IFNAR1-H6, IFNAR1-H10) and His-tag mediated stabilization of multicomponent protein complexes. Bis3NTA and ^{AT565}tetrakisNTA were incubated with 4-5 μM his-tagged proteins in various molar ratios in HBS buffer for 30 min at room temperature followed by SEC. Ternary complex stabilization assays were carried out with a 1.5-fold molar excess of IFNAR2 to ensure full engagement of IFNAR1 into a ternary

complex for separation by SEC. Typically 1.2-2 µM IFNAR1-EC, IFNAR2-EC, IFNα2, and MCHs were mixed in HBS buffer in molar ratio of 1.0:1.5:1.5:1.5 and then incubated the same way as described above. For analytical assays 20 µl sample was loaded onto a SEC column (Superdex^{TM} 200 3.2/30, GE Healthcare) in an HPLC system (Jasco) and elution was monitored at 0.07 ml·min^{-1} by a diode array detector (MD-2015 plus, Jasco) at 280 nm, 488 nm, 650 nm or additionally at 565 nm for ^{AT565}tetrakisNTA clamp, the resulting chromatograms were normalized. For preparative ternary complex purification typically 50 µl sample was loaded onto the same column and fractions were collected at 0.5 minute intervals.

4.2.6 Instrumentation for dual-colour fluorescence cross-correlation spectroscopy

Fluorescence cross-correlation experiments were carried with a Fluoview 1000 confocal laser scanning microscope from Olympus equipped with a 60x water immersion objective (NA=1.2, Olympus) and a Lifetime/FCS upgrade from PicoQuant. Laser diodes at 485 nm and 638 nm were used for pulsed interleaved excitation (PIE) to avoid spectral cross-talk.

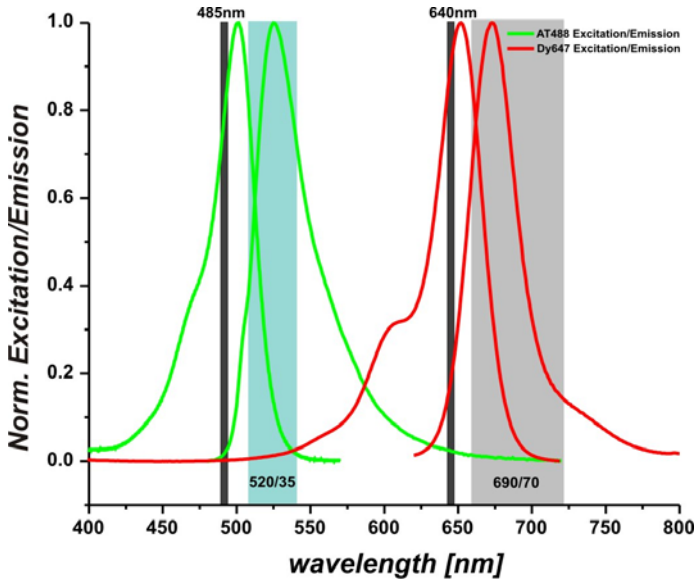

Figure 4.4 Spectral separation of fluorescence excitation and emission spectra of the fluorescence probes employed in FCCS analysis.

Green - ATTO488 excitation and emission spectra, red – Dy647 excitation and emission spectra, the dark grey bars indicate 485 nm and 640 nm excitation laser beams, the light blue bar – 520/35 nm OD emission filter and the light grey bar – 690/70 nm OD emission filter.

Fluorescence signals were detected by two single photon avalanche diodes with the emission filters FF1 520/35 (Semrock) and HQ 690/70 (AHF Analysentechnik) (Figure 4.4). Photon traces were recorded with time-correlated single photon counting (TCSPC), which allowed

time gating - required for (PIE) - and the application of lifetime filters to remove detector afterpulsing, for background reduction and FRET analysis.

4.2.7 FCCS data recording and evaluation

Diffusion experiments in solution were recorded for 60 s at room temperature on 140 µm thick cover slides, 50 µm above the glass interface and with a pinhole size of 120 µm. Measurements were conducted with 15 µW at 485 nm and 50 µW at 638 nm at a pulse frequency of 40 MHz. Effective volumes were calibrated with a solution of the two fluorescent dyes Oregon Green 488 (OG488) and ATTO 655-maleimide (AT655M) at a concentration of 2 nM each. The collected stabilized protein complex fractions were analysed by FCCS directly after HPLC purification and diluting of the samples in HBS complemented with 1 $mg \cdot mL^{-1}$ bovine serum albumin to concentrations of ~0.5-1.8 nM. For the chasing experiments label-free IFNα2-YNS-α8tail was added to a final concentration of 1 µM from a high concentrated stock solution to keep dilution effects minimal. For the spontaneous dissociation experiments samples were kept in the experimental chamber and data traces were recorded at 30 min and 60 min intervals.

Data analysis was performed with the Symphotime software package from PicoQuant. The autocorrelation curve of AT655M was fitted to a simple free diffusion model (Equation 4.1), whereas the autocorrelation of OG488 and AT488 was evaluated by a free three-dimensional diffusion model with Triplet state (Equation 4.2).

$$G(\tau) = \frac{1}{N}\left(1+\frac{\tau}{\tau_D}\right)^{-1} \cdot \left(1+\frac{\tau}{\tau_D \mathrm{K}^2}\right)^{-1/2} \qquad \textbf{Equation 4.1}$$

$$G(\tau) = \left[1+\frac{\mathrm{T}}{(1-T)} \cdot e^{\frac{-\tau}{\tau_\mathrm{T}}}\right] \cdot \frac{1}{N}\left(1+\frac{\tau}{\tau_D}\right)^{-1} \cdot \left(1+\frac{\tau}{\tau_D \mathrm{K}^2}\right)^{-1/2} \qquad \textbf{Equation 4.2}$$

$G(\tau)$: Autocorrelation function at delay time τ; τ_D: Diffusion time; N: Number of particles, $K = \frac{z_0}{\omega_0}$: Eccentricity of focal volume; T: Triplet fraction; τ_T: Lifetime of Triplet state; $\rho = G(0) \cdot (1-T) = \frac{1}{N}$: Correlation amplitude of diffusing species at $\tau = 0$. Based on the diffusion coefficients D_{OG488}=411 $\mu m^2 \cdot s^{-1}$ and D_{AT655M}=407 $\mu m^2 \cdot s^{-1}$ from the literature [35] we determined effective volumes of 1.1 fL and 2.0 fL according to Equation 4.3 and Equation 4.4.

$$D = \frac{\omega_0^2}{4\tau_i}$$ **Equation 4.3**

$$V_{eff} = \pi^{3/2} \cdot \omega_0^2 \cdot z_0$$ **Equation 4.4**

The effective detection volume for the double labelled species $V_{Eff,X}$=1.022 fL was calculated according to Equation 4.5 [36].

$$V_{eff,X} = \pi^{3/2} \cdot \omega_{0,g} \cdot \omega_{0,r} \cdot \sqrt{z_g \cdot z_r}$$ **Equation 4.5**

The concentrations of single- and double-labelled species can be calculated form the auto- and cross-correlation amplitudes by Equation 4.6, Equation 4.7 and Equation 4.8.

$$c_g = \frac{N_g}{V_{Eff,g} \cdot N_A}$$ **Equation 4.6**

Respectively:

$$c_r = \frac{N_r}{V_{Eff,r} \cdot N_A}$$ **Equation 4.7**

N_A: Avogadro constant.

$$\frac{c_x}{c_r} = \frac{\rho_x \cdot V_{Eff,x}}{\rho_g \cdot V_{Eff,g}}$$ **Equation 4.8**

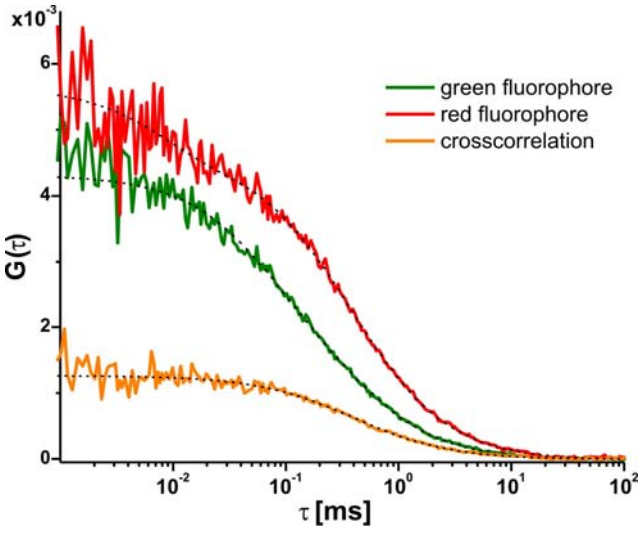

Figure 4.5 Calibration fluorescence cross-correlation measurement using the IBA '*In vitro* standard probe for FCCS'.

Green autocorrelation curve – 488 probe, red autocorrelation curve – 633 probe, orange – cross-correlation. Respective fits indicated as dotted lines.

As a reference for cross-correlation (Figure 4.5) we used the '*In vitro* standard probe for FCCS' (SP) from IBA Gmbh which is comprised of double-labelled dsDNA with excitation wavelengths 488/633 nm. The standard probe was measured at a dilution 1:50 in HBS and a ratio of double labelled to single red-labelled species $\frac{c_{x,SP}}{c_{r,SP}} = 0.2666$ was obtained.

Due to experimental limitations we consider this to be the maximum cross-correlation that can be observed with our setup, even for a fully double-labelled species. Hence, all sample measurements were normalized to the SP.

4.2.8 Life time based FRET analysis with pulsed interleaved excitation

Förster resonance energy transfer (FRET) in the stabilized protein complexes was analysed by evaluation of fluorescence lifetimes. For this purpose TCSPC histograms were generated from the time-correlated time-tagged photon traces that were also used for FCCS analysis. Since PIE was employed the direct acceptor excitation should not affect the reduced donor fluorescence lifetime in presence of an acceptor.

Two component lifetime fitting with a double exponential decay model was applied for experiments where both, the donor and acceptor probes were present. The longer lifetime reference was found by one component (monoexponential decay model) fitting analysis in a control experiment, where only IFNAR1 was labelled with a donor dye. The FRET efficiency (E) was obtained from the intensity amplitudes A_i of the shorter fitted lifetime component A_{DA} (donor in presence of acceptor) and the amplitude of the longer lifetime component A_D (unquenched donor) (Equation 4.9).

$$E = \frac{A_{AD}}{\sum_i A_i}$$ **Equation 4.9**

4.3 Results

4.3.1 Entropic clamp interaction with His6- and His10- tagged proteins

Following the idea that the binding stoichiometry is driven by the thermodynamic selectivity we explored discrepancies related to the multivalent interaction of bis3NTA with individual hexahistidine (H6-) and decahistidine (H10-) tagged proteins.

At first bis3NTA entropic clamp interaction with oligohistidine tags was tested on a model protein, maltose binding protein (MBP, ~43 kDa), known for its intrinsic capability to sustain monomeric form. Two constructs carrying C-terminal tags were selected for this study: hexahistidine-tagged MBP (MBP-H6) and decahistidine-tagged MBP (MBP-H10). All proteins were preliminarily gel-filtrated in order to ensure efficient removal of aggregates.

The multivalent chelator head clamp was titrated at different adaptor-to-protein ratios and analysed by analytical size exclusion chromatography (Figure 4.6).

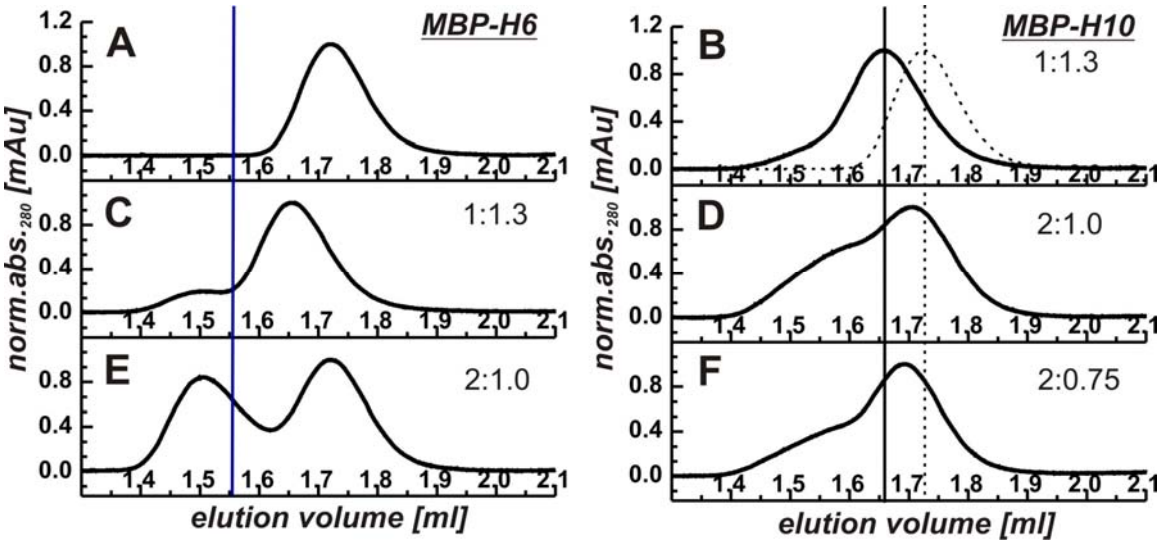

Figure 4.6 Bis3NTA interaction with MBP-H6 and MBP-H10.

Analytical SE chromatograms of H6- and H10- tagged MBP mixed with bis3NTA clamp at different molar ratios. **A** Elution of free MBP-H6. **B** MBP-H10 with 1.3-fold molar excess of bis3NTA, for comparison, dashed line indicates elution of free MBP-H10. **C** MBP-H6 with 1.3-fold molar excess of bis3NTA. **D** SEC with 2-fold molar excess of MBP-H10. **E** SEC with 2-fold molar excess of MBP-H6. **F** SEC with MBP-H10 and bis3NTA mixed at 2:0.75 molar ratio. Blue solid line separates the position of MBP-H6 dimers; black solid line corresponds to the elution of MBP-H10 bound to bis3NTA, black dotted line – to monomeric free protein peak. The peaks were normalized for visual comparison.

We monitored retention time of individual His-tagged MBP or preincubated with bis3NTA with an excess of a clamp, equimolar or sub-equimolar ratios. Monomeric free hexa- and decahistidine tagged MBP peaks elute at about ~1.72 ml retention volume which is in a good

agreement with calibration results for 43 kDa protein (column calibration data not shown). Interestingly that already at a slight stoichiometric excess of bis3NTA over H6-tagged protein (1.3:1) a little extent of dimerization could be observed (Figure 4.6, C) and a peak of MBP fully complexed by multivalent adaptor shifted to shorter retention time (~1.56 mL). In contrast, for MBP-H10 at the same clamp-to-protein molar ratio only a little shoulder of dimers at 1.52 mL was observed (Figure 4.6 B). Subsequent reduction of bis3NTA mixing stoichiometry till one half of the protein molar ratio further enforces the dimerization of MBP-H6 (Figure 4.6 E) whereas the peak of monomeric protein insufficiently complexed with bis3NTA shifts back to the longer retention time of free MBP-H6 (1.72 mL). As expected, for MBP-H10 at the same molar clamp-to-protein rations only a little extent of protein homodimerized and eluted as a shoulder at 1.52 mL significantly overlapping with a peak of protein (~1.7 mL) comprised of free MBP and bound to bis3NTA (Figure 4.6 D). Indeed, further reduction of bis3NTA/His10 ratio (0.75:2) does not increase the extent of MBP-H10 dimerization (Figure 4.6 E). Moreover it reduces the fraction of bis3NTA-bound monomeric MBP-H10 and drives the main peak to longer elution time (~1.7 mL) of free protein due to the sub-stoichiometric interaction with bis3NTA. These results are fully in line with the predicted preferences for the stoichiometries of bis3NTA/oligohistidine complexes. At sub-stoichiometric ratios each tris-NTA moiety of the homobifunctional entropic clamp yields stable non-redundant highly-coordinated complexes with six histidines of individual H6-tags (Figure 4.1 A) gaining the maximum free energy at enthalpy. Thus two hexahistidine-tagged proteins are readily homodimerized by bis3NTA clamp. Whereas under conditions of redundancy, a 1:1 stoichiometry of bis3NTA complex with decahistidine peptide (Figure 4.2 A) appears to be energetically favourable due to the gain in entropy.

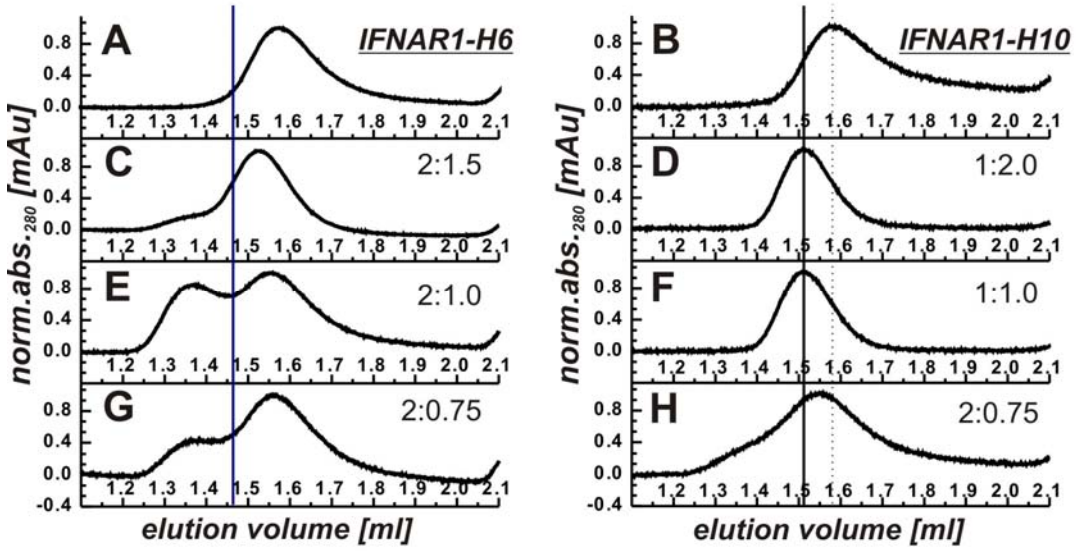

Figure 4.7 Bis3NTA interaction with IFNAR1-H6 and IFNAR1-H10.

Analytical SE chromatograms of H6- and H10- tagged IFNAR1 mixed with bis3NTA clamp at different molar ratios. **A** Elution of free IFNAR1-H6. **B** Elution of free IFNAR1-H10. **C** IFNAR1-H6 with 1.5-fold molar excess of bis3NTA. **D** IFNAR1-H10 with 2-fold molar excess of bis3NTA. **E** SEC with 2-fold molar excess of IFNAR1-H6. **F** IFNAR1-H10 mixed with bis3NTA at equimolar 1:1 ratio. **G** SEC with IFNAR1-H6 with bis3NTA mixed at 2:0.75 molar ratio. **H** SEC with IFNAR1-H10 and bis3NTA mixed at 2:0.75 molar ratio. Blue solid line separates the position of IFNAR1-H6 dimers; black solid line corresponds to the elution of IFNAR1-H10 bound to bis3NTA, black dotted line – to monomeric free protein peak. The peaks were normalized for visual comparison.

Very similar chromatograms were obtained for the interaction of bis3NTA with IFNAR1-H6 and IFNAR1-H10 (Figure 4.7). At substoichiometric mixing ratios bis3NTA clamp preferentially crosslinked two H6-tagged IFNAR1 receptors resulting in a significant fraction of dimers (Figure 4.7 E and G). Still, under similar conditions for bis3NTA interaction with IFNAR1-H10 one-to-one complex stoichiometry was preferred (Figure 4.7 H). These observations further corroborate the entropic selectivity of bis3NTA clamp in forming complexes with oligohistidine peptides. Similar results obtained for MBP and IFNAR1 with hexahistidine and decahistidine tags indicate that the observed effects are not attributed to specific nature of one protein. Further tuning of oligohistidine tag to H11 by adding of NTA moiety would be useful. It would enable the maximum gain in free energy at enthalpy and have the same entropic impact.

4.3.2 Stabilization of ternary complex by my means of entropic clamp

Next, we aimed to explore the selectivity of bis3NTA entropic clamp for stabilizing protein complexes preassembeled by intrinsic low affinity but not crosslinking of H10-tagged protein complexes which do not interact.

To this end, ternary complex formation with wild type IFNα2 in the presence and absence of bis3NTA clamp was studied by analytical SEC. No ternary complex was detected by SEC at given concentrations (4.2.5) upon mixing IFNAR1-H10, IFNAR2-H10 and IFNα2 at a molar ratio 1:1.5:1.5 in the absence of bis3NTA clamp (Figure 4.8). Typically IFNα2/IFNAR1/IFNAR2 ternary complex elutes at ~1.4 mL retention volume as shown by further assays (Figure 4.9) and previous studies [37]. Taking into account 1000-fold higher wild type IFN affinity to IFNAR2 than to IFNAR1, under the experimental conditions equilibrium is shifted towards individual IFNAR1-H10 and IFNα2/IFNAR2-H10 binary complex as illustrated by a comparison with elution of IFNAR1-H10 and IFNAR2-H10 individual receptor subunits (Figure 4.8).

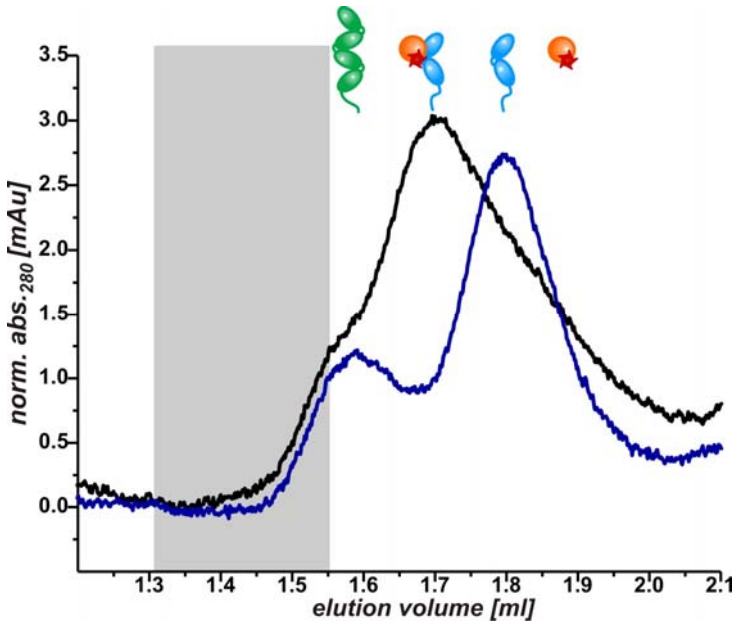

Figure 4.8 Ternary complex formation in the absence of entropic clamp.

Ternary complex formation without an addition of bis3NTA clamp as detected by analytical SEC. Black curve: ternary complex formation of IFNAR1-H10 and IFNAR2-H10 with IFNα2. Blue curve: elution of IFNAR1-H10 and IFNAR2-H10 without a ligand. Typical elution time for the stabilized ternary complex is indicated by the grey bar.

Moreover, under the same experimental conditions, no stable ternary complex was obtained when IFNAR1-H10 and IFNAR2-H10 were mixed with IFNα2-YNS-α8tail (not shown), the IFN mutant with the highest affinity for both receptor subunits [38], indicating that without an additional stabilization ternary complex dissociates during the SEC run.

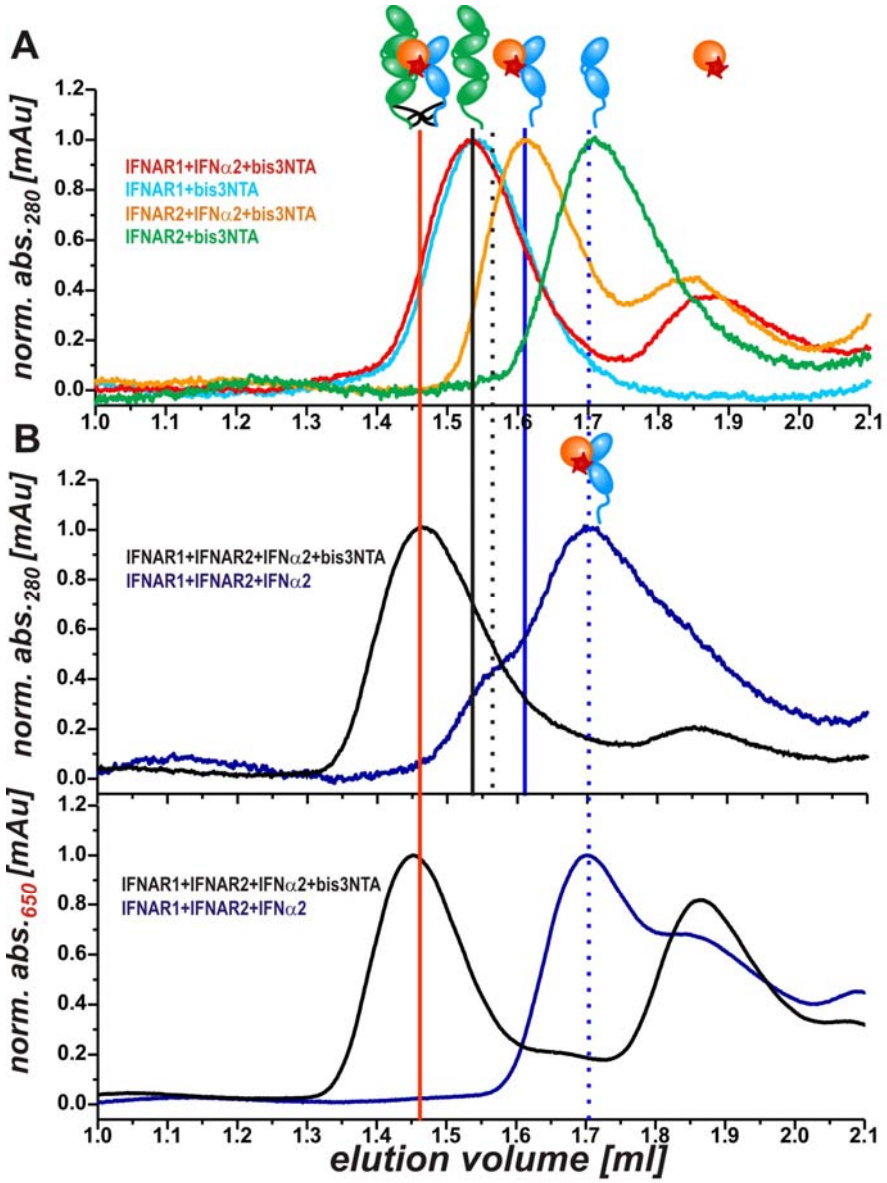

Figure 4.9 Stabilization of ternary complex by means of bis3NTA clamp as detected by multichannel analytical SEC detection.

A Analytical SEC detection of individual receptor subunits conjugated to bis3NTA or in binary complexes with ^{Dy647}IFNα2: ^{Dy647}IFNα2/IFNAR1-H10 binary complex with bis3NTA (red curve), IFNAR1-H10 with bis3NTA (cyan curve), ^{Dy647}IFNα2/ IFNAR2-H10 binary complex with bis3NTA (orange curve) and IFNAR2-H10 with bis3NTA (green curve). **B** Ternary complex formation of IFNAR1-H10, IFNAR2-H10 with ^{Dy647}IFNα2 and bis3NTA (black curves) mixed at 1:1.5:1.5:1.5 molar ratio as detected at 280 nm (upper panel) and 650 nm (bottom panel). For comparison, elution of non-stabilized ternary complex without bis3NTA is shown as blue curves. Red solid line marks the position of the ternary complex peak. Black solid line corresponds to IFNAR1 conjugated with bis3NTA, black dotted line – to the elution of free IFNAR1. Blue solid line marks the elution of ^{Dy647}IFNα2/IFNAR2-H10 binary complex with coordinated bis3NTA and dotted line corresponds to IFNAR2-H10 bound to bis3NTA (in A) and to binary complex ^{Dy647}IFNα2/IFNAR2-H10 (in B). The peaks were normalized for visual comparison.

Nevertheless when bis3NTA is added to the IFNAR1-H10 and IFNAR2-H10 subunits with C-terminal H10-tags mixed with labelled ^{Dy647}IFNα2, the equilibrium readily shifts towards elution of the ternary complex at 1.45 mL (Figure 4.9 B). This observation is further corroborated by monitoring this chromatogram at 650 nm channel. It detects the engagement of labelled ^{Dy647}IFNα2 into the ternary complex peak in comparison to the same experiment carried out without bis3NTA, showing ^{Dy647}IFNα2 elution in a binary complex with IFNAR2-H10 or as an individual peak.

The peak at 1.45 mL clearly corresponds to the bis3NTA-stabilized IFNα2/IFNAR1/IFNAR2 complex since much longer retention times are detected for IFNAR1-H10/bis3NTA and IFNα2/IFNAR2-H10/bis3NTA binary complex and no binary complex of IFNα2 with IFNAR1-H10 is formed under these conditions (Figure 4.9 A). The same elution profiles were observed for bis3NTA-stabilized ternary complexes formed with high affinity interferon mutants ^{Dy647}IFNα2-YNS and ^{Dy647}IFNα2-YNS-α8tail (not shown) corroborating to the generic nature of the selected stabilizations strategy. However it appears that IFNα2 binding towards lower affinity subunit IFNAR1 contributes strongly to the combined complex affinity and transient complex assembly in solution for the bis3NTA-mediated stabilization. Upon further significant decrease of affinity towards IFNAR1 by the IFNα2-R120A mutant ($K_D >> 10$ μM) [39] no bis3NTA-stabilized ternary complex peak was obtained in a similar SEC experiment (not shown). In an additional control SEC experiment set different final equimolar concentrations of IFNAR1-H10 and IFNAR2-H10 where mixed with bis3NTA clamp and eluted as individual IFNAR1-H10/bis3NTA and IFNAR2-H10/bis3NTA peaks (not shown), pointing towards that no transient interaction occurs between the two receptor ectodomains in solution in the absence of ligand.

As predicted, the preferential crosslinking of two H10-tags in the ternary complex preassembled by intrinsic affinity can be ascribed to entropic selectivity of bis3NTA clamp. High redundancy in histidines of each H10 tag provides docking sites for multivalent coordination of all NTA moieties of the clamp and increases the possibility to adopt a complex at maximum energy. Bis3NTA simultaneous interaction with two proximate hexahistidine peptides gains more free energy and entropy at crosslinking in contrast to the 1:1 complex formation stoichiometry with individual H10 tags.

These observations indicate that the low-affinity IFN/IFNAR1/IFNAR2 complex assembly in solution mediated by wild type IFNα2 can be efficiently “zipped-up” by bis3NTA entropic clamp. The selective bis3NTA–mediated crosslinking of the C–terminal receptor decahistidine tags brought into close proximity upon ternary complex formation is

energetically favourable and appears to be suitable as a generic tool for short-term stabilization of low affinity multiprotein complexes for functional analysis.

4.3.3 N-terminal vs. C-terminal complex stabilization

A similar set of analytical SEC assays was carried out in order to compare the bis3NTA-mediated stabilization of ternary complexes formed by wild type IFNα2 ligand and receptor subunits carrying N- or C- terminal His10-tags.

As before, IFNAR1-H10, IFNAR2-H10 and ^{Dy647}IFNα2 were mixed with the bis3NTA clamp at a molar ratio 1:1.5:1.5:1.5 and chromatographed with simultaneous detection at 650 nm (Figure 4.10 A). A clear ternary complex peak was detected at ~1.43 mL retention volume and the excess of the labelled ligand eluted at 1.85 mL. Interestingly under the same experimental conditions when SEC was carried out with the ternary complex formed with H10-IFNAR1 and H10-IFNAR2 receptors carrying N-terminal decahistidine tags, about two-fold reduction of the ternary complex peak at 1.43 mL was observed (Figure 4.10 B). Broadening of the peak at short retention time and a significant increase of the ^{Dy647}IFNα2/H10-IFNAR2 binary complex peak point towards that crosslinking of the receptor N-termini in the interferon ternary complex is less efficient than the stabilization via C-terminal His-tags. This discrepancy can arise from the longer distance between N- termini than between receptor C- termini in the ternary complex as well as from the protein conformational flexibility in solution, lowering the probability of their capture by the clamp. The distance between the N-terminal receptor residues in the X-ray structures of ternary complex is about 7 nm (Figure 4.10 C). Taking into account the length and flexibility of the fused decahistidine tags, the 12 nm maximal distance between the coordination groups of bis3NTA clamp should be sufficient for crosslinking these termini. Comparison of the unliganded and bound receptor subunits in X-ray structures (Figure 1.9) reveals a large movement of the membrane-distal SD1 of IFNAR1 towards ligand upon complex assembly. Fluorescence quenching based FCS experiments suggested dynamic fluctuations of the IFNAR1 conformation (~200 μs transition time) which are lost once complex with the ligand is formed [40]. It provides insights that the SD1 of IFNAR1 is highly flexible in solution. When H10-tag is fused to the N-terminus of SD1, the dynamic distance change between the two receptor N-termini in the ternary complex may result in their partial stabilization efficiency by bis3NTA.

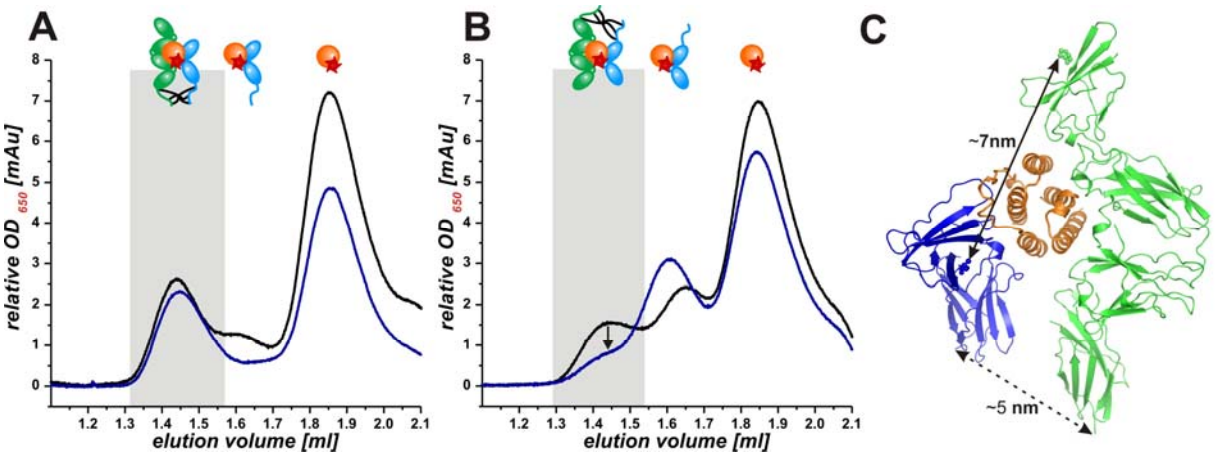

Figure 4.10 Ternary complex stabilization via N- and C-terminal receptor His-tags by bis3NTA and tetrakis-NTA clamps.

SE chromatograms of IFNα2/IFNAR1/IFNAR2 stabilized ternary complex as detected at 650 nm. **A** Stabilized ternary complexes formed by ^{Dy647}IFNα2 and receptor subunits IFNAR1-H10 and IFNAR2-H10 with C-terminal His tags in the presence of bis3NTA (black curve) and ^{AT565}tetrakis-NTA (blue curve). **B** Stabilized ternary complexes formed by ^{Dy647}IFNα2 and receptor subunits H10-IFNAR1 and H10-IFNAR2 with N-terminal His-tags in the presence of bis3NTA (black curve) and ^{AT565}tetrakis-NTA (blue curve). Elution time for the stabilized ternary complex is indicated by the grey bar. Arrow points at the ternary complex peak obtained for the stabilization of N-terminal receptor His-tags by means of ^{AT565}tetrakis-NTA. **C** Schematic comparison of the distances between receptor N- and C- termini in the X-ray structure of IFN2/IFNAR1/IFNAR2 ternary complex. Membrane-proximal SD4 of IFNAR1 was not visible in the X-ray structure and was modelled for clarity.

To further dissect the distance-dependent selectivity of clamps on protein complex stabilization we employed a multivalent chelator head adaptor tetrakis-NTA (4NTA) with four functional NTA moieties (Figure 4.3 B) and the maximum distance of 3.8 nm between the end coordination groups. The same set of SEC assays was carried out with 4NTA and the receptors fused to H10 tags at N- and C- termini. They demonstrated that similarly to bis3NTA, 4NTA efficiently crosslinks the C-terminal receptor His-tags, driving the equilibrium to ternary complex stabilization (Figure 4.10 A). This might indicate the relatively close proximity (about 5 nm or less) of the receptor C-termini in the assembled ternary complex. Though, the position of IFNAR1 C-terminus is not defined since the membrane-proximal SD4 of this receptor was not visible in the X-ray structure (Figure 4.10 C) [1]. As expected, further reduction of the ternary complex peak was observed when 4NTA was employed for stabilizing the complex with receptors carrying N-terminal His tags (Figure 4.10 B). Thus multivalent chelator clamps demonstrate entropic selectivity yet distance-dependence at His tag bridging due to the discrepancy in the size of the clamps. Bis3NTA

clamp can cover H10-tag crosslinking over much longer distances serving a more generic tool for protein complex stabilization.

4.3.4 Preparation of the ternary complex for FCCS analysis

FCCS analysis of the stabilized ternary complex required SEC purification of the complex carrying green and red fluorescence reporters. The ternary complex was formed by mixing ^{AT488}IFNAR1-H10 with IFNAR2-H10 and wild type ^{Dy647}IFNα2 in presence of bis3NTA clamp at the same molar ratios as for analytical SEC in 4.3.2 and subsequent fractionation by size exclusion chromatography (Figure 4.11 A) Accurate determination of the ternary complex elution time was essential for the fraction separation from IFNAR1/bis3NTA and binary IFNAR2/IFN/bis3NTA complex.

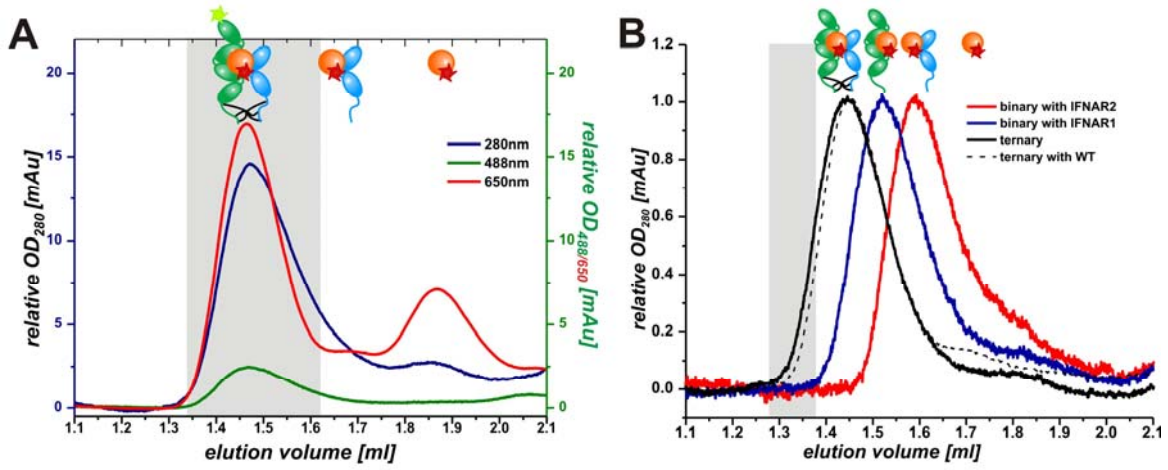

Figure 4.11 Ternary complex preparation for FCCS analysis.

A Purification of a fluorescence labelled ternary complex by size exclusion chromatography. Elution profiles of ^{AT488}IFNAR1-H10 mixed with IFNAR2-H10 and ^{Dy647}IFNα2 in presence of bis3NTA clamp as detected at 280 nm (blue), 488 nm (green), and 650 nm (red). Elution time of the stabilized ternary complex is indicated by the grey bar. **B** Analytical SEC for calibrating the retention time of ternary and binary complexes. All SEC assays carried out in presence of bis3NTA clamp. Solid line chromatograms correspond to complexes formed with ^{Dy647}IFNα2-YNS-α8tail: black – ternary complex, blue – binary complex with IFNAR1-H10, red - binary complex with IFNAR2-H10. For reference, black dashed curve shows the elution of the ternary complex formed with WT ^{Dy647}IFNα2. Ternary complex fractions, taken for FCCS analysis are indicated by the grey bar. The peaks were normalized for visual comparison.

To this end we exploited IFNα2-YNS-α8tail, an interferon mutant with high affinity to both receptors, to calibrate the peak retention time for the individual binary complexes (Figure 4.11 B). Though under applied experimental conditions no binary complex with IFNAR1 and wild type IFNα2 would be formed, defining its retention time would ensure good separation of the ternary complex from elution of IFNAR1/bis3NTA as well. As it is seen from SEC,

IFNAR1/IFN/bis3NTA binary complex peak starts at ~1.4 mL and the ternary complex peak for both interferons, IFNα2 and IFNα2-YNS-α8tail, starts at ~1.3 mL. Therefore in the preparative SEC ^{AT488}IFNAR1/IFNAR2/^{Dy647}IFNα2/bis3NTA complex fractions eluted between 1.3-1.4 mL were collected and taken for subsequent analysis by FCCS. Monitoring SEC at 280 nm, 488 nm, and 650 nm confirmed that the complex contained two fluorescent dyes (Figure 4.11 A).

For FCCS control experiments with a single green fluorescence reporter, ternary complex preparation was carried out the same way but using label-free IFNα2.

4.3.5 Probing the stabilized ternary complex by FCCS

Dual-colour fluorescence cross-correlation spectroscopy (FCCS) was employed in order to probe *in vitro* the stabilized ^{AT488}IFNAR1/IFNAR2/^{Dy647}IFNα2 complex with respect to stability and Förster resonance energy transfer (FRET).

Unlike autocorrelation (AC) amplitudes, cross-correlation (CC) amplitudes are not directly proportional to the concentration of species carrying both, green and red labels. Since cross-correlation depends on autocorrelation amplitudes, higher concentration of either of fluorescence reporters results in the decrease of the cross-correlated signal. In addition, an adequate overlap of the observation volumes for two laser spots is required in order to measure an unbiased cross-correlation. To calibrate the experimental setup we employed the '*In vitro* standard probe for FCCS' (SP) from IBA which is comprised of double-labelled dsDNA with excitation wavelengths 488/633 nm (Figure 4.5). Owing to experimental limitations this is the maximum cross-correlation that can be observed with our setup, even for 100% double-labelled species. Therefore all cross-correlated components of ternary complex measured for the samples were normalized to the respective reference value obtained for the SP.

Since the applied stabilization approach is a reversible process, fractionated ternary complex was analysed by FCCS directly after HPLC-purification. FCCS traces were recorded in succession for each fraction readily after diluting them to working concentrations of nanomolar range which further accelerates complex dissociation. Cross-correlation for typical FCCS measurements (Figure 4.12 A) yielded about 40 to 60% of molecules in complex confirming feasibility of the employed stabilization approach. As a control for the proof of concept no significant cross-correlation was obtained for the high affinity mutant ^{Dy647}IFNα2-YNS-α8tail mixed *in situ* with the respective receptor subunits ^{AT488}IFNAR1 and IFNAR2 without bis3NTA stabilization and diluted to FCCS working concentrations (not shown).

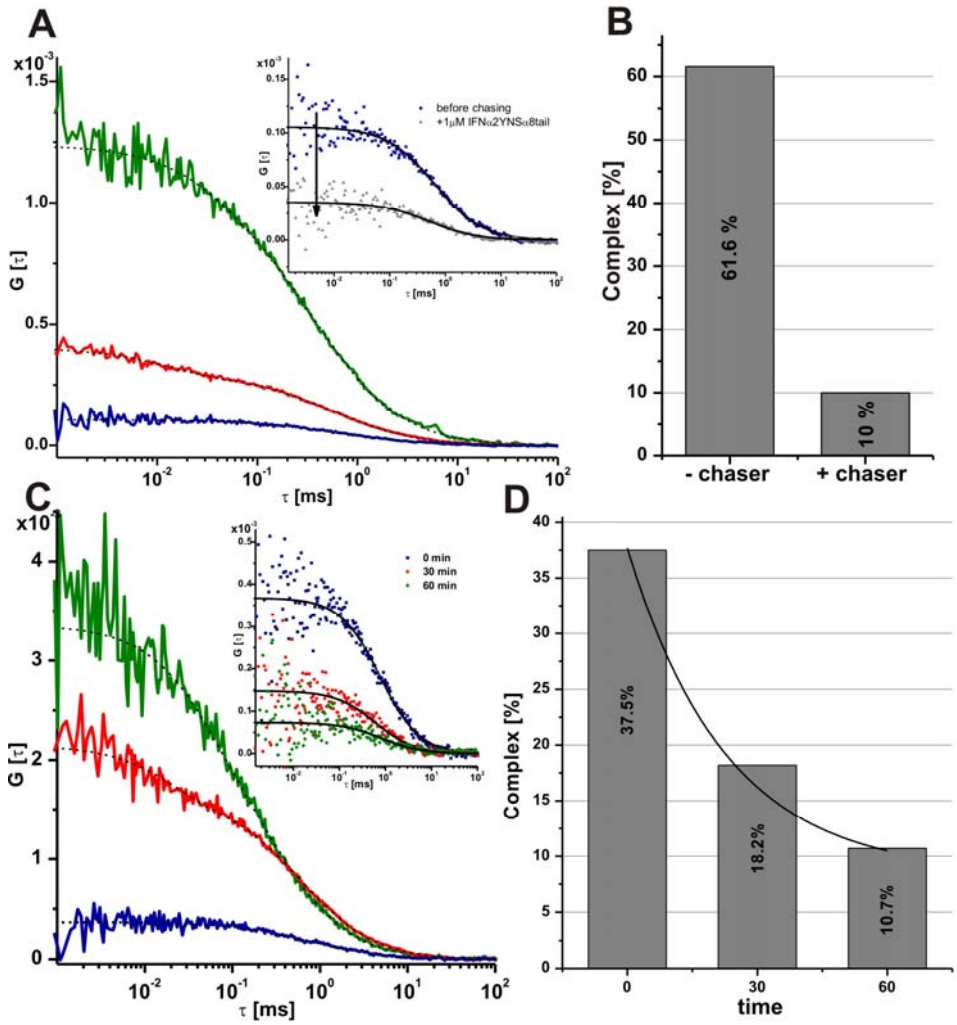

Figure 4.12 Probing the stabilized ternary complex by fluorescence cross-correlation spectroscopy.

A Typical fluorescence autocorrelation (AC) and cross-correlation (CC) curves of the bis3NTA-stabilized ^{AT488}IFNAR1-H10/IFNAR2-H10/^{Dy647}IFNα2 complex measured before chasing. Green curve denotes the ATTO488 autocorrelation, red the Dy647 autocorrelation, and blue the cross-correlation between the two, the fits of the curves are shown as dotted lines. Inset figure shows the reduction of CC upon chasing with 1 µM of label-free IFNα2-YNS-α8tail (blue: CC before chasing; grey: CC 5 min after addition of IFNα2-YNS-α8tail; the fits of the CC curves are shown as black solid lines). **B** The decrease of the cross-correlated fraction of molecules upon chasing with 1 µM of label-free IFNα2-YNS-α8tail. **C** Fluorescence AC and CC curves of the stabilized ^{AT488}IFNAR1-H10/IFNAR2-H10/^{Dy647}IFNα2 complex measured before the dissociation time course. Green curve denotes the ATTO488 autocorrelation, red the Dy647 autocorrelation, and blue the cross-correlation between the two, the fits of the curves are shown as dotted lines. Inset figure shows the reduction of CC as observed during spontaneous dissociation time course (blue: 0 min, red: 30 min, green: 60 min, black solid lines: the fits of the curves are shown as black solid lines). **D** Time-course of the cross-correlation function upon spontaneous complex dissociation. The decrease of the cross-correlated fraction of complex with time is fitted by the monoexponential model shown as solid line, the estimated complex lifetime is τ=23 min.

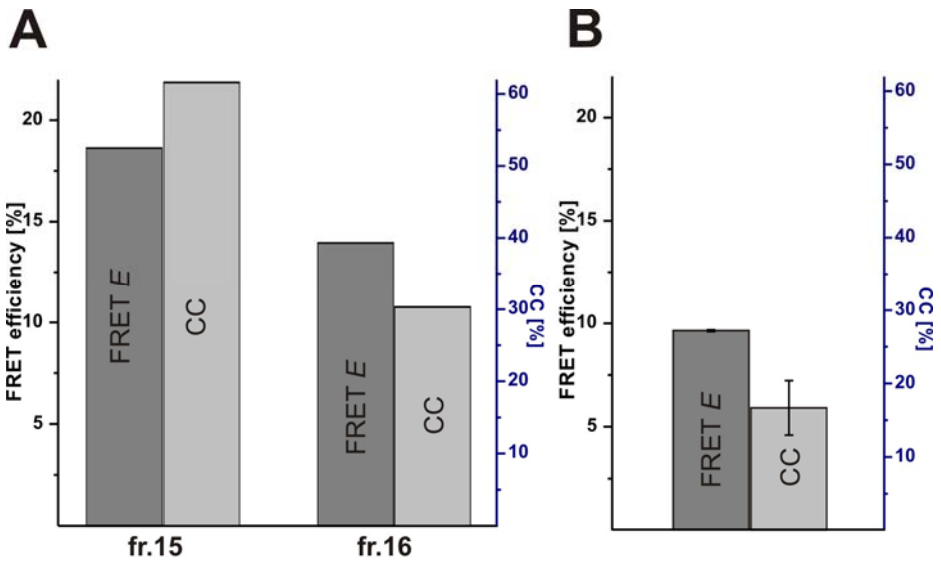

Figure 4.13 Correlation of FRET efficiency and cross-correlated ternary complex upon chasing with label-free IFNα2-YNS-α8tail.

A Correlation of FRET efficiency (*E*) and cross-correlated (CC) percent of total complex before chasing. **B** Comparison of the change in average FRET efficiency (*E*) and cross-correlated (CC) complex after chasing the fractions with 1 μM label-free IFNα2-YNS-α8tail. Fr. 15 and fr. 16 - fraction numbers.

To further confirm that the observed cross-correlation arises from the double-labelled stabilized complex it was chased with 1 μM label-free IFNα2-YNS-α8tail. Five minutes after addition of IFNα2-YNS-α8tail, the cross-correlated fraction of molecules decreased on average to nearly 10% (Figure 4.12 B and Figure 4.13 B), which is close to a baseline value recorded for negative control FCCS experiment in the absence of the red dye. Exchange of the labelled wild type ligand to the unlabelled IFNα2-YNS-α8tail upon complex chasing was also monitored by the decrease of the FRET efficiency between ^{AT488}IFNAR10 and ^{Dy647}IFNα2 (Figure 4.13). The FRET efficiency (*E*) was estimated PIE from the same FCCS traces and was based on the fitted lifetimes of quenched and unquenched donor dye. The maximum calculated FRET efficiency is about 27%, taking into account the Förster radius for this fluorophore pair $R_{0,AT488/Dy647}$=51 Å, the distance between N-termini of IFNAR1 and IFN and the length of ybbR-tags for enzymatic labelling with the dye flexible linkers. Hence, FRET efficiencies of 12-18% obtained for more than 50% cross-correlated complex (Figure 4.13 A) are in line with the theoretical estimation. The decrease in the percent of cross-correlated complex and FRET efficiency for the same samples is well qualitatively correlated pointing towards the reduction of double-labelled ternary complex concentration upon chasing.

Yet, owing to a reversible non-covalent nature of the entropic clamp-mediated stabilization approach, ternary complex falls apart over time, especially at single molecule working concentrations. Spontaneous dissociation of the stabilized ternary complex upon dilution was

assessed from the FCCS time-lapse experiment (Figure 4.12 C and D). Ternary complex lifetime in solution for the time course experiment was estimated as τ=23 min comparatively to ~3 s stability without the stabilizing on solid supports. Thus exploiting the entropic clamp enabled enhancement of the complex stability over two orders of magnitude for measuring substantial cross-correlation and FRET in the assembled wild type interferon receptor complex. However the stabilization is still reversible which is expected for the high affinity yet non-covalent crosslinker dissociating from the complex at working concentrations of nanomolar range. This is a limitation of the chosen strategy which can be detoured by combining it with an additional crosslinking technique for already purified stabilized protein complex.

4.4 Conclusions

We have developed a generic method for stabilizing *in vitro* protein complexes formed by intrinsic low affinity. In contrast to conventional methods such as chemical crosslinking or recombinant self-dimerizing tag fusions, our new "bis3NTA entropic clamp" approach enables site-specific reactivity through already available oligohistidine tags as well as selective crosslinking, because it is based on the entropic preferences for forming multicoordinated NTA/histidine complexes selectively crosslinking only the His-tags of proteins which naturally interact. This introduces the flexibility to selectively stabilize protein complexes preassembled by intrinsic affinity and to suppress the non-specific crosslinking of proteins which do not interact. This crosslinking has numerous advantages over other methods such as it can be applied in one step, does not require additional introduced site-specific protein modifications, withstands size exclusion purification, bridges protein tags spaced by the distance about ten nanometres. Importantly, it enables entropic selectivity at stabilizing only protein complexes which interact and provides high affinity reactivity for working with micromolar protein affinities diluted further at nanomolar concentrations. This technique has been applied to stabilize type I interferon receptor complex with intrinsic affinity of a micromolar range. We subsequently probed the stabilized ternary complex by FCCS and FRET. FCCS chasing assay established that the observed high level of cross-correlation is due to the double-labelled complex particles and it could not have been obtained without the stabilizer. Moreover, significant FRET was detected between the reporter probes placed at two different proteins in the fixed complex. This indicates the utility of the employed stabilization approach for measuring resonance energy transfer in multiprotein complexes which naturally fall apart at single molecule working concentrations. The estimated complex lifetime increased by a factor over two orders of magnitude upon stabilization. However the

observed cross-correlation and FRET diminish to background level in the FCCS spontaneous dissociation time-course assay in solution. It is an expected limitation of the applied technique since the entropic clamp non-covalently interacts with His-tags and eventually dissociates. A potential enhancement of this method is to use an additional crosslinking reaction performed on a purified stabilized complex. The possibility to monitor weakly interacting protein complexes in solution for extended time will enable for further probing by FCCS the dynamic functional processes such as protein conformational crosstalk. Our findings only open up perspectives for further studies in this direction.

4.5 Summary

This last section described a method to stabilize low affinity protein complexes using a multicoordinated reversible interaction of NTA-based entropic clamps with protein oligohistidine tags. Entropic selectivity of the clamp binding enables to suppress non-specific crosslinking of proteins which do not interact. Thus only proteins which have intrinsic affinity to form complexes could be specifically fixed through their His-tags. Crosslinking could also be achieved for N- or C-terminal protein His-tags in a distance-dependent manner via the short-range and long-range entropic clamps covering the distances of four to ten nanometres. This strategy enabled to increase the affinity of type I interferon receptor subunits to form a stable ternary complex with wild type IFNα2. Significant fraction of this stabilized complex was cross-correlated by dual colour FCCS and FRET between the two labelled proteins of the ternary complex was demonstrated.

4.6 References

1. Thomas, C., et al., *Structural linkage between ligand discrimination and receptor activation by type I interferons.* Cell, 2011. **146**(4): p. 621-32.

2. Gavutis, M., et al., *Determination of the two-dimensional interaction rate constants of a cytokine receptor complex.* Biophysical journal, 2006. **90**(9): p. 3345-55.

3. Lamken, P., et al., *Ligand-induced assembling of the type I interferon receptor on supported lipid bilayers.* Journal of molecular biology, 2004. **341**(1): p. 303-18.

4. Benitez, J.J., A.M. Keller, and P. Chen, *Nanovesicle trapping for studying weak protein interactions by single-molecule FRET.* Methods in enzymology, 2010. **472**: p. 41-60.

5. Leitner, A., et al., *Probing native protein structures by chemical cross-linking, mass spectrometry, and bioinformatics.* Molecular & cellular proteomics : MCP, 2010. **9**(8): p. 1634-49.

6. Tang, X. and J.E. Bruce, *Chemical cross-linking for protein-protein interaction studies.* Methods in molecular biology, 2009. **492**: p. 283-93.

7. Brocker, C., et al., *Molecular architecture of the multisubunit homotypic fusion and vacuole protein sorting (HOPS) tethering complex.* Proceedings of the National Academy of Sciences of the United States of America, 2012. **109**(6): p. 1991-6.

8. Yan, F., et al., *Nonprotein based enrichment method to analyze peptide cross-linking in protein complexes.* Analytical chemistry, 2009. **81**(17): p. 7149-59.

9. Brunner, J., *New photolabeling and crosslinking methods.* Annual review of biochemistry, 1993. **62**: p. 483-514.

10. Hino, N., et al., *Protein photo-cross-linking in mammalian cells by site-specific incorporation of a photoreactive amino acid.* Nature methods, 2005. **2**(3): p. 201-6.

11. Kimmerlin, T. and D. Seebach, *'100 years of peptide synthesis': ligation methods for peptide and protein synthesis with applications to beta-peptide assemblies.* The journal of peptide research : official journal of the American Peptide Society, 2005. **65**(2): p. 229-60.

12. Okumura, M., S. Shimamoto, and Y. Hidaka, *A chemical method for investigating disulfide-coupled peptide and protein folding.* The FEBS journal, 2012. **279**(13): p. 2283-95.

13. Mootz, H.D., *Split inteins as versatile tools for protein semisynthesis.* Chembiochem : a European journal of chemical biology, 2009. **10**(16): p. 2579-89.

14. Volkmann, G. and H.D. Mootz, *Recent progress in intein research: from mechanism to directed evolution and applications.* Cellular and molecular life sciences : CMLS, 2012.

15. Vila-Perello, M. and T.W. Muir, *Biological applications of protein splicing.* Cell, 2010. **143**(2): p. 191-200.

16. Chao, H., et al., *Use of a heterodimeric coiled-coil system for biosensor application and affinity purification.* Journal of chromatography. B, Biomedical sciences and applications, 1998. **715**(1): p. 307-29.

17. Fernandez-Rodriguez, J. and T.C. Marlovits, *Induced heterodimerization and purification of two target proteins by a synthetic coiled-coil tag.* Protein Science, 2012. **21**(4): p. 511-519.

18. Hornig, N. and A. Farber-Schwarz, *Production of bispecific antibodies: diabodies and tandem scFv.* Methods in molecular biology, 2012. **907**: p. 713-27.

19. Holliger, P., T. Prospero, and G. Winter, *"Diabodies": small bivalent and bispecific antibody fragments.* Proceedings of the National Academy of Sciences of the United States of America, 1993. **90**(14): p. 6444-8.

20. Kanno, A., T. Ozawa, and Y. Umezawa, *Detection of protein-protein interactions in bacteria by GFP-fragment reconstitution.* Methods in molecular biology, 2011. **705**: p. 251-8.

21. Ando, T., et al., *Construction of a small-molecule-integrated semisynthetic split intein for in vivo protein ligation.* Chemical communications, 2007(47): p. 4995-7.

22. Apostolovic, B. and H.A. Klok, *pH-sensitivity of the E3/K3 heterodimeric coiled coil.* Biomacromolecules, 2008. **9**(11): p. 3173-80.

23. Lata, S. and J. Piehler, *Stable and functional immobilization of histidine-tagged proteins via multivalent chelator headgroups on a molecular poly(ethylene glycol) brush.* Analytical chemistry, 2005. **77**(4): p. 1096-105.

24. Lata, S., et al., *High-affinity adaptors for switchable recognition of histidine-tagged proteins.* Journal of the American Chemical Society, 2005. **127**(29): p. 10205-15.

25. You, C., et al., *Self-controlled monofunctionalization of quantum dots for multiplexed protein tracking in live cells.* Angewandte Chemie, 2010. **49**(24): p. 4108-12.

26. Lata, S., et al., *Specific and stable fluorescence labeling of histidine-tagged proteins for dissecting multi-protein complex formation.* Journal of the American Chemical Society, 2006. **128**(7): p. 2365-72.

27. Reichel, A., et al., *Noncovalent, site-specific biotinylation of histidine-tagged proteins.* Analytical chemistry, 2007. **79**(22): p. 8590-600.

28. Yin, J., et al., *Genetically encoded short peptide tag for versatile protein labeling by Sfp phosphopantetheinyl transferase.* Proceedings of the National Academy of Sciences of the United States of America, 2005. **102**(44): p. 15815-20.

29. Zhou, Z., et al., *Genetically encoded short peptide tags for orthogonal protein labeling by Sfp and AcpS phosphopantetheinyl transferases.* ACS chemical biology, 2007. **2**(5): p. 337-46.

30. Piehler, J. and G. Schreiber, *Biophysical analysis of the interaction of human ifnar2 expressed in E. coli with IFNalpha2.* Journal of molecular biology, 1999. **289**(1): p. 57-67.

31. Griffin, A.M. and H.G. Griffin, *Molecular Biology: Current Innovations and Future Trends* 1997, Norfolk, UK Horizon Scientific Press. 176.

32. Kalie, E., et al., *An interferon alpha2 mutant optimized by phage display for IFNAR1 binding confers specifically enhanced antitumor activities.* The Journal of biological chemistry, 2007. **282**(15): p. 11602-11.

33. Piehler, J. and G. Schreiber, *Mutational and structural analysis of the binding interface between type I interferons and their receptor Ifnar2.* Journal of molecular biology, 1999. **294**(1): p. 223-37.

34. Waichman, S., et al., *Functional immobilization and patterning of proteins by an enzymatic transfer reaction.* Analytical chemistry, 2010. **82**(4): p. 1478-85.

35. Müller, C.B., et al., *Precise measurement of diffusion by multi-color dual-focus fluorescence correlation spectroscopy.* EPL (Europhysics Letters), 2008. **83**(4): p. 46001.

36. Weidemann, T. and P. Schwille, *Fluorescence Correlation Spectroscopy in Living Cells*, in *Handbook of Single-Molecule Biophysics*, P. Hinterdorfer and A. Oijen, Editors. 2009, Springer US. p. 217-241.

37. Li, Z., et al., *The EM structure of a type I interferon-receptor complex reveals a novel mechanism for cytokine signaling.* Journal of molecular biology, 2008. **377**(3): p. 715-24.

38. Levin, D., D. Harari, and G. Schreiber, *Stochastic receptor expression determines cell fate upon interferon treatment.* Molecular and cellular biology, 2011. **31**(16): p. 3252-66.

39. Pan, M., et al., *Mutation of the IFNAR-1 receptor binding site of human IFN-alpha2 generates type I IFN competitive antagonists.* Biochemistry, 2008. **47**(46): p. 12018-27.

40. Strunk, J.J., et al., *Probing protein conformations by in situ non-covalent fluorescence labeling.* Bioconjugate chemistry, 2009. **20**(1): p. 41-6.

5 Conclusions and outlook

This thesis aimed to establish biochemical and biophysical approaches for exploring *in vitro* the type I IFN receptor assembly with respect to interactions, allostery and conformational changes. Elucidation of the molecular basis of these effects for type II cytokine receptors is particularly challenging since typically these proteins are incompatible with conventional site-diercted cysteine-based labelling chemistry. This required a tunable combination of site-specific protein modifications for their surface immobilization, incorporation of fluorescent dyes or crosslinkers. Also in the course of this study the specific advantages of covalent versus non-covalent protein modification chemistries by the use of PPT tags and His tags were exploited to provide versatility and orthogonality in their biological assay applications.

We utilized a generic method of site-directed genetic protein tagging with short PCP/ACP-based peptides (such as ybbR, S6 and A-tag) [1, 2], for attaching small molecule probes and immobilizing proteins onto surface in a covalent manner. The enzymatic PPTase-catalysed labelling of a specific conservative serine residue on these tags was shown in this work to be very robust and efficient for transferring a variety of small molecules from CoA-probe conjugates, including biotin and fluorophores. The substrate promiscuity of the enzyme offers versatility in probe selection through one-step chemical coupling of CoA [3] with spectroscopic reporters or any other functional element, so that a further synthesis of CoA-based crosslinker should be feasible. Interaction assays between soluble labelled wild type and mutant IFNα2 with individual surface-immobilized receptor ectodomains confirmed that the proteins maintained a high degree of activity even after labelling. The orthogonality of this enzymatic reaction to conventional cysteine-based chemistry enables covalent site-directed dual-colour fluorescence labelling of one protein molecule for subsequent probing of intramolecular distances by FRET, but requires substantial amounts of purified protein.

Since the specific serine residue of these peptide tags can be further reacted with the phosphopantetheinyl group of CoA presented on a surface, this approach was also applied for biocompatible covalent protein immobilization. The advantage of this covalent tethering is a good degree of protein activity maintained over several hours which could not have been obtained previously, in particular for IFN ligand surface immobilization. Moreover, there are several short PCP/ACP tags available, for sequential and orthogonal modification by means of Acp and Sfp transferases [2]. Though we did not explore them in greater details, their orthogonal multiplexed application should be possible. Furthermore these tags were successfully labelled when inserted at either of protein termini, but more efficient surface immobilization was achieved for proteins tagged at N-terminus. Additionally, the reactions of

almost all such tags with their specific ligands suffer from slow binding kinetics and thus require comparatively large protein concentrations for surface immobilization. These shortcomings were elegantly overcome by using combined tags comprising of an ybbR- and a His-tag (k_a~10^5 $M^{-1}\cdot s^{-1}$) placed onto different termini of IFNAR1 receptor for achieving much greater immobilization efficiency onto suitably double-functionalized surfaces as compared to proteins with the ybbR tag alone. In the same way as the tethering via a single ybbR peptide, this strategy is orthogonal to His-tag chemistry since Ni^{2+} coordination sites are eliminated from the surfaces after it is being enzymatically reacted with PCP-tag. This would give further an advantage in probing the interactions of irreversibly immobilized analyte with suitable soluble binding partners produced as oligohistidine tag fusion.

Methods of covalent and non-covalent site-specific protein modifications introduced in the section 11 were then systematically explored. Based on the specific reversible interaction of oligohistidine tags with tris-NTA moieties on a surface a rapid immobilization assay have been devised to selectively capture His-tagged proteins directly from cell expression supernatants as well as to quantify their relative surface amount from binding amplitudes. We used it to explore the interaction of IFNAR1 with various IFN subtypes labelled with fluorescence reporters by a covalent and by a reversible His-tag based approaches. Although this assay is not fully orthogonal to probe interactions with ligands sensitive to surface transition metal ions such as interferon β or His-tagged interferons, it enabled a good assessment of the binding kinetics and affinities after complete blocking of excessive Ni^{2+}coordination sites with maltose binding protein. In prospect, full orthogonality can be achieved by devising a direct coupling of ybbR- or ybbR/His-tagged receptors from supernatants through covalent enzymatic surface immobilization chemistry or combined double-tag assay. Since direct quantitative binding assay from crude expression supernatants was proven to be very simple and robust, it could be applicable as a generic method for rapid high-throughput screening of protein binding interfaces.

To analyse in detail the chemistries involved in the IFNAR1 receptor recognition of various IFNs the established direct rapid surface immobilization assay was employed. It enabled to dissect in an alanine screen the conservative versus subtype-specific chemistries in the IFNAR1 binding interface for IFNα/β/ω subtypes. So with the help of the implemented *in vitro* screening technique a distinct recognition of IFNAR1 residues was revealed and subsequently correlated with the cellular response pattern evoked by various IFNs thus suggesting the mechanism of their differential signalling. Since cooperative binding was reported for some other members from cytokine receptor family, we have been looking for

suitable means to address this effect in *in vitro* assays for interferon receptor. A bottom-up interaction assay have been devised to probe simultaneous binding of both soluble receptor ectodomains IFNAR1 and IFNAR2 to IFN stably immobilized onto surface via the covalent PPTase-catalysed approach . This allowed abating the possible receptor-receptor contacts through C-terminal His-tags and membrane-proximal domains and their influence onto the observed little cooperative stabilization of the ternary complex during simultaneous receptor binding. Thus the mechanism of cooperativity was proposed to be mediated through local conformational changes on the ligand binding sites for the receptors. Yet a potential contribution of receptor transmembrane domains in a three-body assembly of IFN receptor still has to be elucidated. Apparently, cellular assays with endogenous full length receptors carried out with IFN mutants targeting both receptor subunits corroborated the independent ligand binding to FNAR1 and IFNAR2. Our *in vitro* solid phase measurements with combined IFNAR1/2 interferon mutants on artificial membranes contributed to that study. An elegant assay was implemented in order to probe ternary complex assembly with label-free ligands. Ligand binding-induced conformational change in labelled IFNAR1 was exploited as fluorescence readout. This enabled to explore the stability of ternary complexes with the combined mutants on lipid bilayers and to correlate them with the effects observed in cells. Thus the integral binding affinity comprised of the affinities towards individual receptor subunits was proposed to play a role in dictating the cellular response pattern.

Although through the course of the carried out experiments on solid supports we could demonstrate differential binding chemistries, allostery or conformational changes involved in the formation of type I IFN receptor complex, the dynamic processes such as conformational crosstalk or dynamic ligand-receptor interactions remained concealed. To evaluate by FCCS in solution a conformational crosstalk in a ternary complex formed with wild type IFNα2 we sought to design an approach of stabilizing its natural low affinity-based assembly. A method to stabilize preformed protein complexes by means of multivalent chelator head entropic clamps was confirmed to be very efficient to increase their naturally low binding affinities. The bis3NTA entropic clamp forms multicoordinated non-covalent complexes with oligohistidine peptide tags at well-defined energetically favourable stoichiometry, depending on gain or loss in entropy. Owing to the clamp entropic selectivity feature, suppression of unspecific crosslinking of non-interacting proteins is feasible. Thus bis3NTA clamp specifically crosslinks only His-tagged proteins interacting with each other with intrinsic affinity targeting them to form stable complexes. With the His-tag being far the most frequently used affinity tag for protein purification, highly generic application of this

technique can be envisioned for stabilization of low affinity multiprotein complexes for functional analysis. Owing to the simplicity of this method and rapid NTA/histidine complexation this clamping technique can be used even *in situ* such as for direct fixing of protein complexes for electron microscopy studies. This approach allows only a short-term reversible complex stabilization since the His-tags were crosslinked by bis3NTA in a non-covalent manner. As it was demonstrated by FCCS experiments in solution, bis3NTA-mediated stabilization of IFN receptor complex was sufficient to significantly increase its life time in order to detect the high level of cross-correlated double-labelled complex particles and FRET within them. However for further assessment of the complex conformational crosstalk, more robust irreversible crosslinking is needed. As a solution to this drawback an approach of combination the His-tag clamping with subsequent covalent chemical crosslinking can be developed. In addition, site-specific chemical reactivity can be introduced into His-tags such as the insertion of a lysine residue for site-directed amine chemistry. For combining the His-tags with ybbR-tag covalent modification chemistry, an implementation of ybbR-tag-reactive CoA-based clamp can be as well envisaged. The current study laid the first stone for broad and challenging future developments in this field.

5.1 References

1. Yin, J., et al., *Genetically encoded short peptide tag for versatile protein labeling by Sfp phosphopantetheinyl transferase.* Proceedings of the National Academy of Sciences of the United States of America, 2005. **102**(44): p. 15815-20.

2. Zhou, Z., et al., *Genetically encoded short peptide tags for orthogonal protein labeling by Sfp and AcpS phosphopantetheinyl transferases.* ACS chemical biology, 2007. **2**(5): p. 337-46.

3. Yin, J., et al., *Site-specific protein labeling by Sfp phosphopantetheinyl transferase.* Nature protocols, 2006. **1**(1): p. 280-5.

6 Summary

Signal propagation across the membrane by cytokine receptor signalling involves a complex interplay of receptor-ligand interactions, allostery and conformational changes. Type I interferons (IFNs) exert their biological activities through binding to a shared receptor consisting of the type II cytokine receptor subunits IFNAR1 and IFNAR2. The aim of this thesis was to establish biochemical and biophysical approaches for exploring *in vitro* interactions and conformational changes accompanying the formation of type I IFN receptor complex. For these purposes, in this work a versatile combination of covalent vs. non-covalent reversible site-specific protein modification chemistries was exploited for their surface immobilization, incorporation of fluorescence probes or crosslinkers. The generic bioorthogonal strategy of PPTase-catalysed covalent modification of ybbR short peptide tag fused to a protein of interest enabled highly efficient site-directed fluorescence labelling of wild type IFNα2 and mutants, IFNAR1 and IFNAR2 receptors as well as their functional immobilization onto surfaces. These modified proteins were confirmed to be active by studying their interactions in ligand-receptor surface binding assays in real time by total internal reflection fluorescence spectroscopy and reflectance interference. A rapid quantitative surface assay for probing binding kinetics of proteins captured directly via His-tags from cell supernatants was established and employed for screening of IFNAR1 mutants in order to identify the residues responsible for differential recognition of various IFN subtypes. Thus the fine-tuned IFN binding chemistries through few ligand-specific interaction points as the basis for receptor plasticity was identified. Site-specific covalent immobilization allowed exploring cooperativity in ligand recognition by the receptor subunits. The observed small allosteric effect is apparently not related to the potential contact of membrane-proximal receptor domains but probably mediated through conformational cross-communication of binding sites on the ligand. Substantial conformational changes of IFNAR1 upon ligand binding were exploited as fluorescence readout to monitor the assembly of ternary complexes on artificial membranes. This enabled exploring the life times of ternary complexes with IFNα2 combined mutants targeting binding to IFNAR1 and IFNAR2 and corroborated to the suggestion that the differential physiological activity of IFN subtypes is related to the total ternary complex affinity and not to ligand affinity towards individual receptor subunits. Finally, *in vitro* stabilization of dual-colour labelled weakly interacting IFNα2/IFNAR1/IFNAR2 complex by means of an entropic clamp was implemented, enabling to analyze ternary complexes by fluorescence cross-correlation spectroscopy Förster resonance energy transfer on the single

molecule level. These novel tools will prove valuable for unravelling the subtle interplay of interactions and conformational changes in cytokine receptor complexes.

7 Appendix

7.1 Publications

1. Kalie, E., et al., *The stability of the ternary interferon-receptor complex rather than the affinity to the individual subunits dictates differential biological activities.* The Journal of biological chemistry, 2008. 283(47): p. 32925-36.

2. Waichman, S., et al., *Functional immobilization and patterning of proteins by an enzymatic transfer reaction.* Analytical chemistry, 2010. 82(4): p. 1478-85.

3. You, C., et al., *Self-controlled monofunctionalization of quantum dots for multiplexed protein tracking in live cells.* Angewandte Chemie, 2010. 49(24): p. 4108-12.

4. Thomas, C., et al., *Structural linkage between ligand discrimination and receptor activation by type I interferons.* Cell, 2011. 146(4): p. 621-32.

7.2 List of figures

7.3 Tables

Table 7.1 Protein molar absorption values used in the current study.

Protein	ε, [$M^{-1} \cdot cm^{-1}$]
IFNα2, IFNα2-YNS, IFNα2-YNS-α8tail	18 070

YbbR-IFNα2, ybbR-IFNα2-YNS, ybbR-IFNα2-α8tail, ybbR-IFNα2-YNS-α8tail	18 070
IFNAR2, FNAR2-H10, ybbR-IFNAR2, IFNAR2-ybbR, ybbR-FNAR2-H10	26 500
IFNAR1-H6, IFNAR1-H10, H10-IFNAR1-ybbR, ybbR-IFNAR1-H10	84 830
IFNAR1-H10 cysteine and alanine mutants	84 830
Sfp, Sfp tagless	95 230

Table 7.2 Fluorescent dyes molar extinction coefficients with respective correction factors at 280 nm.

Fluorescent dye	Vendor	Absorption maximum (λ_{abs}), nm	ε, $M^{-1} \cdot cm^{-1}$	CF_{280}
Alexa Fluor 488	Molecular Probes	489	71 000	0.11
ATTO 488	ATTO-TEC GmbH	501	90 000	0.10
Oregon Green 488	Molecular Probes	498	70 000	0.12
Alexa Fluor 594	Molecular Probes	591	73 000	0.56
ATTO 565	ATTO-TEC GmbH	563	120 000	0.16
DY 647	Dyomics GmbH	653	250 000	0.04
ATTO 655	ATTO-TEC GmbH	663	125 000	0.08

Table 7.3 Course of chasing experiments in the cooperativity assays and specification of studied effects.

Ligand	Receptor	Chaser	Studied effect
YbbR-IFNα2-YNS	20 nM AT488IFNAR2	500 nM IFNα2	Suppression of rebinding
YbbR-IFNα2-YNS	20 nM AT488IFNAR2	3 μM IFNAR-H10, 500 nM IFNα2	Cooperativity proof for

			IFNAR2-EC
YbbR-IFNα2-YNS	20 nM AT488IFNAR2	3 µM IFNAR1-SD123, 500 nM IFNα2	Role of SD4 in cooperativity
YbbR-IFNα2-YNS	20 nM AT488IFNAR2	3 µM IFNAR1-tagless, 500 nM IFNα2	Role of H10-tag in cooperativity
YbbR-IFNα2-YNS	100 nM OG488IFNAR1-H10	Buffer	-
YbbR-IFNα2-YNS	100 nM OG488IFNAR1-H10	3 µM IFNAR2-H10	Cooperativity proof for IFNAR1-EC
YbbR-IFNα2	500 nM IFNα2 20 nM AT488IFNAR2	-	Binding inhibition assay
YbbR-IFNα2	20 nM AT488IFNAR2	Buffer	-
YbbR-IFNα2	20 nM AT488IFNAR2	500 nM IFNα2	Suppression of rebinding
YbbR-IFNα2	20 nM AT488IFNAR2	10 µM IFNAR1-H10	Cooperativity proof for IFNAR2-EC

7.4 Abbreviations

AC	autocorrelation
ACP	acyl carrier protein
bis3NTA	tris-(nitrilotriacetic acid)-EG7-disulfide
BSA	bovine serum albumin
CC	cross-correlation
CCW	counterclockwise
CoA	coenzyme A
CW	clockwise
D	domain
DOL	degree of labelling
DTT	dithiotheitol

EC	ectodomain, extracellular subunit
EDTA	ethylenediaminetetraacetic acid
EGF	epidermal growth factor
EGFR	epidermal growth factor receptor
EGFP	enhanced green fluorescent protein
EM	electron microscopy
Epo	erythropoietin
EpoR	erythropoietin receptor
FCS	fluorescence correlation spectroscopy
FCCS	fluorescence cross correlation spectroscopy
FN	fibronectin
FRET	Förster resonance energy transfer
GH	growth hormone
GHR	growth hormone receptor
H6	hexahistidine-tag
H10	decahistidine-tag
HBS	Hepes buffered saline
His	histidine-tag
HTL	HaloTag ligand
HTP	HaloTag protein
ICD	intracellular domain
IFN	interferon
IFNAR	interferon alpha receptor
IFNAR1	type I interferon receptor subunit 1
IFNAR2	type I interferon receptor subunit 1
Ig	immunoglobulin
IL	interleukin
IMAC	immobilized metal affinity chromatography
Jak	Janus kinase
mAb	monoclonal antibody
k_a	association rate constant
kDa	kilo Dalton
K_D	dissociation constant
k_d	dissociation rate constant

MCH	multivalent chelator head
MBP	maltose binding protein
NCL	native chemical ligation
NTA	nitrilotriacetic acid
PAGE	polyacrylamide gelelectrophoresis
PCP	peptidyl carrier protein
PCR	polymerase chain reaction
PEG	polyethylene glycol
PIE	pulsed interleaved excitation
Ppant	phosphopantetheinyl
PPT-tag	phosphopantetheinyl-tag
PPTase	phosphopantetheinyl transferase
RIf(S)	reflectance interference (spectroscopy)
RMS	root-mean-square deviation
RTK	receptor tyrosine kinase
SD	subdomain
SDS	sodiumdodecylsulfate
SE	size exclusion
SEC	size exclusion chromatography
Sf9	*Spodoptera frugiperda 9*
smFRET	single molecule Förster resonance energy transfer
SP	standard probe
STAT	signal transducer and activator of transcription
STD	standard deviation of the mean
TCEP	tricarboxyethtlphosphine
TCSPC	time-correlated single photon counting
tetrakis-NTA	tetrakis(nitrilotriacetic acid)
TIRFS	total internal reflection fluorescence spectroscopy
tl	tagless
TMD	transmembrane domain
tris-NTA	tris(nitrilotriacetic acid)
UUA	unnatural amino acid
WT	wild type

CURRICULUM VITAE

NAME **Yulia Podoplelova**

DATE OF BIRTH 26th July 1981

CONTACT DETAILS Department of Biophysics

Faculty of Biology/Chemistry, University of Osnabrück

Barbara Str. 11

49076 Osnabrück, Germany

Cell: +49 (0) 151 539 10141

E-mail: yuliapodoplelova@yahoo.com

EDUCATION

2007 - present **PhD candidate in Biophysics**

University of Osnabrück, Germany

Thesis title: "Site-specific modification strategies for unravelling energetics and dynamics of type I interferon receptor complex"

1998 - 2003 **M.S. (Diploma) in Biology**

Lomonosov's Moscow State University (MSU), Moscow, Russia

Thesis title: "Comparative anatomy of primary bark and secondary phloem of Tribe Galegeae"

SCHOLARSHIPS AND AWARDS

2005 – 2006 DAAD Scholarship for postgraduate research

RESEARCH EXPERIENCE

2007 – present **PhD Student**

Dept. of Biophysics, Faculty of Biology/Chemistry, University of Osnabrück, Germany

2005 - 2006 **Internship Research Student**

Dept. of Plant Mol.Biol., Institute of Biology II, A. Ludwigs University of Freiburg, Freiburg, Germany

2003 - 2005 **Research Assistant/Internship Student**

Dept. of Bioengineering, Faculty of Biology, Lomonosov Moscow State University, Moscow, Russia

Declaration

I hereby declare that the presented thesis:
"Site-specific modification strategies for unravelling energetics and dynamics of type I interferon receptor complex"
was prepared entirely on my own and I have not used outside sources without declaration in the text. Any concepts or quotations applicable to these sources are clearly attributed to them.

I have never attempted a promotion before.

Osnabrück, 25th February 2013 Yulia Podoplelova